

***Cryptosporidium* Capture and Detection of Ultraviolet
Radiation Induced DNA Damage**

by

Nusrat Jahan Urmi

B.Sc., Microbiology, The University of Dhaka, Bangladesh, 2006
MSc., Microbiology, The University of Dhaka, Bangladesh, 2008

A THESIS SUBMITTED IN PARTIAL FULFILLMENT OF
THE REQUIREMENTS FOR THE DEGREE OF

MASTER OF SCIENCE

in

THE COLLEGE OF GRADUATE STUDIES
(Biochemistry and Molecular Biology)

THE UNIVERSITY OF BRITISH COLUMBIA
(Okanagan)

March 2017

© Nusrat Jahan Urmi, 2017

The undersigned certify that they have read, and recommend to the College of Graduate Studies for acceptance, a thesis entitled:

Cryptosporidium capture and detection of ultraviolet radiation induced DNA damage

submitted by Nusrat Jahan Urmi in partial fulfilment of the requirements of

the degree of Master of Science

Dr. Deborah Roberts, School of Engineering, UBCO

Supervisor, Professor (please print name and faculty/school above the line)

Dr. Mina Hoorfar, School of Engineering, UBCO

Co-supervisor, Professor (please print name and faculty/school above the line)

Dr. Deanna Gibson, IKBSAS, UBCO

Supervisory Committee Member, Professor (please print name and faculty/school in the line above)

Dr. Kristen Wolthers, IKBSAS, UBCO

Supervisory Committee Member, Professor (please print name and faculty/school in the line above)

Dr. Richard Plunkett, IKBSAS, UBCO

University Examiner, Professor (please print name and faculty/school in the line above)

External Examiner, Professor (please print name and university in the line above)

March 29, 2017

(Date Submitted to Grad Studies)

Abstract

Majority of the waterborne outbreaks in USA and Canada are associated with protozoa. *Cryptosporidium*, an obligate intra-cellular human pathogen, is responsible for more than 50% of these outbreaks and has become one of the major public health concerns as they can survive typical chemical disinfection treatments. Early detection of this parasite in the water and determination of ultraviolet treatment efficacy can play a role in reducing this disease burden.

An antibody based capture surface was developed to detect *Cryptosporidium* oocysts in treated water. The surface was able to capture three different species of *Cryptosporidium*: *C. parvum*; *C. muris*; *C. hominis* but not *E. coli* indicating that the capture surface is *Cryptosporidium* genus specific rather than species specific and the chances of capturing microorganisms other than *Cryptosporidium* from water are low. IgG3 was selected as better candidate for the capture surface development due to its higher capture efficiency (~84%-90%) compared to that of IgG1 (~54%-74%). Though the oocysts were successfully released in intact form from the capture surface at pH 1.0, it was not possible to reuse the surface because the capture performance decreased after pH treatment.

An indirect ELISA protocol was optimized to detect UV induced photoproducts (CPDs) in the DNA of UV treated *Cryptosporidium* oocysts using cuvettes in a spectrophotometer. Power soil kit was selected as the preferred DNA extraction kit because of its high recovery from low concentration of *Cryptosporidium* in water with high concentrations of other solids. The optimized ELISA protocol was applied on the samples spiked with different doses (0, 3, 6, 10 and 40 mJ/cm²) of UV irradiated *Cryptosporidium* oocysts. The signal generated from DNA-antibody reaction resulted in an exponential rise to maximum curve which showed that the absorbance (indication of

DNA damage) increased with the increase in UV dose. Adaptation of these techniques for *Cryptosporidium* detection & UV treatment validation is expected to improve the standards for water quality monitoring, providing the communities with assurance that their water is safe to consume.

Preface

All the experiments of this research work was conducted in the Biological Solution Laboratory and the Facility for Environmental and Biological Imaging and Dr. Hoorfar's lab at the University of British Columbia (Okanagan) under the supervision of Dr. Deborah Roberts and Dr. Mina Hoorfar.

Chapter 2 is based on work conceptualized and supervised by Dr. Deborah Roberts. I was responsible for designing and conducting all experiments, data collection, analysis & interpretation and microscopic imaging. The work described in Chapter 2 was funded by IC-IMPACTS (the India-Canada Centre for Innovative Multidisciplinary Partnerships to Accelerate Community Transformation and Sustainability). Gold plating of the glass slides were performed by the PhD students of the School of Engineering, Ehsan Samiei and George Luka. Parts of this work have been presented in a conference "IC-IMPACTS 2015 Annual General Meeting & Research Conference" at Vancouver, BC as a poster presentation on "Direct *Cryptosporidium* Detection for Developed and Developing Nations" by Nusrat Urmi, George Luka, Mina Hoorfar and D. J. Roberts.

The research work described in Chapter 3 was conceptualized and supervised by Dr. Deborah Roberts. The experiments were designed by myself and research technician Belal Hossain. I was responsible for conducting experiments, data collection, analysis & interpretation and microscopic imaging. This part of the research was funded by NSERC-Engage grant and was in collaboration with Hyperion Research Ltd., Alberta. Sample collection and processing was assisted by Belal Hossain. He also helped in performing DNA extraction of the samples. Parts of the work reported in Chapter 2 and Chapter 3 have been presented in the "First Annual Biology Graduate Symposium" in the University of British Columbia, Kelowna, BC, 2015 as a poster presentation on

“*Cryptosporidium* detection and quantification of damaged DNA in UV irradiated oocysts” by Nusrat Urmi, Mina Hoorfar and D. J. Roberts.

Table of Contents

Examination committee.....	ii
Abstract.....	iii
Preface.....	v
Table of Contents.....	vii
List of Tables.....	x
List of Figures.....	xii
List of Abbreviations	xv
Acknowledgements	xvii
Dedication.....	xviii
Chapter 1 Introduction	1
1.1 Statement of problem and significance	2
1.2 Relevant literature review	4
1.2.1 Waterborne disease outbreak	4
1.2.2 <i>Cryptosporidium</i> and Cryptosporidiosis	7
1.2.3 <i>Cryptosporidium</i> detection.....	15
1.2.4 Viability and infectivity assays for <i>Cryptosporidium</i> species	21
1.2.5 Recent progress in capture techniques	23
1.2.6 <i>Cryptosporidium</i> inactivation	31
1.3 Research plan and research objectives	39
Chapter 2 <i>Cryptosporidium</i> detection in water using antibody based capture unit...41	
2.1 Materials	42
2.1.1 <i>Cryptosporidium</i> species.....	42
2.1.2 Antibody selection	44
2.2 Capture surface development	45
2.2.1 Preparation of capture surface	45
2.2.2 Experimental design.....	47

2.2.3 Results.....	48
2.3 Antibody specificity determination within the <i>Cryptosporidium</i> genus	49
2.3.1 Methods.....	49
2.3.2 Results.....	50
2.4 Antibody cross reactivity determination with other genera	52
2.4.1 Methods.....	52
2.4.2 Results.....	53
2.5 Antibody concentration determination	56
2.5.1 Methods.....	56
2.5.2 Results.....	56
2.6 pH dependent release mechanism	59
2.6.1 Methods.....	59
2.6.2 Results.....	60
2.6.3 Facilitating pH dependent release mechanism with extended time exposure and shaking.....	61
2.6.4 Effect of pH on the structure of <i>Cryptosporidium</i> oocysts	63
2.7 Capture surface reusability	65
2.7.1 Methods.....	65
2.7.2 Results.....	65
2.8 Discussion	67
Chapter 3 Detection of damaged DNA in UV treated <i>Cryptosporidium</i>	71
3.1 Selection of DNA extraction method for environmental samples	72
3.1.1 Sample preparation for DNA extraction	73
3.1.2 DNA extraction.....	74

3.1.3 Polymerase Chain Reaction (PCR).....	77
3.1.4 Gel electrophoresis.....	78
3.1.5 Results.....	79
3.2 DNA damage detection using ELISA	80
3.2.1 Steps of ELISA procedure	81
3.2.2 Parameter optimization for ELISA method	82
3.2.3 Indirect ELISA to detect UV photoproducts in DNA.....	91
3.2.4 Results.....	91
3.3 Validating ELISA results via microscopy.....	92
3.3.1 Methods.....	92
3.3.2 Results.....	93
3.4 Discussion	98
Chapter 4 Conclusions.....	103
4.1 Concluding remarks	103
4.2 Limitations of the study.....	104
4.3 Future recommendations	104
References.....	107
Appendices.....	128
Appendix A: Chemical composition.....	128
Appendix B: Raw Data	130
Appendix C: Statistical analyses outputs.....	135

List of Tables

Table 1.1: Biology of recently recognised <i>Cryptosporidium</i> species	9
Table 1.2: Methods for <i>Cryptosporidium</i> oocysts retrieval, concentration, and detection from water samples	17
Table 1.3: Molecular approaches to detect <i>Cryptosporidium</i> oocysts in water	20
Table 1.4: Different classes and isotypes of immunoglobulins	23
Table 2.1: Proof of capture ability of the anti- <i>Cryptosporidium</i> activated capture surface	48
Table 2.2: Mean capture efficiency of IgG3 and IgG1 activated surfaces to capture different <i>Cryptosporidium</i> species.	51
Table-3.1: Properties of selected commercially available DNA extraction kits.....	75
Table 3.2: The primer sequences for the 18S rRNA gene external and internal PCR runs	77
Table 3.3: Reaction composition for external PCR (single reaction)	78
Table 3.4: Reaction composition for internal PCR (single reaction)	78
Table 3.5: Presence of CPD in the DNA of non-irradiated and irradiated <i>Cryptosporidium</i> oocysts	94
Table B.1: Capture efficiency of the antibody capture surfaces with non-significant differences (P value> 0.05).....	130
Table B.2: Capture efficiency of the antibody capture surfaces with significant differences (P value< 0.05).....	131
Table B.3: Capture efficiency of IgG3 activated capture surfaces in respect to different antibody concentrations ranging from 100-0.001 µg/ml	131
Table B.4: Capture efficiency of IgG3 activated capture surfaces in respect to different antibody concentrations ranging from 100-12.5 µg/ml	132

Table B.5: Effect of different pH on the release of <i>Cryptosporidium</i> oocysts from the surface	132
Table B.6: pH dependent release efficiency in terms of different time period.....	133
Table B.7: Changes in capture efficiency with the subsequent use of the same surface	133
Table B.8: Analysis of the presence of CPD in DNA of UV irradiated (40mJ/cm ²) oocysts.....	134
Table C.1: One-way ANOVA for <i>C. parvum</i> vs. IgG3	135
Table C.2: One-way ANOVA for <i>C. parvum</i> vs. IgG1	135
Table C.3: One-way ANOVA for <i>C. muris</i> vs. IgG3	135
Table C.4: One-way ANOVA for <i>C. muris</i> vs. IgG1	136
Table C.5: One-way ANOVA for <i>C. hominis</i> vs. IgG3.....	136
Table C.6: One-way ANOVA for <i>C. hominis</i> vs. IgG1.....	136
Table C.7: One-way ANOVA for IgG3 vs. all 3 <i>Cryptosporidium</i> species	137
Table C.8: One-way ANOVA for IgG1 vs. all 3 <i>Cryptosporidium</i> species	137
Table C.9: t-test IgG3 vs. IgG1 for <i>C. parvum</i>	138
Table C.10: t-test IgG3 vs. IgG1 for <i>C. muris</i>	138
Table C.11: t-test IgG3 vs. IgG1 for <i>C. hominis</i>	139
Table C.12: Statistical analysis of antibody concentration.....	139

List of Figures

Figure 1.1: Global distribution of waterborne protozoan outbreaks from 1954 to 2010....	5
Figure 1.2: Geographical distribution of worldwide outbreaks caused by <i>Cryptosporidium</i> spp.....	6
Figure 1.3: Parasitic life cycle of <i>Cryptosporidium</i> involving fecal-oral contamination .	11
Figure 1.4: Oocyst wall structure of <i>C. parvum</i> showing attachment of sporozoites to the inner wall surface via tethers	12
Figure 1.5: Schematic diagram of a sporozoite showing internal organelles	14
Figure 1.6: Schematic representation of the antibody structure	25
Figure 1.7: Role of functional groups in antibody immobilization (random and oriented)	28
Figure 1.8: Conversion of pyrimidine bases to cys-syn and trans-syn isomers of CPD...34	
Figure 2.1: Anti-Cryptosporidium antibody activated capture surface model (not to scale).	41
Figure 2.2: Fluorescence microscopy images of <i>Cryptosporidium</i> oocysts..	43
Figure 2.3: <i>C. parvum</i> oocysts captured on IgG3 activated capture surface.	49
Figure 2.4: Bright field microscopy images of <i>E. coli</i> cells on a poly L lysine coated sticky slide showing typical morphology (rod shaped) and size (~2 μm in length)..	54
Figure 2.5: Bright field microscopy images of a microscopic field of a gold slide activated with anti-Cryptosporidium IgG3 antibody	55
Figure 2.6: Fluorescence microscopy images of positive and negative controls of anti- <i>Cryptosporidium</i> antibody cross reactivity experiment.....	55
Figure 2.7: Capture efficiency of IgG3 activated capture surfaces in respect to different antibody concentrations.	58

Figure 2.8: The changes in the oocyst release efficiencies with respect to different pH solutions.....	61
Figure 2.9: Morphological changes in <i>Cryptosporidium</i> oocysts due to exposure to different pH solutions observed under epifluorescence microscope	64
Figure 2.10: Recapture efficiency of an IgG3 activated capture surface during multiple attempts.....	66
Figure 3.1: Different sizes of cuvettes used during the optimization step.....	84
Figure 3.2: Absorbance of CPD-antibody reaction in different sizes of cuvettes against <i>Cryptosporidium</i> oocysts irradiated at 40 mJ/cm ²	86
Figure 3.3: Signal to noise ratio in different sizes of cuvettes.....	87
Figure 3.4: Changes in absorbance in response to different combination of primary (1 µg/ml, 2 µg/ml, 4 µg/ml) & secondary antibody (0.3 µg/ml, 0.375 µg/ml, 0.5 µg/ml) concentrations against <i>Cryptosporidium</i> oocysts irradiated at 40 mJ/cm ²	88
Figure 3.5: Signal to noise ratio over different combination of primary (1 µg/ml, 2 µg/ml, 4 µg/ml) & secondary antibody (0.3 µg/ml, 0.375 µg/ml, 0.5 µg/ml) concentrations..	89
Figure 3.6: Changes in absorbance in response to different incubation period of primary & secondary antibodies at 37°C and 4°C with <i>Cryptosporidium</i> oocysts irradiated at 40 mJ/cm ²	90
Figure 3.7: Signal to noise ratio over different incubation period of primary and secondary antibodies at 37°C.....	90
Figure 3.8: Dose response curve to detect CPDs in <i>Cryptosporidium</i> oocysts irradiated with different doses of UV light.	92

Figure 3.9: Black and white images of 40 mJ/cm² UV radiation treated *Cryptosporidium* DNA taken with (a) Alexa fluorescence excitation and (b) DAPI fluorescence excitation using epifluorescence microscope.....95

Figure 3.10: Black and white images of UV non-irradiated *Cryptosporidium* DNA taken with (a) Alexa fluorescence excitation and (b) DAPI fluorescence excitation using epifluorescence microscope.96

Figure 3.11: Crypt-a-Glo stained *Cryptosporidium* oocysts with DAPI stained DNA under epifluorescence microscope.....97

List of Abbreviations

Ab: Antibody

ANOVA: Analysis of variance

AP: Alkaline phosphatase

ASTM: American Society for Testing and Materials

BSA: Bovine serum albumin

COWP: *Cryptosporidium* oocyst wall protein

CPD: Cyclobutyl pyrimidine dimers

DAPI: 4' 6-diamidino-phenylindole

DEPC: Diethylpyrocarbonate

DIC: Differential interference contrast

DNA: Deoxyribonucleic acid

ELISA: Enzyme linked immunosorbent assay

FITC: Fluorescein isothiocyanate

FT: Freeze-thaw

GP: Glycoprotein

HBSS: Hanks' Balanced Salt Solution

HRP: Horseradish peroxidase

ICR: Information Collection Rule

IFA: Immunofluorescence assay

IFM: Immunofluorescence microscopy

IgG: Immunoglobulin G

IgM: Immunoglobulin M

IMS: Immuno-magnetic separation

LP: Low pressure lamp

mAb: Monoclonal antibody

MIC: Microbial inactivation credit

MP: Medium pressure lamp

mRNA: Messenger RNA

NFT: No freeze-thaw

PBS: Phosphate buffered saline

PCR: Polymerase chain reaction

RFLP: Restriction fragment length polymorphism

RT-PCR: Reverse transcription polymerase chain reaction

SNK: Student-Newman-Keuls

TBE: Tris Borate EDTA

TBS: Tris buffered saline

TRI reagent: Total RNA Isolation reagent

USEPA: United States Environmental Protection Agency

UV: Ultraviolet

WHO: World Health Organization

Acknowledgements

I would like to thank my thesis supervisor Dr. Deborah Roberts of the School of Engineering at the University of British Columbia (Okanagan) for all the support she provided since the day I joined the university. She allowed this research to be my own work but was constantly there to guide me in the right direction. Her office door was always open whenever I had a trouble or a question about my research or writing.

I would also like to express my gratitude to my co-supervisor Dr. Mina Hoorfar and my committee members Dr. Deanna Gibson and Dr. Kirsten Wolthers for their valuable suggestions and constructive comments about the research work which helped me to shape up my work. I also want to thank IC-IMPACTS and NSERC-Engage grant as well for providing necessary funds required to conduct this study.

Finally, I am gratefully indebted to my parents for believing in me and to my husband for supporting and encouraging me throughout my years of study and through the process of researching and writing this thesis. This accomplishment would not have been possible without them. Above all, I am grateful to Almighty for making this journey easier for me.

Dedication

**To my beloved husband and my mother
without whose support this journey would not be possible**

Chapter 1 Introduction

According to the recent estimation of World Health Organization (WHO) and United Nations Children's Fund, about 768 million people depend on unimproved water supplies contaminated with high levels of pathogens (Joshi et al., 2013). The consequence of this lack of treated water is 1.3 million deaths each year, the majority of which are reported in developing countries. Although substantial improvement has been achieved in developed countries water treatment technologies remain at risk of experiencing failure, causing outbreaks of waterborne disease on several occasions. Pons et al. (2015) reviewed 293 waterborne disease outbreaks occurring from 1970 to 2014 in Canada and US. The majority of these involved small non-community drinking water systems and showed that water treatment failure (23%) and scarcity of available treatment (20%) were the major causes.

Cryptosporidium is an obligate intra-cellular human pathogen and has become one of the major public health concerns as they can survive typical chemical disinfection treatments. Gradually, the use of ultraviolet (UV) irradiation has been instituted as an effective process to disinfect water containing these resistant organisms. To regulate the presence of protozoa in drinking water, the United States Environmental Protection Agency (USEPA) developed a detection method (EPA-1623.1) which is expensive (\$700 per sample), time consuming and requires skilled technicians in advanced laboratories and can only confirm the cause of an outbreak because they are not timely enough to prevent it (Bridle et al., 2012). The current detection system uses filters to capture the pathogen which have wide ranges of recovery and require significant time to process. Moreover, the detection technique cannot ensure the efficacy of UV treatment. This research was therefore designed to address these problems. During this research, an antibody based capture surface was developed as a part of a detection device with

improved capture capability and specificity. A new assay method was also developed for water treatment process operators to document the efficacy of the widely used UV disinfection method.

1.1 Statement of problem and significance

Motivation for this research stemmed from the recognition of the fact that safe and secure water supplies are vital for human health. Water contaminated with infectious organism can cause hemorrhagic diarrhea, typhoid fever, gastroenteritis, cryptosporidiosis and giardiasis which are responsible for the death of 1,000,000 people each year (Naghavi et al., 2015). Diarrheal diseases alone constitute 4% of the total daily global disease burden and are a leading cause of global death in children (<5 years) (WHO The World Health Report, 2002). Water consumed while waiting for analytical results may lead to outbreaks. Many of these tragedies could be prevented with early detection of the outbreak causing pathogens. There is ample evidence in the literature that both developed and developing countries suffer from the undesirable consequences of waterborne pathogenic infections every year due to the presence of *Cryptosporidium parvum* oocysts (Corso et al., 2003; Karanis et al., 2007; Mackenzie et al., 1994; Snelling et al., 2007).

Existing waterborne pathogen testing technology (EPA 1623.1) suffers from large errors in accuracy (recovery rate 21-100%) and precision (standard deviation 38). On many occasions, large standard deviations of the detection techniques make the results ineffective for quality control. These variances occur due to imprecise methods such as filtration used in separating the pathogens from the large volumes of water that require testing as well as subjective interpretation due to microscopy. Additionally, conventional water treatment techniques such as chlorination are not effective against *Cryptosporidium* due to its environmentally resistant oocyst structure. Due to this resistant structure, the method in practice for *Cryptosporidium* disinfection is UV treatment. There is a converse

relationship between UV exposure and *Cryptosporidium* oocyst viability due to DNA damage (Rochelle et al., 2005), but no test is in practice to check the state of the DNA of the pathogens in UV-treated water samples. Due to previous collaboration of our lab with water suppliers, it is clear that municipalities are interested in a test unit to check whether their UV treatment facilities are operating properly.

This thesis therefore included two unique milestones. First was the development of a reliable and efficient capture unit for a *Cryptosporidium* detection device to determine their existence in water. Second, the methodology was designed to determine the effectiveness of UV radiation treatment in the captured and detected pathogens.

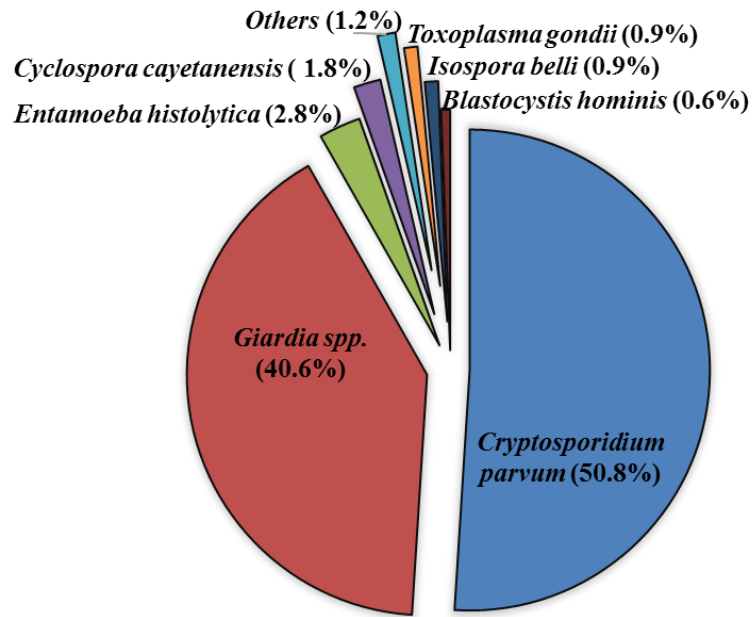
1.2 Relevant literature review

In this section a literature review focusing on the enteric parasite *Cryptosporidium* and its pathogenicity; current detection and treatment methods in practice and their drawbacks are discussed to provide background knowledge about the research.

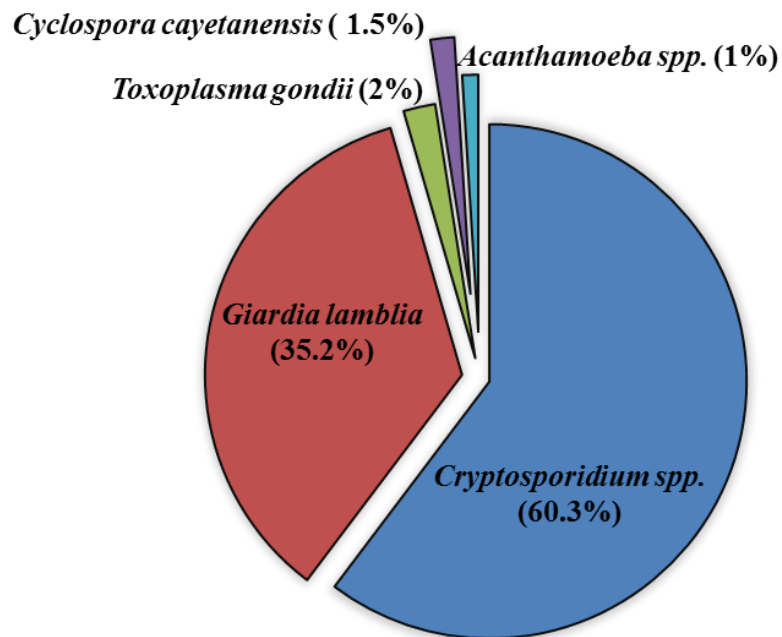
1.2.1 Waterborne disease outbreak

Despite being essential for life, water is also responsible for waterborne diseases. According to WHO a waterborne disease outbreak occurs when two or more epidemiologically-linked persons appeared with similar sicknesses upon consumption of the same water/food (Tirado and Schmidt, 2001). Waterborne disease outbreak often causes diarrheal diseases (1993 Milwaukee, U.S. outbreak, cases=403,000) and rarely causes high mortality (1892 cholera outbreak in Hamburg, Germany, deaths=8500) (MacKenzie et al., 1994; Medema et al., 2003). Ligon and Bartram (2016) reviewed drinking water disease outbreaks and investigated multiple associations such as temporal, geographical, water source, treatment system, and causative agents. It was found that unprocessed water and contamination events were most frequently associated with the outbreaks.

Although the bacterial pathogens are attributed as the leading cause of waterborne diseases in developing countries, the majority waterborne outbreaks in USA and Canada are associated with protozoa (Leclerc et al., 2002). Figure 1.1a and 1.1b represent global distribution of waterborne protozoan outbreaks that occurred worldwide from 1954 to 2001 (325 cases) and from 2004 to 2010 (191 cases) respectively. More than 50% of these outbreaks were reported to be caused by the enteric parasite *Cryptosporidium* spp. (Karanis et al., 2007; Baldursson and Karanis, 2011).



(a)



(b)

Figure 1.1: Global distribution of waterborne protozoan outbreaks from 1954 to 2010 (Adapted from Karanis et al., 2007; Baldursson and Karanis, 2011)

Baldursson and Karanis (2011) also discussed the regional distribution of protozoan outbreaks where 46.7 % outbreaks were reported on the Australian continent, 33.1% on the American continent, 16.5% on the European continent and 3.5% on the Asian continent 3.5% from 2004 to 2010. In developed countries the presence of good

surveillance systems allows them to generate data that show how significantly waterborne diseases contribute to public health concerns. The evidence suggests that inclusion of the detection of these protozoa as an integral part of the quality assurance system in water industries should be emphasized and more investment should be encouraged on designing appropriate workflow for proper detection and diagnosis (Putignani and Menichella, 2010). In developing countries, the infections are potentially greater because of high pollution in water bodies, lack of standard sanitary systems and inadequate quality control in food and water industries. Unfortunately, the evidence generated from this part of the world are underestimated due to a lack of reporting facilities and resources to implement diagnostic algorithms (Putignani and Menichella, 2010). Strong and sustainable surveillance programs need to be introduced in this part of the world to generate evidence for appropriate policy implementation. Figure 1.2 shows the geographical distribution of cryptosporidiosis outbreaks which are classified as water borne diseases, foodborne diseases, HIV related diseases (Immuno-suppressed), travel and community diseases.

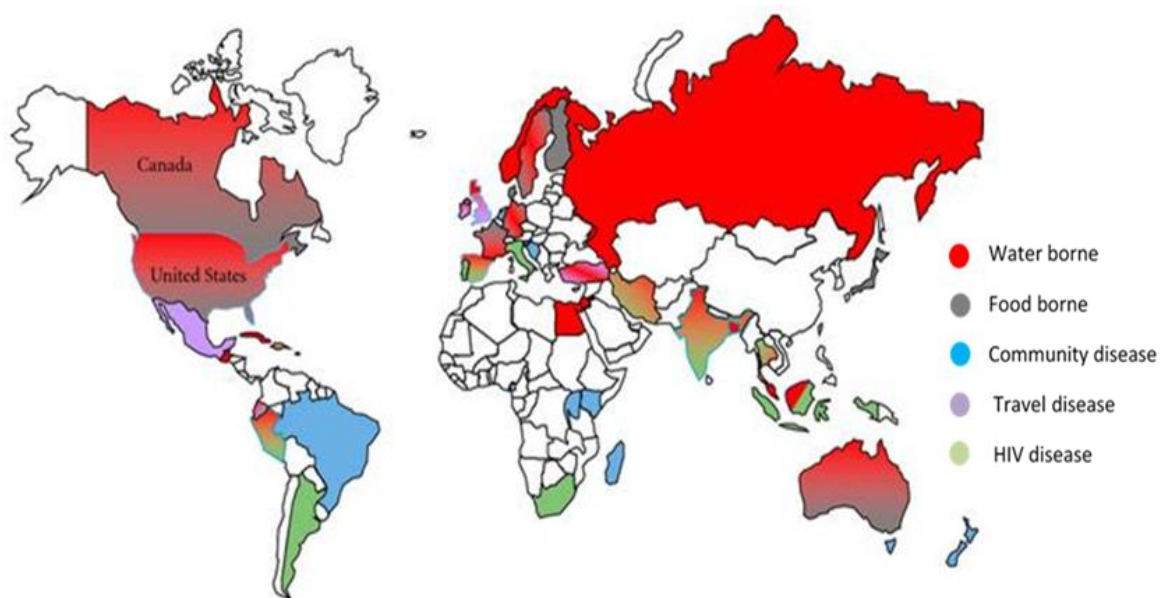


Figure 1.2: Geographical distribution of worldwide outbreaks caused by *Cryptosporidium* spp. (Adapted from Putignani and Menichella, 2010)

The outbreaks due to waterborne and foodborne cryptosporidiosis are more concentrated in Europe, Australia, USA and Canada whereas outbreaks in Russia are due to waterborne cryptosporidiosis (Putignani and Menichella, 2010).

1.2.2 *Cryptosporidium* and Cryptosporidiosis

Cryptosporidium first described by Tyzzer (1910) belongs to the phylum Apicomplexa. Until the reporting of first human case of cryptosporidiosis in 1976 this enteric parasite was considered as an infrequent gastrointestinal pathogen (Nime et al., 1976). An outbreak in Texas involving 2,000 individuals in 1984 first categorized this organism as a waterborne pathogen (D'Antonio et al., 1985). Since then outbreaks have been documented globally including one of the largest epidemic known as 1993 Milwaukee outbreak (Mackenzie et al., 1994). At first, water polluted by livestock feces containing *Cryptosporidium* was thought to be responsible for this sporadic cryptosporidiosis but later human feces containing *Cryptosporidium* oocysts was identified as the cause for this water outbreak (Mackenzie et al., 1994; Peng et al., 1997; Goh et al., 2004).

Age and immune status of the host determine the severity of the disease. Immunocompetent people are more resistant to infection than immunocompromised people and children (Ramirez et al., 2004; Chen et al., 2002; Farthing, 2000). Children from developing countries with history of malnutrition develop severe clinical signs. Cryptosporidiosis can also cause lethal diarrhea in immunosuppressed populations like AIDS patients with low CD4+ T cell counts (Chen et al., 2002; Farthing, 2000). Signs and symptoms may appear within 2 to 14 days after ingestion of oocysts. The predominant sign is diarrhea, sometimes associated with abdominal cramps, malaise, fever, fatigue, loss of appetite as well as nausea. Based on severity, bloody diarrhea, dehydration, weight loss may follow. The duration of clinical signs in immunocompetent

hosts is usually 10-14 days, whereas in immunocompromised patients they can last for years.

1.2.2.1 Taxonomy

Based on host, nomenclature of *Cryptosporidium* species was primarily constructed and over sixty species were reported from diverse sources. Due to morphological similarity, *Cryptosporidium* was also classified based on molecular characteristics, host preference, sites of infection, and cross transmissibility (Smith & Nichols, 2010). *Cryptosporidium* belongs to Cryptosporidiidae (family), Eimeriorina (suborder) and Eucoccidiorida (order) with more than 20 species (Table 1.1) and 60 genotypes (Fayer, 2010; Plutzer & Karanis, 2009; Xiao et al., 1999). It is to be noted that *Cryptosporidium parvum* has been known to infect widespread host types.

From Table 1.1 it can be seen that *Cryptosporidium* particularly *C. parvum* is zoonotic in nature with a broad host range including human and cattle (Hunter et al., 2004). Besides zoonotic cryptosporidial infections, infections from human origin caused by *C. hominis* (the human genotype of *C. parvum*) were reported (Morgan et al., 1998; Ong et al., 2002; Read et al., 2002). Humans are also susceptible to *C. canis*, *C. felis*, *C. muris* harbored by companion animals like dogs, cats and mice (Abe et al., 2002; McGlade et al., 2003; Sterling and Adam, 2004; Thompson, 2003). The prevalence of *Cryptosporidium* species are dominated by *C. parvum* and *C. hominis* and global distribution of these two species regionally varied (Caccio et al., 2005). *C. parvum* was mostly reported in Europe whereas *C. hominis* was the predominant species in Australia, Africa, both American continents and some parts of Asia. These two species were also reported with different seasonality and age group distribution. *C. parvum* dominates in the spring while *C. hominis* occurs mainly in late summer or early autumn and also travels throughout the whole year with travelers. *C. hominis* are more prevalent in <1 year old

children as well as in females of the reproductive age and *C. parvum* was reported to cause significant infection in children <5 years old (Chalmers et al., 2009).

Table 1.1: Biology of recently recognised *Cryptosporidium* species (Adapted from Ghazy et al., 2015; Smith et al., 2007)

Species	Major hosts	Minor hosts
<i>C. hominis</i>	Humans	Dugong, sheep
<i>C. parvum</i>	Cattle, livestock, humans	Deer, mice, pigs
<i>C. meleagridis</i>	Turkey, humans	Parrots
<i>C. canis</i>	Dogs	Humans
<i>C. felis</i>	Cats	Humans, cattle
<i>C. suis</i>	Pigs	Humans
<i>C. wrairi</i>	Guinea pigs	Not known
<i>C. muris</i>	Rodents	Humans, rock hyrax, mountain goat
<i>C. andersoni</i>	Cattle, Bactrian camel	Sheep
<i>C. bovis</i>	Cattle	Sheep
<i>C. ryanae</i>	Cattle, Bos taurus	Not known
<i>C. xiaoi</i>	Sheep	Yak, goat
<i>C. fayeri</i>	Red kangaroo	Not known
<i>C. macropodum</i>	Eastern grey kangaroo	Not known
<i>C. baileyi</i>	Poultry	Quails, ostriches, ducks
<i>C. galli</i>	Finches, chicken	Not known
<i>C. serpentis</i>	Lizards, snakes	Not known
<i>C. varanii</i>	Lizards	Snakes
<i>C. molnari</i>	Fish	Not known
<i>C. scophthalmi</i>	Fish	Not known

1.2.2.2 Transmission

As *Cryptosporidium* is parasitic in nature, it thrives in the gastrointestinal tract of infected humans or animals. From there, the oocysts are excreted in the environment with stool (Carey et al., 2004; Current, 1990). *Cryptosporidium* shedding in the stool starts from the onset of symptoms resulting in millions of oocysts released in a single bowel movement. This shedding can last for weeks even after the symptoms subside. The chemically resistant thick walled structure of the oocysts helps them to survive from fecal deposition through water or through treatment (Robertson et al., 1992). From there *Cryptosporidium* can spread by ingestion of contaminated drinking water, contaminated food, and contact with contaminated materials/people. Recreational water contaminated

with feces or sewage also plays role in spreading cryptosporidiosis. The majority of the outbreaks reported in Canada are due to *C. parvum* from the contamination of drinking water or recreational water (Stirling et al., 2001; Putignani and Menichella, 2010; Macey et al., 2002). Jaidi et al. (2009) used QMRA (Quantitative Microbial Risk Assessment) to assess the risk of *Cryptosporidium* and *Giardia* in Canadian drinking water revealing that the contamination occurred mostly due to the choice of water treatment system.

1.2.2.3 Life cycle

Both asexual and sexual reproduction occur during the *Cryptosporidium* life cycle, all taking place within an individual host (monoxenous). Figure 1.3 describes the parasitic life cycle of *Cryptosporidium*. The parasite survives in the environment as a hard oocyst containing four sporozoites. Following the consumption of contaminated food/water, *Cryptosporidium* attaches to apical surface of the intestinal epithelial cells. The invasion mechanism is not well understood. *Cryptosporidium* may exhibit actin-dependent gliding and enter the epithelial cell of the infected mammalian host using a parasite driven process (Sibley, 2004).

Excystation of the oocyst occurs within the host and the released sporozoites then transform into trophozoites within the parasitophorous vacuoles in the mucosal epithelial microvilli. Trophozoites then enter the asexual stage to form merozoites, which eventually start the sexual phase of the life cycle and produce microgamonts and macrogamonts. During this stage, zygotes form through the fertilization of microgametes and macrogamonts. These zygotes develop into environmentally resistant oocysts which are then discharged outside via the feces of the host (Current, 1990; Carey et al., 2004).

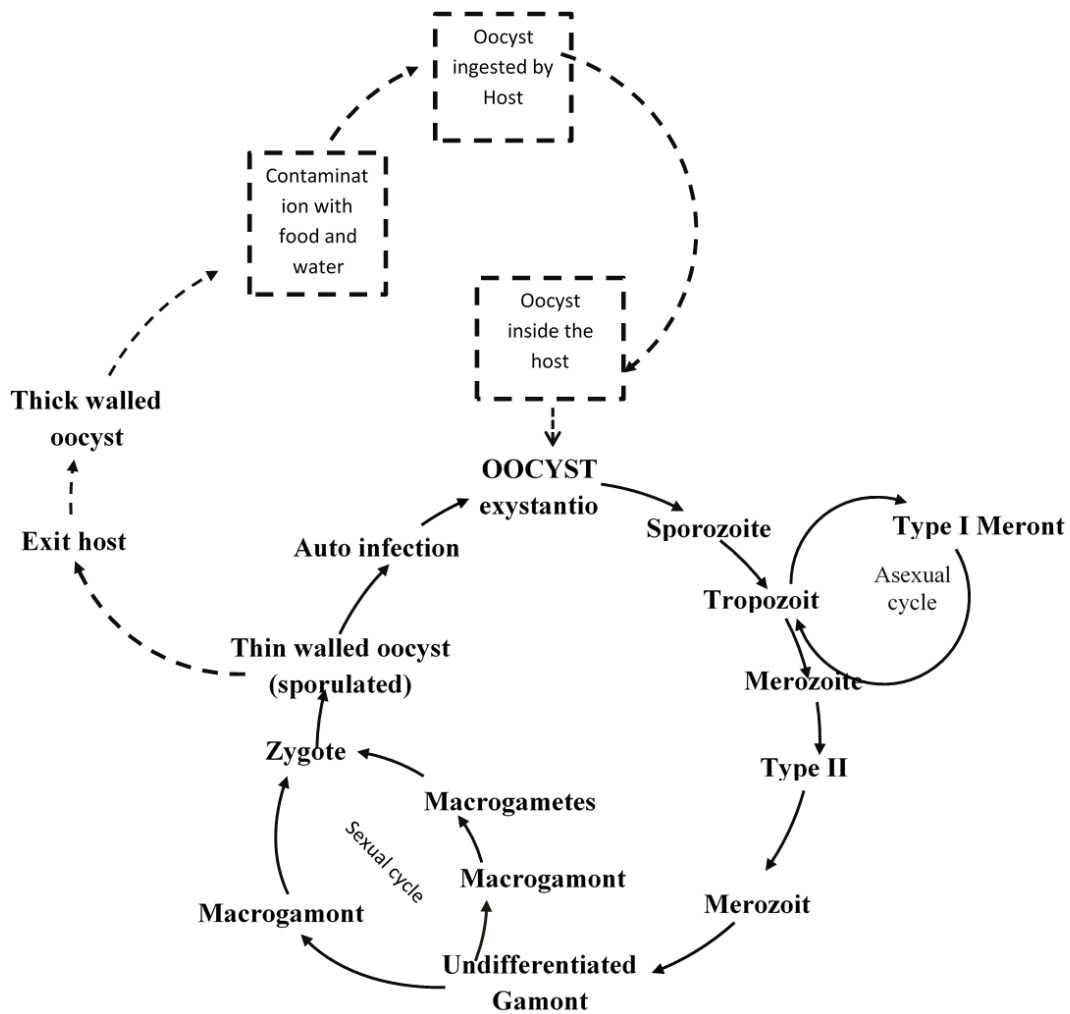


Figure 1.3: Parasitic life cycle of *Cryptosporidium* involving fecal-oral contamination (Adapted from CDC (USA), 2016)

1.2.2.4 Pathogenesis

Cryptosporidium causes an acute malabsorptive and secretory diarrhea in humans with the clinical symptom onset within 2-7 days of infection and a prepatent period of 7-21 days (Ramirez et al., 2004). The attachment and invasion of the sporozoites within the epithelial cells are facilitated by apical complex proteins (Sibley, 2004; Tzipori and Ward, 2002; Ward and Cevallos, 1998). After the initial infection, *Cryptosporidium* multiply within the epithelial cells and disseminate throughout the small and large intestine. The intensity of clinical signs depends on the infection sites; infections in the small intestine result in severe watery diarrhea whereas infections in the distal ileum and large intestine are often asymptomatic. The invasion and colonization of the epithelial cells cause

damage through decrease of intestinal surface area, loss of membrane-bound digestive enzymes and imbalanced electrolyte and nutrient transport (Baker et al., 2005).

Cryptosporidium has also been found to be responsible for increased epithelial permeability by disrupting epithelial tight junctions (Buret et al., 2003).

1.2.2.5 Biological properties

1.2.2.5.1 Oocyst cell wall

National Institutes of Health categorized *C. parvum* as a category B biodefense agent because it possesses a hard oocyst structure which made it resistant to inactivation or difficult to remove from drinking water without filtration (Fayer, 1997; Puiu et al., 2004). As presented in Figure 1.4, *C. parvum* oocysts have a single, multilayered wall consists of firm bilayer of acid-fast lipids and an internal layer of oocyst wall proteins with tethers to sporozoites (Belli et al., 2006; Bushkin et al., 2013; Chatterjee et al., 2010; Samuelson et al., 2013).

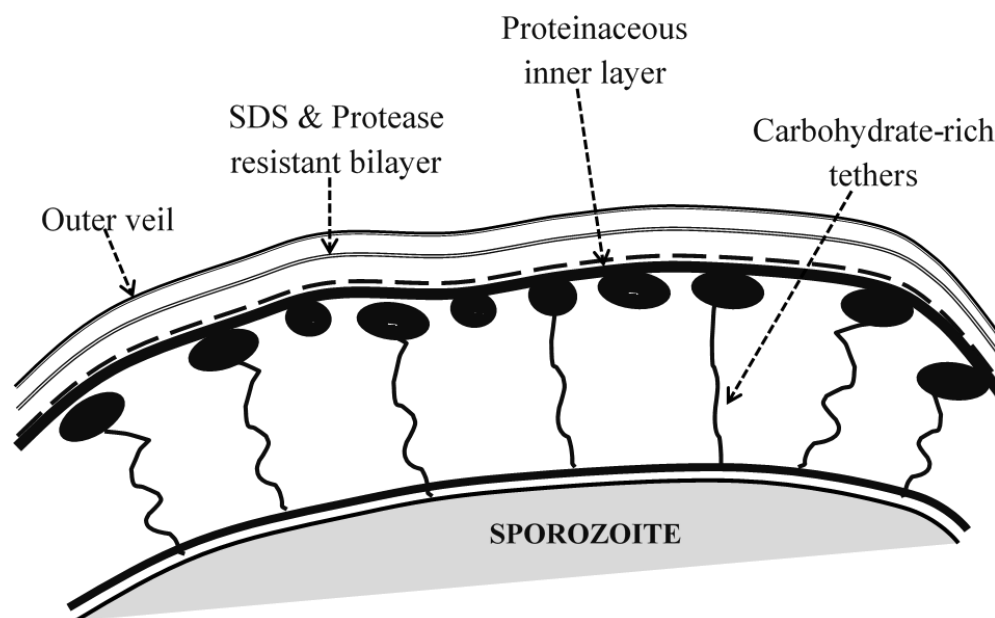


Figure 1.4: Oocyst wall structure of *C. parvum* showing attachment of sporozoites to the inner wall surface via tethers (Adapted from Chatterjee et al., 2010)

Oocyst wall lipids are composed of triglyceride mixtures, including polyhydroxy fatty acyl chains that are responsible for resistance towards environmental stress. The

whole oocyst wall can be dissolved by organic solvents. *Cryptosporidium* oocyst wall protein 1 (COWP1), COWP6 and COWP8 are three major proteins, whereas COWP2, COWP3, and COWP4 are minor proteins. The surface of the sporozoite contains mucin-like glycoproteins that contribute to fibrils or which attach or tether sporozoites to the inside of the oocyst wall (Chatterjee et al., 2010).

1.2.2.5.2 Sporozoites

The sporozoite of *Cryptosporidium* is motile, short lived and invades host cells after attachment to the membrane of a host cell. Tetley et al. (1998) studied profiles of *C. parvum* and obtained number, distribution and arrangement of organelles (3D) by transmission electron microscopy. Figure 1.5 represents the morphological characteristics of a sporozoite where the apical complex is found beneath the tip of the polar ringed region which further lengthen as the entry procedure continues with the liberation of secretory contents (Scholtyseck et al., 1970). Tetley et al. (1998) suggested that sporozoites have a single secretory structure which is called rhoptry. Sporozoites contain one or two crystalline bodies. They do not have conventional golgi apparatus and mitochondria. Sporozoites contain thread-like structures called micronemes which are apparently spherical, presenting 0.8% of total cell, located mostly at the apical complex. The sporozoite also contains dense granules which are less numerous but larger in size accounting for 58% of the cell size. The central region of the sporozoites contain 300-nm-diameter granules (Bonnin et al., 1995). A plastid-like organelle was also observed close to the nucleus in the *Cryptosporidium*.

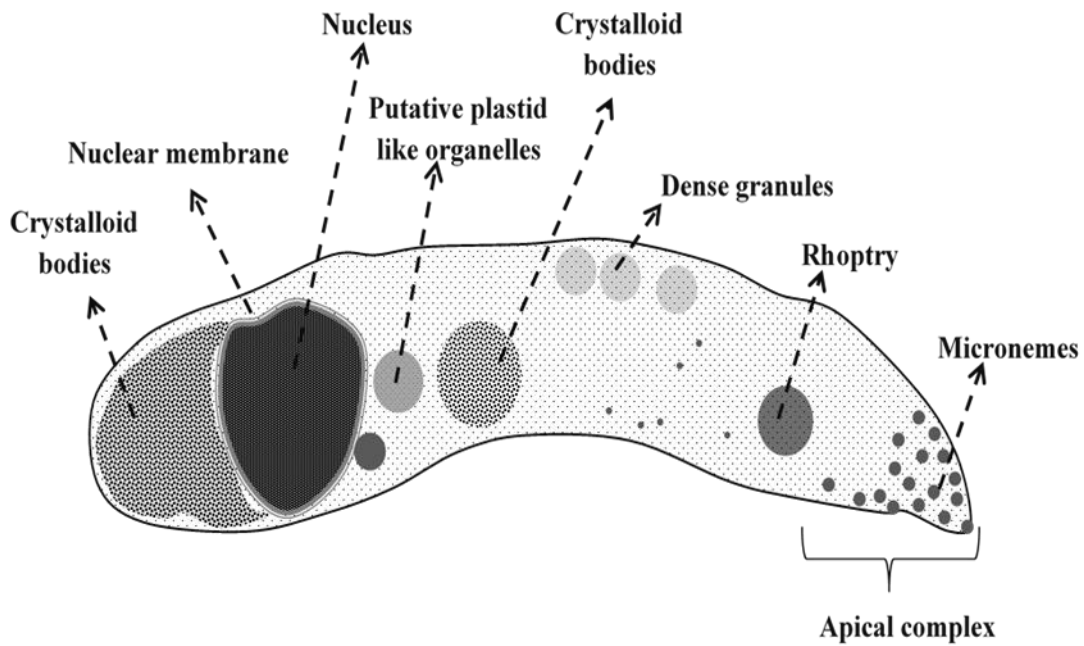


Figure 1.5: Schematic diagram of a sporozoite showing internal organelles (Adapted from Tetley et al., 1998)

1.2.2.6 Antigenic and genomic properties

A number of immunogenic antigens of *Cryptosporidium* have been identified. Most of them are glycoproteins expressed on the surface of oocysts such as circumsporozoite-like antigen, glycoprotein 900 (GP 900), glycoprotein 40 (GP 40), glycoprotein 25-200 (GP 25-200), thrombospondin-related adhesive protein (TRAP C1) (Sibley, 2004). The antigens are connected through a vesicle which lies between sporozoites and the oocyst wall. Eventually they appear on the surface by a mechanism involving vesicle fusion with the wall. Antigens are labile and secretory in nature and can be separated in the supernatant following centrifugation (Entrala et al., 2001; Yu et al., 2002).

During the infection process, antigens contact the host-cell cytoplasm by feeder organelles and host-parasite networks (Lee et al., 2006). The antigenicity causing humoral immunity was reported to locate at various developmental stages of parasites. Lee et al. (2006) showed that oocyst walls contain high amounts of antigen stimulating IgG

antibodies compared to trophozoites. The sporozoite surface stimulate IgG and IgM antibody formation. Weir et al. (2000) conducted an experiment where different mice were immunized with different antigens, such as soluble protein extract of oocyst wall, inactivated whole oocysts, and purified oocyst walls, the immune response against which yielded high IgG, IgM and low IgM/IgG levels respectively.

The *Cryptosporidium* genome consists of 8 chromosomes (9.0-10.4 Mbp) containing ~60%–70% AT and 3807 genes with low copy numbers of rDNA genes (Blunt et al. 1997; Le Blancq et al. 1997; Taghi-Kilani et al., 1994). Bankier et al. (2003) constructed a robust physical map revealing a compact genome, unusually rich in membrane proteins. The full genome sequence of *C. parvum* and *C. hominis* is available on CryptoDB (<http://CryptoDB.org>) database (Puiu, 2004; Xu et al., 2004; Abrahamsen et al., 2004).

1.2.3 *Cryptosporidium* detection

1.2.3.1 Legislation

The effectiveness of water treatment processes designed to eliminate pathogens has been evaluated through water monitoring studies (Quintero-Betancourt et al, 2002). The United States Environmental Protection Agency's "Interim Enhanced Surface Water Treatment Rule" established maximum contaminant level goal of "0" for *Cryptosporidium*. Since such measurement techniques are not readily available, a treatment goal was set at least 99% removal from the water. This was determined based on the performance of water treatment plants and water monitoring indices such as turbidity, filter performance etc. To achieve the goal, a guideline was published in December 1998 followed by the revised version in January 2001, applied from 2002 (Quintero-Betancourt et al., 2002). The water supply regulations in the United Kingdom consider the presence of *Cryptosporidium* oocysts at above 10/100L as a criminal

violation (Fairley et al., 1999). Although detection, quantification and viability determination of waterborne protozoa from the environment is a challenge.

1.2.3.2 Detection of waterborne *Cryptosporidium* in environmental samples

Several approaches were stimulated to develop the retrieval and detection of *Cryptosporidium* after the first *Giardia* outbreak in 1965 (Hass et al., 1999; Rose, 1991). The method developed from these approaches has three basic steps: (i) sample concentration such as filtration to collect parasites present in low numbers; (ii) purification and (iii) detection of oocysts in filtered sample by immunofluorescent microscopy (Jakubowski et al., 1996).

Originally, oocysts were entrapped in filter from water samples either by cartridge or membrane filtration (Musial et al., 1987; Ongerth and Stibbs, 1987) and then detected by immunofluorescent assay (Rose et al., 1989). The principles for observing *Cryptosporidium* oocysts required the oocysts to be stained with fluorescence dye specifically around the oocyst wall. At the beginning of 90's, the American Society for Testing and Materials (ASTM) used cartridge filtration to recover oocysts from water, a percoll-sucrose step to segregate the oocysts from debris and an IFA based method to detect and enumerate oocysts (ASTM, 1991). The average recovery efficiency of the ASTM method was reported between to be 3-29% (LeChevallier et al., 1991; Smith and Hayes, 1997). Though ASTM could handle high volumes of water, the system was costly and required a long execution time compared to membrane filtration. Membrane filtration method was, however, unable to differentiate oocysts from algae (Nieminski et al., 1995). During the 1990s, the United States Environmental Protection Agency (USEPA) approved "Information Collection Rule" (ICR) for detection and quantification of oocysts which was later criticized for several reasons such as being costly, difficult to perform, variances in results, low recovery efficiencies (3%), non-specificity, inability to

determine viability (Quintero-Betancourt et al., 2002). According to LeChevallier et al. (1995) each step of ICR sample processing method was responsible for oocyst loss and suggested modifications in sampling, processing, staining or detection. As suggested by LeChevallier et al. (1995) the USEPA initiated an effort in 1996 to draft Method 1622 for the detection of *Cryptosporidium* which was further confirmed in 1998 through an inter-laboratory study. The method was labelled as 1623 in October 1998 when the detection of *Cryptosporidium* was combined with *Giardia* and finally approved in January 1999. This was further validated by inter laboratory study and finally published as “EPA-1623.1” in 2012 after several revisions and field trials. Method 1623 included filtration (Envirochek™), immunomagnetic separation (IMS) and immunofluorescence assay (IFA) using microscopy with vital dye staining (4' 6-diamidino-phenylindole (DAPI) to detect *Cryptosporidium* and *Giardia* in water (USEPA, 1999a; USEPA, 1999b; USEPA, 2012). Standard techniques that have been used for recovery and detection of *Cryptosporidium* are recorded in Table 1.2.

Table 1.2: Methods for *Cryptosporidium* oocysts retrieval, concentration, and detection from water samples (Adapted from Quintero-Betancourt et al., 2002)

Technique	Filtration and capacity	Concentration	Purification	Detection	Recovery (%)
ASTM, 1991 USEPA, 1996 (USA)	Cartridge filtration (1.0 µm,)100-1000L	Centrifuged at 1050×g, 10 min	Percoll–sucrose density-gradient centrifugation	IFA, DIC microscopy	0–100
Method 1622/1623: USEPA, 1999a USEPA, 1999b (USA)	Membrane filter (Envirochek™ HV) 10-1000L	Centrifuged at 1100×g for 15 min	Dynal IMS		12–93 (21–100)*
SOP 1999, SI No. 1524 † (UK)	Genera Filta-Max™ filter membranes		Dynal IMS	IFA, DIC microscopy	30–50**

1.2.3.3 EPA 1623.1 | *Cryptosporidium* detection in drinking water system

This section covers the details of EPA 1623.1 method, the only currently accepted detection method to regulate the waterborne parasites in drinking water according to the “Safe drinking water act amendments” of USEPA and also the method currently in use in Canada.

Although *Cryptosporidium* spp. is ubiquitous, it exists in low numbers in many water sources. Therefore, the ability to collect *Cryptosporidium* from a large volume of sample is the main concern during sampling. During the EPA method, the filtration step can be performed directly in the field using a portable pump to separate the oocysts from the water and the filter would be transported to the lab maintaining the proper temperature. The method also allows for the collection of water in the field in a container and transportation of this water to a lab for filtration. Wide ranges (0-93%) of recovery efficiency were reported based on different types of filters, pore sizes, and modifications of the basic filtration process. The Envirochek capsule (membrane filter) was included in the EPA protocol because of its capacity to handle up to 40L water without clogging and its application in both lab and sampling field (Quintero-Betancourt et al., 2002).

After filtration, the pathogens are retained on the filter membrane along with other extraneous material. Elution buffers made in the laboratory are then used to elute and recover the oocysts from the filter through mechanical washes. The recovery percentage varies highly from this filtration/ elution process making the filtration step imprecise. The filtration step causes the accumulation of other particles of similar size and properties that could interfere in the detection of oocysts (specificity and sensitivity). So after elution, the sample is purified and concentrated to microvolumes in the next step using IMS kits. Commonly used kits are Dynabeads® anti-*Cryptosporidium* IMS kit (USEPA 1623) and Cryptoscan IMS kit (Bukhari et al., 1998), which consist of super-paramagnetic beads

conjugated with an Immunoglobulin-M (IgM) monoclonal antibody (mAb) and Immunoglobulin-G (IgG) mAb respectively. Different research groups conducted a comparison study with different commercially available IMS kits and showed inconsistency in recapture (Rochelle et al., 1999). The inconsistencies were credited to the bead size, turbidity level and conjugated immunoglobulin type. The acceptable range of final recovery reported by EPA for *Cryptosporidium parvum* was 21-100% (Quintero-Betancourt et al., 2002). The kit designed for only *Cryptosporidium* worked better than the combo kit for detecting *Giardia* and *Cryptosporidium* (Stanfield et al., 2000). The wide range of recovery and precision demonstrated that although the method worked practically, there is much room for improvement.

The oocysts are enumerated and detected from the concentrated and purified sample by epifluorescent microscopy after immunofluorescent staining using *Cryptosporidium* specific fluorescein isothiocyanate conjugated antibody to define size and shape of oocysts. Additional steps included staining of nuclei of oocyst sporozoites through nuclear fluorochrome 4', 6- diamidino-2-phenylindole (DAPI) followed by differential interface contrast (DIC) microscopy to determine internal morphology. The use of DAPI and DIC microscopy in combination with Immunofluorescence assay (IFA) decreased false positive and false negative results (Quintero-Betancourt et al., 2002).

1.2.3.4 Molecular approaches for *Cryptosporidium* detection in water

The detection of waterborne oocysts using polymerase chain reaction (PCR) was reported to generate more specific and sensitive (detection limit 1-10 oocysts) results compared to other conventional methods (Quintero-Betancourt et al., 2002). Some of these molecular approaches are summarized in Table 1.3. In addition to detection, molecular techniques were also applied to determine strain specificity or source of outbreak by identifying genus, species, and genotype of the parasite. Some authors

successfully used ss rRNA-based nested PCR-restriction fragment length polymorphism (RFLP) to distinguish *Cryptosporidium* parasites pathogenic to human from non-pathogenic strains in environmental samples (Xiao et al., 2000; Xiao et al., 2001a; Xiao et al., 2001b). Using micromanipulation technique Sturbaum et al. (2001) inserted desired number of oocysts ranged from 1-10 into PCR tube for DNA extraction and conducted nested PCR-RFLP. The result showed increased rates (38%-100%) in amplification with the increase of cell number (1-10). Although PCR is sensitive enough to detect low number of oocysts in small samples, these approaches are not proven to be mature enough in routine analysis and field conditions for environment sample due to failure to micromanipulate low numbers of oocysts from large sample volume (Xiao et al., 2006).

Table 1.3: Molecular approaches to detect *Cryptosporidium* oocysts in water (Adapted from Quintero-Betancourt et al., 2002)

Target sequence	Approach			Detection limit*	References
	Concentration technique	DNA extraction technique	Detection technique		
<i>C. parvum</i> hsp70	Calcium carbonate flocculation	Freeze-thaw	RT-PCR	1 oocyst	Stinear et al., 1996
<i>C. parvum</i> hsp70 (hsp mRNA)	ICR method	Tri Reagent kit	RT-PCR	10 oocysts	Rochelle et al., 1997b
CPR1 gene encoding oocysts cell wall protein	Membrane filter dissolution	Lysis, TE-sarcosyl-proteinase K-buffer, freeze-thaw: 10 cycles, DNA purification (QIAmp spin columns)	nested PCR	1-10 oocysts	Chung et al., 1999
Unknown genomic region	EPA method 1622	25% (w/v) Chelex 100, freeze-thaw and centrifuged at 13,000×g	nested PCR, dot blot hybridization	1 oocyst	Hallier-Soulier and Guillot, 1999
dsRNA	ICR method	Xtra Bind Capture System	Nested RT-PCR	1 oocyst/l	Kozwicz et al., 2000
* Due to various operational parameters used in each study the detection limit cannot be given as a concentration					

1.2.4 Viability and infectivity assays for *Cryptosporidium* species

As the occurrence of *Cryptosporidium* in the water is considered as a threat to public health, several attempts were taken to determine their ability to be viable or infectious. The following techniques were used to assess infectivity of *C. parvum*:

- i) Three studies used a mouse model to measure the infectivity for *C. parvum* genotype-2. But this method was restricted to only genotype-2 as the *C. parvum* human genotype-1 was unable to infect animals (Korich et al., 1990; Widmer et al., 2000). Moreover, Neumann et al. (2000) showed that the method was tiresome, difficult, costly and not feasible for water industries.
- ii) Cell culture showed the greatest application to determine the direct infectivity of *Cryptosporidium* from samples containing small numbers of oocysts. Human illeocecal adenocarcinoma cells (HCT-8) was frequently used in detection schemes used (Di Giovanni et al., 1999). During this method, oocysts initiated infection in the cells upon excystation and infected cells were quantified by microscopy using probed antibodies (Slifko et al., 1997; Slifko et al., 1999) or by PCR/ RT-PCR after DNA extraction from the cell (Rochelle et al., 1997a; Di Giovanni et al., 1999). This method has been applied in water laboratories and UV inactivation studies (Huffman et al., 2000). Cell culture has several advantages, for example, this was easier than animal studies and detects both genotypes 1 & 2. The result of cell culture significantly correlates with animal infectivity ($r=0.78$) result (Slifko, 2001). But still there are interpretation issues as well as chances of contamination making this process a difficult choice.

As infectivity assays are not always convenient practical solutions, some other tests have been developed which can give us an indication of the viability of *Cryptosporidium*:

- i) In vitro excystation was applied in laboratory disinfection and survival studies, but was found to not be suitable to measure oocyst viability in environmental samples as the test required $>10^5$ oocysts/ml (Quintero-Betancourt et al., 2002).
- ii) The inclusion or exclusion of vital dyes has been used as an indicator of the presence of internal features and intact membranes in *Cryptosporidium* oocysts (Robertson et al., 2014). Due to its fluorogenic property, it was used to assess the viability of oocysts in environment samples by IFA and microscopy which correlated with in-vitro excystation assays and the standard mouse infectivity assay (Campbell et al., 1992; Quintero-Betancourt et al., 2002; Smith et al., 1991). The dye permeability assay differentiated viable *Cryptosporidium* from non-viable strain based on the differential uptake of DAPI and propidium iodide (Gasser and O'Donoghue, 1999). Sporozoite nuclei of viable oocysts absorbed DAPI but not propidium iodide as it would not pass through an intact membrane due to its large size. Whereas nuclear material of non-viable oocyst stained with both fluorochromes. However, overestimation of viability and heterogenous staining were two major drawbacks which demanded careful interpretation of the test to avoid false result (Black et al., 1996; Campbell et al., 1992; Neumann et al., 2000; Quintero-Betancourt et al., 2002).
- iii) The viable status of *C. parvum* oocysts were also identified in drinking water sources by staining the nucleic acids with SYTO-9, SYTO-59 and hexidium (Belosevic et al., 1997a; Belosevic et al., 1997b; Neumann et al., 2000) Among them SYTO-59 was used in combination with fluorescein isothiocyanate conjugated antibodies to determine the viability of oocysts in environmental samples as they did not overlap in their fluorescence spectrum (Neumann et al., 2000). However, this technique is also dependent on microscopy which requires skills and a good laboratory setup.

- iv) The amplification of messenger RNA (mRNA) has also been reported for the detection of infectivity of oocysts by reverse transcriptase polymerase chain reaction (RT-PCR) (Wiedenmann et al., 1998; Stinear et al., 1996; Rochelle et al., 1997b; Kaucner and Stinear, 1998; Jenkins et al., 2000). However, it suffered from some disadvantages such as inefficient extraction of RNA, interferences by environmental constituents and low concentration of oocysts in volumes for RT-PCR (Wiedenmann et al., 1998).
- v) Fluorescence in situ hybridization technique was reported to identify the viability of *Cryptosporidium* when a fluorescent DNA probe was directed to the 18S rRNA of *C. parvum* (Vesey et al., 1995; Vesey et al., 1998). Viable organisms showed positive result as they contained intact 18S rRNA but in dead cells this rRNA was destroyed by cellular RNase enzymes.

1.2.5 Recent progress in capture techniques

1.2.5.1 Use of antibodies as capture molecules

Antibodies (immunoglobulins, Ig) have been used as the capture molecules because they are specific to antigens that exposed on the surface of the organism. Igs are highly soluble molecule divided into five classes based on their heavy chain constant region; they are IgM, IgD, IgE and IgA (Weiner et al., 2010) (Table 1.4).

Table 1.4: Different classes and isotypes of immunoglobulins

Class	Isotype	Functions	Source (predominant)
IgG	1,2,3,4	Enter tissue spaces, coat antigen ad speeding up uptake	Blood (80%)
IgA (Mono/dimeric)	1,2	Concentrates in body fluids to guard the entrance of the body	Extravascular secretion (Predominant)
IgM (Pentameric)	None	Leads to efficient killing of bacteria	Blood
IgD	None	Regulate B cell's activation	Membrane bound
IgE	None	Triger allergies	Blood (Trace)

IgG is the most abundant antibody which used as a prototype to describe the basic structure of Immunoglobulins. IgG molecules are joined together by a peptide bond which readily hydrolyzes through papain (proteolytic enzyme) and produces 3 fragments. Two of these are called Fab fragments (fragments of antigen binding) each will bind with antigen (Figure 1.6A). The third fragment is not responsive against antigen and becomes crystallized during cold storage so is called Fc (fragment for crystallization) (Figure 1.6A). The joint between Fab and Fc has segmental flexibility (hinge) that allows Fab to rotate from 60-180 degrees. IgG treated with pepsin yielded one large fragment which contain Fab and a portion of Fc and is called F(ab')₂. The remaining fragments are the degraded portion of Fc. The variability of Ig's is concentrated in complementary determining regions (CDR) which confer the antigen specificity, are located in antigen binding site (Fab). The constant region (Fc) plays an important role to mediate effector functions such and also regulate cell activation and proliferation. (Elgert, 1996; Sharma et al., 2016). Reduction with dithiotheritol breaks disulfide bonds in IgG and produces two heavy (H) kappa chain and two light (L) lambda chains (Figure 1.6B). The constant part of the two heavy chains are identical and are composed of amino acid (residues 109-214) ends with carboxy terminal. The opposite part of the k chain showed great variety in amino acid sequence (residue 1-108) and ends with amino terminal (Figure 1.6B). Each antibody possesses a tandem series of repeating homology (approximately 110 amino acid residues) called immunoglobulin domain that folded individually into a dense spherical form. Light and heavy chains consist of two and four domains respectively: the light chain has one variable (V_L) and one constant region (C_L), whereas the heavy chain has one variable (V_H) and three constant regions (C_{H1}, C_{H2} and C_{H3}).

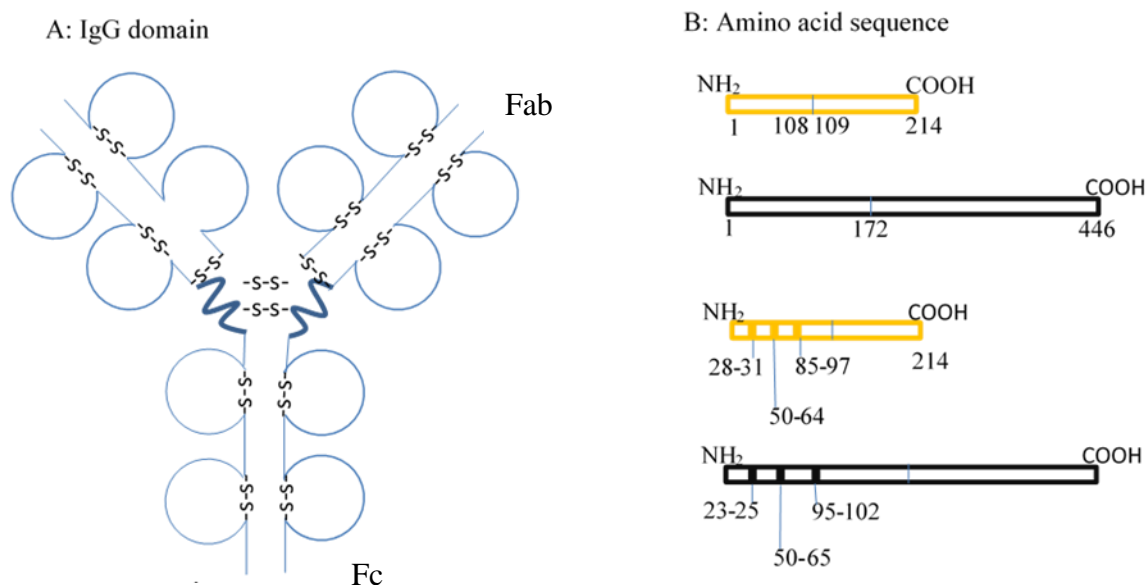


Figure 1.6: Schematic representation of the antibody structure (Adapted from Elgert, 1996)

The antibody is a vital player in eliminating foreign particles in the body because it can identify each different antigen individually. Scientists use this exquisite characteristic as diagnostic tools in many different setups (Borrebaeck, 2000). In general, serum can contain 10^{16} molecules of antibody per ml produced after an immune response (Elgert, 1996). The antiserum containing antibodies can be produced by repeated immunization of animals such as rabbit, sheep and goat which results in the production of non-homogeneous antibody with different specificity and affinity referred to as polyclonal antibody (Morgan and Levinsky, 1985). In order to retrieve homogeneous antibody with single specificity, scientists fused B cell from immunized mice into an immortal myeloma cell line of the same species. After selective cloning the hybridoma cell will produce unlimited antibody of single idio type which are called monoclonal antibodies.

1.2.5.2 Antibody immobilization and linkers

The immunosensor is a widely used device where antibodies are immobilized onto a solid surface. Antibodies are used as a detection element for immunosensor antibody-antigen interaction because they are highly specific and sensitive (Lu et al., 1996; Rao et

al., 1998; Wiseman, 1993). However, the immobilization step affects the detection limit, sensitivity and overall performance of immunosensors (Trilling et al., 2013a). In order to improve the performance of immunosensors, antibodies should be immobilized on the surface through low nonspecific absorption without altering their binding activity as well as the material accessibility of the material to be detected in the sample (Sharma et al., 2016). Antibody can be immobilized in different orientations either in a specific or random fashion. Specific orientation allows the F_c portion to attach on solid surface leaving the F_{ab} site free facilitating the increased antigen binding capacity on the immunosensor. On the other hand, random orientation allows antibody to anchor on surface using F_{ab} portion thus limiting the antigen binding capacity of the immunosensor (Sharma et al., 2016). Figure 1.7 summarizes the different approaches to antibody immobilization which are based on non-covalent and covalent binding chemistry that described below.

A. Covalent immobilization:

Technically, covalent immobilization offers better option for longevity and sensitivity of the antibody activated surface due to a strong bonding and specific orientation respectively (Trilling, 2013a). The following are some examples of the chemistry deployed to covalently immobilize antibodies on surfaces.

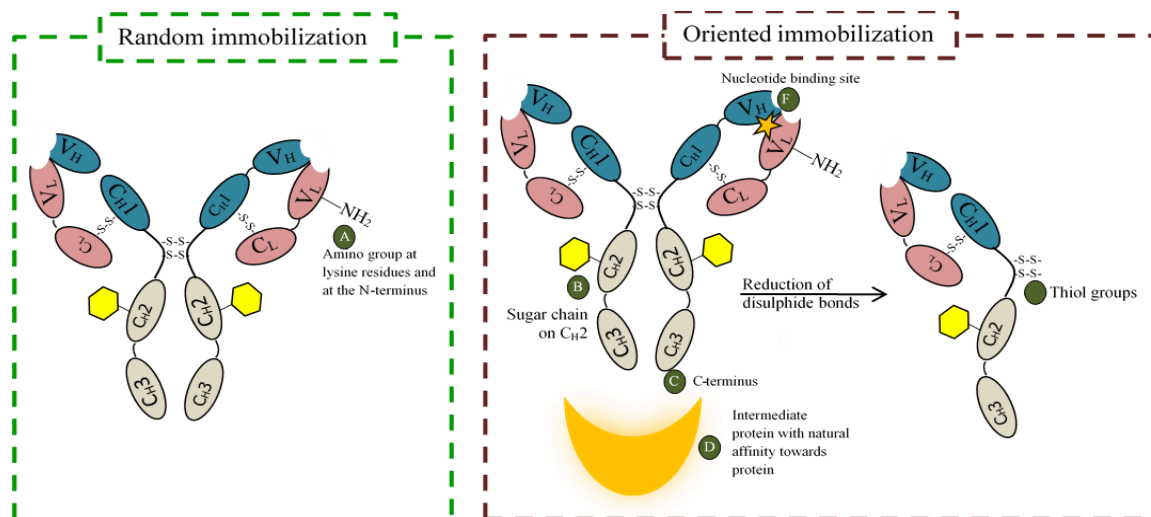
Covalent immobilization in random orientation can be achieved by using amine (NH_2) groups exposed on the lysine side chain of the antibody. Epoxide-functionalized polymer brushes and glutaraldehyde-functionalized surfaces also allow covalent immobilization of antibody via the amine group (Huy et al., 2011; Liu et al., 2011; Yuan et al., 2011) (Figure 1.7). The sugar present on the F_c portion of the antibody also contributes in covalent immobilization. Upon oxidation of hydroxyl groups, carbohydrates yield aldehydes which react with aminated surfaces (Figure 1.7; Yuan et

al., 2011), surface with hydrazine-functionalized dendrimers (Han et al., 2010) and surface with boronic acid (Ho et al., 2010) resulting in oriented covalent immobilization of antibody.

Antibodies can also be immobilized covalently using their conserved nucleotide binding site located in the variable domain. Nucleotide binding site contain highly aromatic amino acids that reacts with indole-3-butyrac acid. This interaction showed covalent immobilization in oriented manner without interrupting the antigen binding site (Alves et al., 2012). Another example of covalent immobilization is utilization of thiol groups on metal surface resulting in more stable oriented immobilization. Thiol groups are usually generated either by mild reduction of disulfide bonds of intact antibody or by breaking bond through UV light absorbed by adjacent aromatic amino acids (Figure 1.7) (Ventura et al. 2011). Balevicius et al. (2011) used amine groups for random immobilization of intact antibodies and showed that oriented antibody fragments possess more than two times analyte binding capacity than intact antibodies.

B. Non-covalent immobilization:

Typically, non-covalent immobilization is obtained by adsorbing the antibody physically or chemically on surfaces via electrostatic interactions, ionic bonds, hydrophobic interactions and van der Waals forces. Um et al. (2011) showed that electrochemical immobilization (attributed to tail-on orientation) improved activity over the physically adsorbed immobilization which usually results in flat-on orientation. The concentration of salt and pH effect the amount of antibody adsorption and analyte binding in physio-adsorbed immobilization but do not influence the orientation of immobilized antibody (Zhao et al., 2012). Electrochemical immobilization can be achieved using poly-(2-cyano-ethylpyrrole)-coated gold electrodes. The cyano group on the surface interact electrostatically with OH group of antibody present in Fc portion (Um et al. 2011).



Functional group	Reacted with
A Amine group	Carboxy-methylated dextran layers (Trilling et al., 2013a; Vashist et al., 2011) Glutaraldehyde exposed surface (Tajima et al., 2011; Huy et al., 2011) Epoxide-functionalized polymer brushes (Liu et al., 2011) NHS-activated biotin* (Park et al., 2011)
B Sugar chain	Boronic acid presenting surfaces (Ho et al., 2010) Hydrazine biotin* (Kang et al., 2007) Oxidated sugar chain (reactive aldehyde) Aminated surfaces (Yuan et al., 2011) Hydrazine-functionalized dendrimers on surfaces (Han et al., 2010)
C C-terminus	Enzyme yielding biotinylation* (Franco et al., 2006)
D Intermediate protien	Protein A & G (Non covalent) (Le Brun et al., 2011; Liu et al., 2012; Lee et al., 2011; Ko et al., 2010) Protein A & G then chemical-crosslinking (covalent) (Song et al., 2012; Bereli et al., 2011)
E Thiol group	Gold (Yoshimoto et al., 2010; Balevicius et al., 2011) Maleimide-functionalized biotin* (Park et al., 2011) Maleimide-functionalized surfaces (Baio et al., 2011)
F Nucleotide binding site	Indole 3-butyric acid followed by photo-cross-linking with UV light. (Alves et al., 2012) *Followed by the immunization on Streptavidin functionalized surfaces
G Disulphide bond	Reduced with 2-mercaptoethanol (Trilling et al., 2013a; Vashist et al., 2011) UV-light absorption by nearby aromatic amino acids

Figure 1.7: Role of functional groups in antibody immobilization (random and oriented) (Adapted from Trilling, 2013a)

However, the non-covalent interactions are weak and subject to alteration due to change in conditions such as pH, temperature or salt concentration which cause reduced analytical performance.

The performance of non-covalent antibody binding can be improved using streptavidin–biotin interaction resulting in either random or oriented immobilization. For random immobilization antibodies are biotinylated at the amine groups whereas for site specific orientated immobilization biotinylation is done at the hinge region of the antibodies. Although in both strategies antibodies immobilize in tail-on orientation, site-specific orientation immobilizes faster the random one (Cho et al., 2011; Park et al., 2011). Several approaches have been applied to achieve successful biotin mediated immobilization such as biotinylation of the antibody at the C-terminus using the enzyme carboxypeptidase Y (Franco et al., 2006), site-specific biotinylation of the antibody using a sugar moiety (Kang et al., 2007), in vivo biotinylation of VHH using the Avi-tag (Trilling et al., 2013b).

Another method used for immobilization was done by fusing of a polyhistidine (His6) affinity-tag on the recombinant antibody (C- or N-terminus). His6 tag have great affinity ($K = 10^7 \text{ M}^{-1}$) to surfaces coated with divalent metals such as Ni^{2+} , Co^{2+} and Cu^{2+} which makes bonds by chelating the His residue. Using this principle, recombinant proteins containing His6 tag can be purified via metal ion chromatography. His6 tag should be available to divalent metal ions to ensure optimum binding and maximum recovery. Many support materials such as iminodiacetic acid, nickel-nitrilotriacetic acid (Ni-NTA), cobalt-carboxymethylaspartate (Co-CMA) are used to control the coordination of His6 tag. Several approaches were attempted which revealed with unsatisfactory affinity and unwanted protein detachment while using the His6 tag (Baio et al., 2011).

Alternative approach involves the use of an intermediate protein such as protein A or protein G to immobilize untreated antibodies on the surface in an orientated fashion. These proteins use antibody Fc portion specific binding domains, 5 in protein A and 2 in protein G. Several studies showed that biosensor performance improves when antibodies are immobilized in oriented manner using protein A or G compared to random immobilization (Huy et al., 2011; Ryu et al., 2011; Shen et al., 2011; Vashist et al., 2011). In addition to orienting antibodies, orientation of protein A or G also resulted in increased affinity for analytes. Researchers frequently use Cysteine residues or thiol residues to immobilize protein A or G to surfaces in oriented fashion (Liu et al., 2012; Lee et al., 2011). Biosensor activity enhanced 10 fold when Cys-protein G trimers were used compared to Cys-protein G monomers (Lee et al., 2011). Oriented antibody immobilization was also achieved by generating polyethylene glycol monolayer on gold using protein A which was fused with *Escherichia coli* protein OmpA exposing Cysteine (Le Brun et al., 2011). Another example is GBP-ProtA, this is a fusion of protein A with gold binding protein which produced a highly compact self-assembled monolayer on gold than protein A only and increased antibody binding capacity of the surface (Ko et al., 2010). Protein G has stronger immobilization ability onto metal surfaces when thiol residue is used. These immobilized thiolated protein G ensured tail-on orientation of antibodies on the copper surface (Liu et al., 2012). These strictly orientated antibody immobilization techniques increased the affinity of biosensors than the randomly orientated ones.

1.2.5.3 Self-assembled monolayer formation on metal surface

Formation of self-assembled monolayers of thiolates on substrate is an important step to achieve oriented immobilization of antibodies. A substrate is a physical object that supports the metal surface on which self-assembled monolayer forms. Glass, plastics,

silicon wafers, mica are common substrates on which thin films of metal are generated using different deposition techniques like sputtering, electrodeposition, vacuum deposition (Malinsky et al., 2012; Schlesinger and Paunovic, 2010; Venables, 2000). Besides gold which is the most popular choice for metal layer formation, copper, platinum, silver and nickel are also used (Love et al., 2005). An intermediate adhesion layer of chromium or titanium is used in between because these noble metals exhibit weak adhesion to the inert substrates such as glass or silicon wafers and this adhesion layer could improve the binding between metal and substrate due to its oxidative nature (Love et al., 2005). Gold is considered as the standard to coat the surface as it has several advantages over other materials. Gold provides an inert surface for biological experiments, it is resistant to oxidation and it is easy to generate thiolated self-assembled monolayer on the gold surface due to its high affinity for sulphur-containing molecules (Xue et al., 2014). Another reason to choose gold is that it is electrically conductive and could be built into a sensing surface changing the capture surface from capture only to capture & sense (Li et al., 2010; Vidic et al., 2007; Wu et al., 2016).

Based on these principles an antibody-based capture surface was designed for this research. Though it may possible to develop a system that can capture and sense the presence of *Cryptosporidium* in the water, this system tells us nothing about the viability status of the organism. This leads to the concern that water treatment plants have about the efficiency of the UV treatment technology they have been using. So it would be helpful if we have an additional test to show that UV treatment is working.

1.2.6 *Cryptosporidium* inactivation

This section discusses the use of UV radiation as a disinfection measure, UV damage mechanism, the response of *Cryptosporidium* to UV treatment, and the use of monoclonal antibody in UV damage detection.

Cryptosporidium is resistant to typical chemical disinfection methods such as chlorination, ozonation. Chlorine derivatives are used as the primary disinfectants in the water industries but the concentrations at which these chlorine-based disinfectants are usually applied have limited effect on *Cryptosporidium* inactivation. For example, *E. coli* inactivation (>99%) is achievable at a CT value (contact time & concentration) of 0.04 mg min⁻¹L⁻¹. In case of *Cryptosporidium*, this value is quite high (7200 mg min⁻¹L⁻¹) demanding much higher chlorine concentrations during treatment (Korich et al., 1990; Chauret et al., 2001). Similarly, ozone treatment can play role in *Cryptosporidium* inactivation at a CT value of 5.4 mg min⁻¹L⁻¹ at 14°C but the efficiency declines with the decreasing temperature of water (Oppenheimer et al., 2000). All these findings indicate the necessity of developing alternative treatment approaches with higher efficiency. UV irradiation is considered as a popular treatment alternative due to its germicidal potency without effecting water quality.

1.2.6.1 UV radiation as a disinfection measure

UV irradiation was first applied in 1910 to disinfect water when mercury vapor lamp and quartz tubes were established as a source of UV irradiation (Bolton et al., 2008). Wolfe (1990) and Hoyer (2004) described the limitations of the general application of UV irradiation which includes their high expense, poor apparatus dependability, maintenance difficulties and the existence of cheaper and reliable chlorination technique. However, UV irradiation has recently received significant attention as it produces almost no byproducts and does not affect water stability unlike chlorination and ozonation. The use of UV as a decontamination procedure for water received further attention when Clancy et al. (1998) reported that *Cryptosporidium* oocysts lost their infectivity in mice after the UV treatment. The susceptibility of *C. parvum* oocysts to UV disinfection was again demonstrated by using infectivity assay to establish its application in drinking water

treatment facility (DVGW, 1997; NIPH, 2002). Europe had initiated wide utilization of UV irradiation in 1980 to control incidental contamination of drinking water (Kruithof et al., 1992). North America and Europe considered UV irradiation as a primary disinfection technology when high efficiency of UV as a disinfectant was proved against protozoa (Clancy et al., 1998).

Water treatment facilities mainly use two mercury lamps for UV irradiation, they are low-pressure (LP) and medium-pressure (MP) lamps. LP emits a sharp line at 254nm when low pressure (10^{-3} to 10^{-2} Torr) is applied inside the lamps (Bolton, 2001). In contrast to LP lamps, MP lamps require amplified pressure (10^2 to 10^4 Torr) that creates an increased radiation intensity ranging from 185nm to 1367nm (Bolton, 2001; Linden & Mofidi, 1999). Both LP and MP lamps are considered to be germicidal, but MP lights are widely used for industrial water treatment due to the amplified radiation intensity. UV irradiation causes cell damage and loss of viability by destroying DNA function (Friedberg et al., 1995). The most detrimental/ germicidal UV wavelengths ranged between 200-300nm, with full absorption at 260nm by DNA bases (Friedberg et al., 1995). The inactivation rate constant k (cm^2/mJ) and the maximum inactivation are key parameters used to describe inactivation of a particular organism. Microbial inactivation credit ($\text{MIC} \frac{1}{4}$ ‘log-credits’) for a particular UV dose is calculated based on these parameters. UV sensitivity of different organisms varies significantly for example, *Cryptosporidium*, *Giardia*, and bacteria are more susceptible with a dose requirement of 0.9-13.1 mJ/cm^2 whereas viruses particularly Adenovirus (8-306 mJ/cm^2) and bacterial spores (5-78 mJ/cm^2) show more resistance to UV radiation (Malley et al., 2004; Rochelle et al., 2004; Sommer et al., 2000; Zimmer and Slawson, 2002).

1.2.6.2 Damage mechanism

UV light can travel through the shell of *Cryptosporidium* oocysts and reach the DNA. UV radiation interacts specifically with the pyrimidine (thymine and cytosine) molecules in the DNA backbone causing them to link together across the structure forming cyclobutyl pyrimidine dimers (CPD) as presented in Figure 1.8 (Balajee et al., 1999; Torizawa et al., 2000). Other evidence proposes that pyrimidine (6-4) pyrimidone and Dewar photoproducts (6-4) are other UV induced byproducts in DNA and may also possibly be responsible for cell damage and mutation (Brash, 1988; Cleaver et al., 1987; Cleaver et al., 1988; Mitchell, 1988). Accumulations of these UV photoproducts inhibit the replication and transcription process of DNA, thus rendering the organism nonviable and non-infective (Gentil et al., 1996; Hijnen et al., 2006; Maher et al., 1982; Rochelle et al., 2004; Setlow, 1978; Suzuki et al., 1981). Among all of the UV photoproducts, the most noticeable one is CPD which is identified with 2 isomers *cis-syn* [*c,s*] and *trans-syn* [*t,s*] (Figure 1.8) resulting from the photo [2+2] cycloaddition of 5,6-double bond of two adjacent pyrimidine nucleotides. The *trans-syn* and *cis-syn* pyrimidine dimers have *syn* glycosyl and anti glycosyl conformations respectively. Generally, the *cis-syn* pyrimidine dimers are the main photoproducts of UV-irradiation.

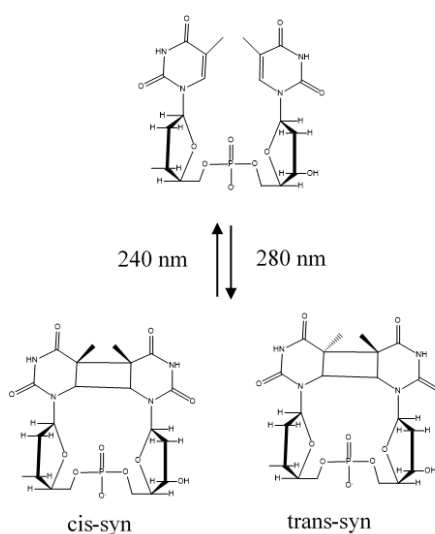


Figure 1.8: Conversion of pyrimidine bases to *cis-syn* and *trans-syn* isomers of CPD

1.2.6.3 Repair mechanism

Many organisms can repair UV induced DNA damage by photo reactivation and nucleotide excision repair mechanisms which is reported as a major problem for disinfection technology (Thoma, 1999; Rochelle et al., 2005; Friedberg et al., 1995). Photo-reactivation directly repairs DNA impairments within minutes to hours, it is induced by visible light (300-500 nm) using DNA photolyase which was reported in several organisms (Sommer et al., 2000; Zimmer & Slawson, 2002). Photo repair could jeopardize the disinfection process if light exposure occurs after UV treatment at the processing unit or following distribution unless enough damage is done to prevent the repair genes from being expressed. Nucleotide excision repair obviates the need for visible light induction and so is often known as the dark repair mechanism. This involves a more complex repair process with the synchronization of many enzymes to recover DNA damages (Friedberg et al., 1995). *C. parvum* should have the capacity to recover infectivity after exposure to UV as they possess genes encoding UV repair proteins (Rochelle et al., 2005). However, there is growing evidence that the organism is unable to reactivate after UV irradiation (Morita et al. 2002; Oguma et al. 2001; Rochelle et al., 2005). Zimmer et al. (2003) investigated the level of inactivation and the potential for *C. parvum* to repair the damage even on low doses (1 and 3 mJ/cm²) of UV irradiation. No indication of repair was detected when incubated in light or dark conditions following UV irradiation. This evidence shows *Cryptosporidium* does not express DNA repair genes.

1.2.6.4 DNA damage detection

There is no commercially or industrially accepted procedure for the detection of DNA damage in *Cryptosporidium* to date. The literature (Peccia and Hernandez, 2002; Al Adhami et al., 2007) presented research converting procedures from the field of clinical

skin cancer testing to the application of *Cryptosporidium*. This relies on the use of antibodies specific for UV photoproducts.

DNA damage in UV irradiated *Cryptosporidium* can be detected using monoclonal antibodies specific for the photoproducts. Establishment of two different types of monoclonal antibodies TDM and 64M against CPDs and UV-induced (6-4) photoproduct respectively have been reported from the same mouse (Mori et al., 1991). TDM-2 binds to DNA containing a *cis-syn*-cyclobutane thymine dimer (T[c,s]T). Torizawa et al. (2000) presented the interaction between the TDM-2 F_{ab} and CPD-containing DNA analogs. They reported that the nucleotides on both sides (5' & 3') of d(T[c,s]T) augment the attraction for TDM-2 and are also involved in binding to TDM-2 which preferentially binds to single-stranded(ss) DNA (Komatsu et al., 1997). Komatsu (1997) studied the structural necessities of antigen recognition by the antibody TDM-2 which bound with *cis-syn*, in chemically synthesized antigen analogs. The study revealed that TDM-2 strongly binds with four nucleotide analogs when the *cis-syn* pyrimidine dimer was positioned in the center. Additionally, it was shown that the phosphate group at either side of CPDs was required for the affinity to TDM-2. Various tests have been developed to determine the photoproduct concentration sufficient to render *Cryptosporidium* inactive.

1.2.6.4.1 Immunofluorescence microscopy (IFM)

A review article by Kumari et al. (2008) recommended an immunofluorescence assay as a useful tool for estimating UV photoproducts. Preliminary research suggested a fluorescence based localization system for detecting thymine dimer (common forms of CPDs) in intact irradiated bacterial cells (Peccia and Hernandez, 2002). Later in 2007, Al Adhami et al. detected CPD in intact *Cryptosporidium* (both oocyst and sporozoite) through immunofluorescence microscopy using commercially available anti-thymine

dimer monoclonal antibody. Author exposed oocysts to 4,10, 20 and 40 mJ/cm² doses of UV irradiation and incubated with primary antibody followed by florescent labeled secondary antibody to examine the production of CPDs in intact *Cryptosporidium*. This study detected CPDs in the oocyst that irradiated above 10 mJ/cm² and the result was correlated with mouse infectivity assay. However, this method is laborious, time intensive, expensive, requires special skills and facilities, and is subjective to interpretation which limits its use for water suppliers and analysis service laboratories.

1.2.6.4.2 Enzyme linked immunosorbent assay (ELISA)

The CPD-antibody reaction can also be detected by using enzyme linked immunosorbent assay (ELISA) (Matsunaga et al., 1990; Mori et al., 1991). ELISA, commonly used in medical researches to detect and quantify a particular protein or DNA, was initially described by Engvall and Perlmann (1971) (Nishiwaki et al., 2004). Later the method was established due to the revolution in several related fields, particularly production of monoclonal antibody by Kohler and Milstein (1975) used as a probe to detect individual molecules. In the beginning, detection was performed by radioimmunoassay but due to the health risk it was further replaced by antibody chemically linked with an enzyme which can react in solution containing appropriate substrate and produces a measurable signal (Avrameas, 1969; Nakane and Pierce, 1967).

There are two different mechanisms for ELISA: direct and indirect. In both cases the antigen attaches to the plate by passive adsorption. Then this antigen is recognised using labeled primary antibody during direct ELISA, whereas in indirect ELISA the antigen-primary antibody is detected by a secondary antibody with conjugate enzyme. Another approach is sandwich ELISA where surface is coated with first antibody that capture the antigen and a second antibody detects the immobilized antigen (Shah and Maghsoudlou, 2016). This principle is mostly used for low levels of antigen or if antigen

does not adhere to the well. The ELISA application typically uses either alkaline phosphatase (AP) or horseradish peroxidase (HRP) as the enzyme. AP is a large enzyme (140 KDa) restricted to one/two molecules per antibody, therefore it generates less signal and is less stable. HRP is a small molecule (40KDa) allows more molecules to bind with antibody thus generates more signal than AP and is also capable of reacting with a wide range of substrate such as TMB (3,3',5,5'-tetramethylbenzidine), OPD (o-phenylenediamine dihydrochloride), ABTS (2,2'-Azinobis [3-ethylbenzothiazoline-6-sulfonic acid]-diammonium salt). The substrate reacts with the enzyme and develops a colored product which is relative to the presence of enzyme in the well. The higher numbers of antigen generate a high intensity of signal.

The ELISA protocol may vary by situation but consists of the same basic elements including immobilization of antigens on an appropriate surface, covering of all of the unsaturated surface to block irrelevant proteins, incubation with antigen specific antibody and measurement of the signal produced by the tagged antibody. Optimization of these elements is essential otherwise signal can not be captured due to suboptimal condition of any of these factors.

ELISA plates are usually made of polystyrene but are also available in polypropylene, polycarbonate and nylon. To facilitate coating with antigen, now plates are also positively charged by gamma-irradiation. The bottom should be clear and flat as the absorbance is measured by shining a laser through the base. Passive adsorption mediated by hydrophobic interaction is commonly used for most attachment but electrostatic forces also contribute to some extent. The blocking buffer designed to inhibit capture of non-specific proteins should be optimized to maximize the signal to noise ratio. The signal-to-noise ratio is calculated by dividing the absorbance of test sample by the absorbance of negative control. A low signal-to-noise ratio is one of the common

occurrences due to weak signal and high background. A weak signal can be due to several factor such as a low concentration antigen or antibody, degradation or contamination of reagents, inefficient antibody antigen match pair, and insensitivities of substrates. High background signal can be due to inefficient washing, improper blocking, cross reactivity of reagents and antibody with blocking agent or high amount of enzymes. Tris or phosphate-buffered salines (TBS or PBS) containing 0.05% (v/v) Tween®-20 are commonly used buffers for the washing step in ELISA application. Optimization of washing steps helps to washout the irrelevant proteins.

1.3 Research plan and research objectives

Previous work has been done in our laboratory on the development of pathogen detection device. The proposed detection device consists of two units: a capture unit and a detection unit. Development of this device requires the expertise from the field of both biology and engineering. The capture technique is based on antibody specificity. The detection technique is based on capacitive immunosensor. The capture unit is designed to effectively sample water and separate specific waterborne pathogens, if any, in the water (i.e., *Cryptosporidium*). In the proposed design, the water will enter the capture unit through the inlet and will pass through a series of parallel plates with slotted holes directing the flow over a capture surface activated with antibodies. For detection, a highly sensitive and label-free *Cryptosporidium* capacitive immunosensor based detection unit will be developed using gold interdigitated electrodes capacitor arrays by School of Engineering of UBCO. The detection of *Cryptosporidium* will be based on relative change in capacitive/dielectric properties which will provide a detectable signal. An advantage of this device is that it can be modified for use at any specified location by adding antibodies directed at the species of interest in that location.

In early work Rony Das (2010) developed a system to recover *Cryptosporidium* oocysts from environmental samples using fragmented antibodies with limited capture efficiency (11.45%). Dr. Jomeh designed the microfluidic flow cell using numerical stimulation/modeling to separate *Cryptosporidium* oocysts based on their physical properties with the target of replacing the filtration and IMS steps used in EPA 1623 (Jomeh and Hoorfar, 2012; Jomeh, 2013). The binding efficiency and specificity of the antibody based capture surfaces were not explored during the previous research. Therefore, this research was focused on the development of a sensitive pathogen specific capture surface for water quality monitoring technology that is expected to test for the presence of *Cryptosporidium* pathogens in treated water. Though the device is expected to determine if the *Cryptosporidium* is present but it would not be able to determine whether or not the oocysts are damaged by UV disinfection which leads to another task that is development of a test assay for UV damage detection in *Cryptosporidium* oocysts. Therefore, the following objectives were developed for this research:

1. Development of an antibody based capture surface to identify *Cryptosporidium* oocysts in treated water with increased capture ability and specificity.

The hypothesis is that it is possible to develop a capture surface with improved capture ability and specificity by changing it from fragmented antibodies used by Das (2010) to whole antibodies linked to surface through binding proteins.

2. Development of an assay method for water treatment process operators to document the efficacy of the widely used UV disinfection method.

The hypothesis is that using anti-CPD antibodies described in previous research it is possible to establish an ELISA based DNA damage detection assay.

Chapter 2 *Cryptosporidium* detection in water using antibody based capture unit

One objective of this thesis was to develop an antibody based capture surface specific for *Cryptosporidium* (Figure 2.1). This includes the selection of antibodies as capture molecules, development of the capture device, determination of capture specificity and cross reactivity with other organisms, as well as the assessment of pH dependent release mechanism to determine the reusability of the capture surface.

The rationale behind achieving this objective was that the current EPA method possesses several limitations including use of the filtration/elution process which have been shown to have a wide range of mean recoveries (21-100%) and large standard deviations, thus leaves much room for improvement. In addition, use of IMS and microscopy requires skilled personnel as well as advanced expensive equipment. To address these issues an antibody based capture surface was developed as a part of the proposed detection device during this research to capture pathogen from the water.

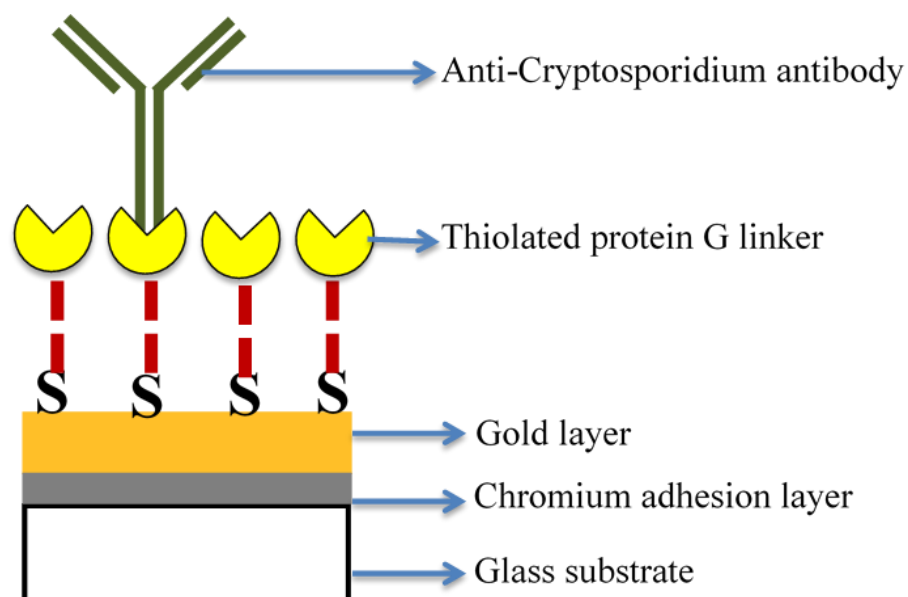


Figure 2.1: Anti-*Cryptosporidium* antibody activated capture surface model (not to scale).

For the development of the capture unit (Figure 2.1), antibodies were used as the capture molecules because they are specific to the antigens that are exposed on the surface of the organism. Orientated immobilization of antibodies was ensured by using recombinant protein G-thiol conjugate as a linker. Protein G binds with the Fc portion of the antibody and the thiol portion of the linker binds with gold coated glass surface to generate self-assembled monolayers.

2.1 Materials

2.1.1 *Cryptosporidium* species

C. parvum (IOWA isolate) and *C. muris* (RN66 isolate, Japan) were acquired from Waterborne™, Inc. (New Orleans, USA). Oocysts of *C. parvum* were developed in calves and *C. muris* oocysts were raised in rodents by experimentally infecting them. Both types of oocysts were initially extracted from feces using diethyl ether and further purified via sucrose and Percoll™ density gradient centrifugation. *C. hominis* (human source, UK) oocysts were received from *Cryptosporidium* Reference Unit, Public Health Wales Microbiology, Singleton Hospital, UK. Oocyst stocks were stored in the lab at 4°C.

A Petroff-Hausser counting chamber (Hausser Scientific) was used to determine the concentration of *Cryptosporidium* species in the stock suspension. For each strain, 30µl of stock suspension (1×10^6 oocysts/ml for *C. parvum* & *C. muris*; 1.8×10^6 oocysts/500µl for *C. hominis*) was mixed well using a vortex mixer and was loaded then into a cell counting chamber. The counting chamber was placed on the microscope stage (Zeiss Axioimager M1 microscope, Germany) and fields were examined after a 2 minute settling period. The number of oocysts per ml of stock suspension was counted at 400X magnification via phase contrast microscopy. Working dilutions of the following concentrations were prepared by diluting the stock suspension with PBS buffer (pH 7.4):

C. parvum (5.5×10^3 oocysts/ml), *C. muris* (7.5×10^3 oocysts/ml), *C. hominis* (4×10^3 oocysts/ml). Figure 2.2 presents Cypt-a-Glo stained oocysts (see Section 2.2.2) of three different *Cryptosporidium* species, *C. parvum* and *C. hominis* were found to be quite similar in shape (round), whereas *C. muris* oocysts appeared to have a more oval shape.

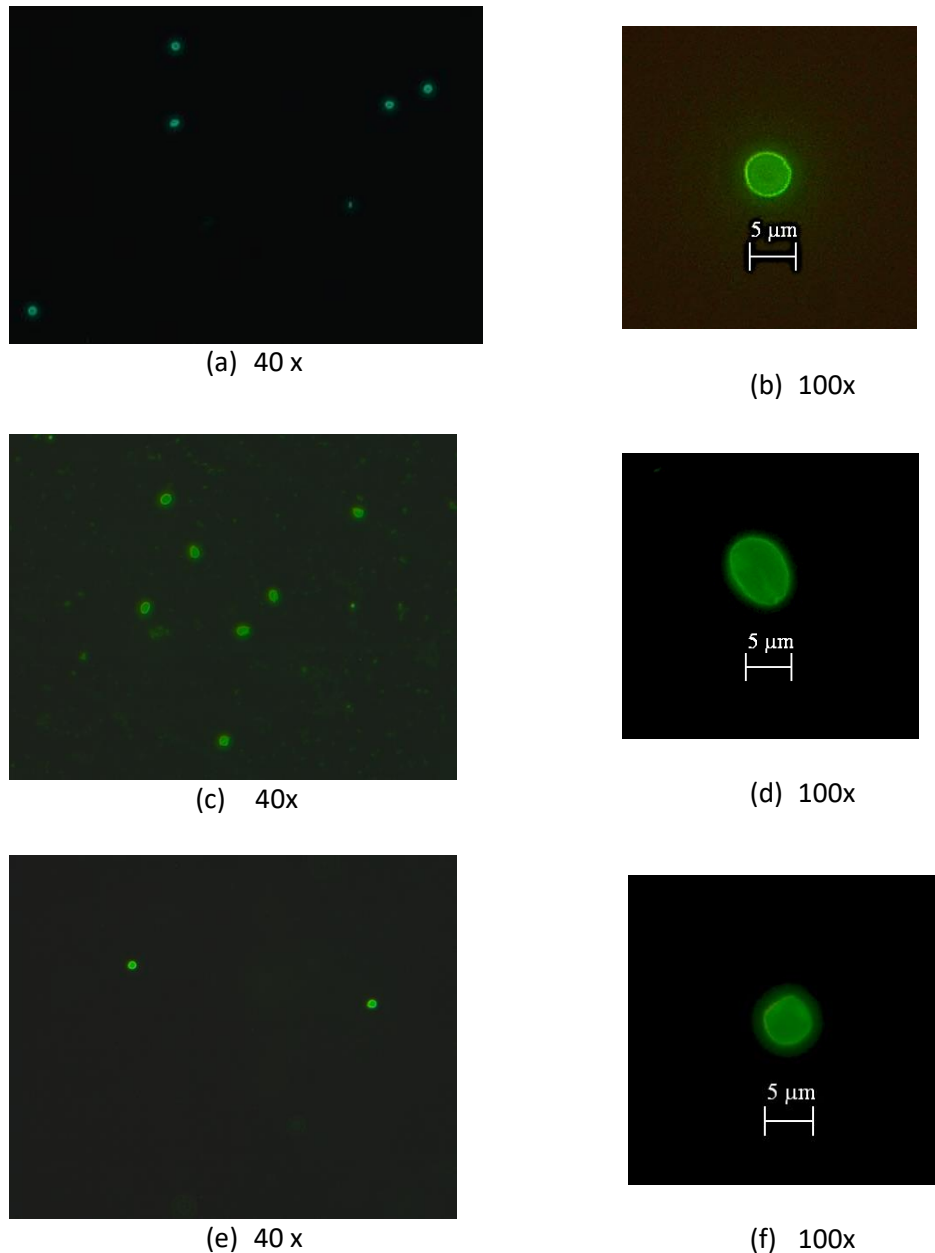


Figure 2.2: Fluorescence microscopy images of *Cryptosporidium* oocysts. *Cryptosporidium* oocysts were stained using Crypt-a-Glo, a fluorescein-labeled mouse monoclonal antibody (mAb) agent which is responsible for green fluorescence. Figure 2.2a & 2.2b represents the microscopic fields of *C. parvum* observed under 40x and 100x objective lenses respectively. Similarly, Figure 2.2c & 2.2d and figure 2.2e & 2.2f represents the microscopic fields of *C. muris* and *C. hominis* respectively.

2.1.2 Antibody selection

This task was initiated with a search of the commercially available antibodies. All the antibodies found to belong to two different isotypes: IgG1 & IgG3. Of these products, *C. parvum* specific mouse monoclonal antibody clone 7613 (isotype IgG1) and *Cryptosporidium* specific mouse monoclonal antibody clone BEL0126 (isotype IgG3) were selected as they represent the most common clones that are commercially produced. IgG1(7631) and IgG3 (BEL0126) were obtained from Bio-Rad company. Another *Cryptosporidium* specific antibody IgM (clone 2C9) manufactured by Waterborne Inc. was also used as this antibody is the basis of the fluorescein based stain Cypt-a-glo antibody reagent (see Section 2.2.2) widely used to detect *Cryptosporidium* (Waterborne Inc. personal communication). IgM was purified by precipitation from mouse ascites fluid using 2% boric acid, followed by dialysis versus phosphate-buffered saline (PBS)/0.02% sodium azide, and extraction from fatty material using 1,1,2- trichlorotrifluoroethene by Waterborne Inc. Both IgG1 and IgG3 were purified by affinity chromatography on protein A and preserved in phosphate buffer saline using 0.1% sodium azide (NaN₃) as preservative by their respective suppliers.

Though some of the commercial antibodies were raised specifically to *C. parvum*, in most cases the companies have not performed any cross-reactivity tests against other species of *Cryptosporidium*. Only two of these commercially available antibodies have been tested for specificity against different hosts. The IgM clone was tested against and reacts positively with *C. muris*, *C. meleagridis* (turkeys), *C. hominis*, *C. andersoni* (cattle) and *C. baileyi* (chickens) (Waterborne Inc. personal communication). This antibody is genus specific and does not react with *Giardia*. The IgG1 (7631) has been tested against various bacterial isolates (*E. coli*, *Shigella* sp., *Klebsiella pneumonia*, *Salmonella* sp., *Enterococcus faecium*, *Yersinia entetorcolitica*, *Toxoplasma gondii*) as well as against

human cells and found to be non-reactive but not against other species of *Cryptosporidium* (Bio-Rad Laboratories, Inc. personal communication).

Among the three available isotypes, IgG1 & IgG3 antibodies were selected for capture surface development because IgG antibodies have free Fc portions which will bind specifically with protein G leaving antigen specific Fab parts free for antigen-antibody binding (Hjelm et al., 1975; Guss et al., 1986; Janeway, 2001). As IgM lacks a free Fc part, this antibody would not be able to interact with the linker and thereby was not used for the development of antibody based capture surface (Janeway et al., 2001).

2.2 Capture surface development

2.2.1 Preparation of capture surface

The glass slides were immersed in piranha solution (a 3:1 mixture of concentrated sulfuric acid, H₂SO₄ with 30% hydrogen peroxide, H₂O₂) overnight, and then rinsed with a stream of isopropanol for 20 seconds and dried with a stream of air. They were treated with oxygen plasma for 10 min to remove any remaining residues and organic contaminations (Baxter et al., 2009). Afterwards, 50 nm of Chromium (Cr) and 100 nm of Gold (Au) were sputtered using Magnetron Sputtering System (Angstrom Engineering Inc., Canada) on the clean surface of the glass slides.

Both protein A & protein G have the ability to bind with IgG. Their binding specificities and affinities differ among species and IgG subclasses. Protein G has a higher affinity for a broader range of human and mouse IgG subclasses than protein A which has more affinity for rabbit, cat, pig & dog IgG (Akerstrom and Bjorck, 1986; Akerstrom et al., 1985; Bjorck and Kronvall, 1984; Eliasson et al., 1988; Kronvall and Williams, 1969). It has also been shown that in many cases monoclonal antibodies do not bind to protein A, especially mouse IgG (Kronvall et al., 1970). Thus protein G was a better selection to confirm orientated immobilization of mouse anti-*Cryptosporidium*

monoclonal antibodies targeted for the capture surface. The recombinant version of this protein has an advantage over the native one as it lacks albumin and cell surface binding domains, thereby reducing non-specific bindings and increasing IgG specific bindings (Akerstrom, et al., 1987; Fahnestock et al., 1986; Fahnestock, 1987; Guss et al., 1986; Olsson et al., 1987; Sjobring et al., 1988).

Recombinant thiolated protein G (23 kDa) was purchased from Protein Mods Inc. (USA). According to the manufacturers, protein-G was purified from *E. coli* and thiolation was carried out by the amino-reactive reagent iminothiolane. The thiolated protein G (concentration 2mg/ml) was diluted in 1xPBS (phosphate buffer, pH 7.0) to make a working dilution of 0.1 mg/ml. Subsamples of 50 μ l were placed in several 5 mm diameter circles (outlined in wax pencil) on the gold coated slides and incubated at 4°C overnight to generate self-assembled monolayer of thiolated protein G (Bae et al., 2005; Lee et al., 2013). The surface was then cleaned with 1X PBS buffer and type 1 water to remove excess thiolated protein G and allowed to air dry.

Bovine serum albumin (BSA) (1%) was selected as the blocking agent to restrict the non-specific binding of antibodies with the binding surface on the gold surface (Xiao et al., 2012). BSA does not block the antibody binding sites on thiolated Protein G, as the recombinant version of protein G does not have albumin binding domains (Akerstrom, et al., 1987). 1% BSA was prepared by dissolving lyophilized bovine serum albumin (Sigma-Aldrich, USA) powder in 1xPBS. 50 μ l of 1% BSA then applied to the thiolated gold surface, kept at 4°C for 1 hour and rinsed with PBS buffer and type 1 water before final air drying.

The concentration of the IgG1 in the stock solution was 0.1mg/ml and IgG3 (1.0 mg/ml) was diluted to the working concentration of 0.1mg/ml. Both IgG1 and IgG3 activated capture surfaces were developed by adding 50 μ l of solutions (0.1mg/ml) of

respective antibodies on the thiolated protein-G activated gold surface. Loaded slides were then incubated at 4°C for 48 hours to facilitate the orientated immobilization of antibodies (Lee et al., 2013; Jung et al., 2008). Activated slides were gently washed with PBS buffer and type 1 water to remove unbound antibodies and then air dried.

2.2.2 Experimental design

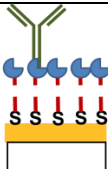
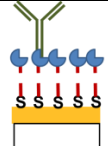

The initial capture test was carried out with *C. parvum* against IgG3 activated capture surface. An aliquot of 20µl of *C. parvum* (5.5×10^3 oocysts/ml) was placed on each of the three IgG3 activated spots (5 mm diameter size) on the gold slide and kept at 4°C for 1 hour, it was then gently rinsed with PBS and type 1 water sequentially. As a negative control, another spot on the capture surface was loaded with type 1 water instead of *C. parvum*. To determine the role of thiolated-linker in the capture process another spot lacking linker but loaded with BSA and antibody was also tested with *C. parvum*. The captured *C. parvum* oocysts were then stained using Crypt-a-Glo, a fluorescein-labeled mouse monoclonal antibody (mAb) agent (A400FLK Crypt-a-Glo™ Comprehensive Kit, Waterborne™ Inc., USA). Each spot received 20 µl of Crypt-a-Glo and was incubated for 30 min at 4°C before washing with 100 µl of SureRinse™ wash buffer (Waterborne™ Inc., USA) by tilting the slide long edge down and absorbing excess fluid using absorbent material without disturbing the surface.

The slide was then air dried and viewed under Zeiss Axioimager M1 microscope (Germany). Using Fluorescein excitation/emission filters of the microscope, the total number of captured oocysts was determined. Crypt-a-Glo stained oocysts on the antibody activated area were directly counted by scanning the area (5mm in diameter) from top to bottom and left to right using a 40X objective lens. The structural characteristics of the oocysts were observed using a 100X objective lens using immersion oil.

2.2.3 Results

As can be seen in Table 2.1 and Figure 2.3, anti-*Cryptosporidium* (IgG3) activated capture surface successfully captured *Cryptosporidium* oocysts. This was confirmed by visualization via Zeiss Axioimager M1 fluorescence microscope using 100x magnification whereas no oocyst was found on the one loaded with type 1 water (negative control). This capture surface was then compared with the spot without thiol-linker to find out the significance of linker. As antibodies did not bind in the absence of linker on BSA coated gold surface, slides without linker gave no cell count. The absence of *Cryptosporidium* indicated the necessity of linker to ensure successful orientated immobilization of antibodies for *Cryptosporidium* capture. All these findings showed that successful assembly of all surface components was required to develop a *Cryptosporidium* specific capture surface.

Table 2.1: Proof of capture ability of the anti-*Cryptosporidium* activated capture surface

Capture surface	Diagram	Loading agent	Microscopic observation
IgG3 activated capture surface		<i>C. parvum</i>	Oocysts present
IgG3 activated capture surface		Type 1 water	Oocysts absent
Capture surface lacking linker (BSA & antibody added)		<i>C. parvum</i>	Oocysts absent

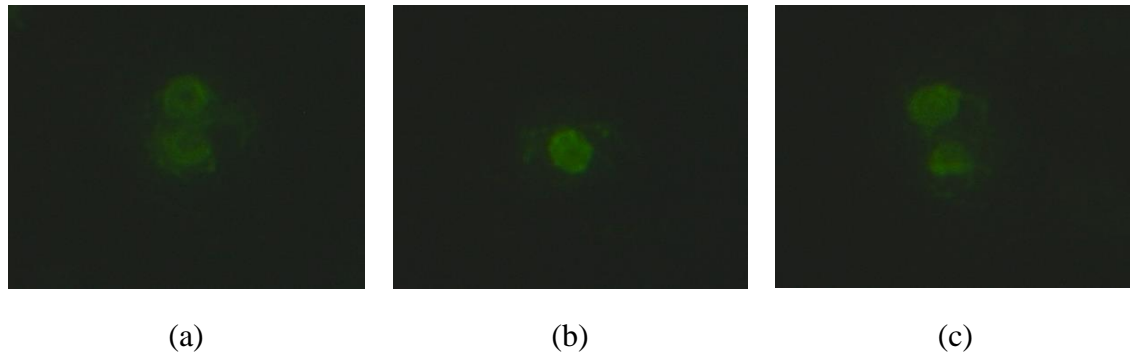


Figure 2.3: *C. parvum* oocysts captured on IgG3 activated capture surface. Figure 2.3 a, b & c represent example images of three different microscopic fields of an antibody activated spot showing captured oocysts. *C. parvum* oocysts were placed on the IgG3 activated spot and kept at 4°C for 1 hour. After washing *Cryptosporidium* oocysts were stained using Crypt-a-Glo, a fluorescein-labeled mouse monoclonal antibody (mAb) agent and observed under epifluorescence microscope using 100x oil immersion objective lens.

2.3 Antibody specificity determination within the *Cryptosporidium* genus

2.3.1 Methods

To determine the specificity and the capture efficiency of different anti-*Cryptosporidium* antibodies, capture surfaces activated with IgG1 & IgG3 (prepared as described in Section 2.2.1) were tested against three *Cryptosporidium* species: *C. parvum*, *C. muris* & *C. hominis*. A set of three gold slides were used in this experiment, each of which contained three spots activated with IgG3 antibodies. For each slide, an aliquot of 80 µl of *C. parvum* was taken from the working dilution (5.5×10^3 oocysts/ml) and 20 µl from this aliquot were used for microscopic examination (re-counting), the rest of the 60 µl were equally distributed on the three activated spots (20 µl each) on the gold slide. *C. parvum* oocysts were allowed to settle on three activated spots for 1 hour at 4°C followed by a gentle rinsing with PBS buffer and Type 1 water. The same experiment was repeated with *C. muris* (7.5×10^3 oocysts/ml) and *C. hominis* (4×10^3 oocysts/ml) respectively with the same experimental set up. After the washing steps, the captured cells were stained with Crypt-a-Glo (as described in Section 2.2.2). The slides were then observed under the epifluorescence microscope and all captured oocysts were counted by direct enumeration

according to the process described in Section 2.2.2. The total number of captured cells was divided by total cell number in the tested volume to figure out the capture efficiency. Following the same procedure, all three *Cryptosporidium* species were also placed on an IgG1 coated capture surface and capture efficiency was determined. During each combination of antigen-antibody experiment, one antibody activated spot was loaded with type 1 water instead of designated organism as a negative control.

A paired t-test was used to compare the capture efficiencies between two different antibodies (IgG3 & IgG1) in case of each *Cryptosporidium* species. Results were considered as significantly different when the P value was < 0.05. Statistical analysis of the results for more than two tests was done by analysis of variance (ANOVA). When the ANOVA showed the null hypothesis was rejected, a Post Hoc test (Student-Newman-Keuls) was performed to determine the differences of the means.

2.3.2 Results

The results of the antibody specificity test are presented in Appendix B (Table B.1 & B.2). Before calculating the average capture efficiency, one-way ANOVA analysis was carried out for each antigen-antibody combination to determine how the data should be aggregated. For each *Cryptosporidium*-IgG combination, a one-way ANOVA analysis showed that the differences in mean capture efficiency with IgG1 against three *Cryptosporidium* species were not significant enough to reject the null hypothesis (P value for *C. parvum*= 0.512, *C. muris*= 0.166 & *C. hominis*= 0.704 respectively). The similar non-significant change in capture efficiency was also observed with IgG3 against *C. parvum* (P value= 0.358). For these cases, all nine subsets could be considered as the same population (Appendix C; Table C.1, C.2, C.4, C.6) for analyzing capture efficiency. The capture efficiency varied significantly in case of IgG3- *C. muris* (P value= 0.047) and IgG3-*C. hominis* (P value= 0.04) suggesting that each of the 3 sets of data for these cases

should be processed as individual populations (Appendix C; Table C.3 & C.5). A pair wise comparison among 3 sets of each antigen-antibody experiment was also done using Student Newman-Keuls (SNK) method (Appendix C; Table C.3 & C.5). Following these statistical interpretation, the mean capture efficiency of IgG3 and IgG1 against different species were calculated (Appendix B; Table B.1 & B.2) which has been summarized in Table 2.2.

Table 2.2: Mean capture efficiency of IgG3 and IgG1 activated surfaces to capture different *Cryptosporidium* species. Both IgG1 and IgG3 activated capture surfaces were developed by adding 50 μ l of solutions (0.1mg/ml) of respective antibodies on the thiolated protein-G activated gold surface. 20 μ l of known concentration of *Cryptosporidium* oocysts was placed on each of the IgG3 & IgG1 activated spots (5 mm diameter size) on the gold slide for 1 hour at 4°C. After washing with PBS and type 1 water, the slides were stained with Crypt-a-Glo and counted under fluorescence microscope.

Antibody	<i>Cryptosporidium</i> species	Mean Capture efficiency (%) \pm Standard Deviation	Coefficient Variance (CV)
IgG3	<i>C. parvum</i>	92.60 \pm 2.79	3.02
	<i>C. muris</i>	93.59 \pm 1.86	1.99
	<i>C. hominis</i>	84.13 \pm 2.92	3.47
IgG1	<i>C. parvum</i>	74.32 \pm 3.42	4.61
	<i>C. muris</i>	65.84 \pm 3.35	5.08
	<i>C. hominis</i>	54.13 \pm 3.69	6.82

It can be inferred from Table 2.2, IgG3 has good binding (more than 90% capture) with *C. parvum* and *C. muris* compared to *C. hominis* (~84% capture). This finding was supported statistically by conducting one-way ANOVA. ANOVA result showed the oocyst recovery was significantly different among these groups (P value = 0.000). The SNK method compared these antigen-antibody combinations pair wise revealing that there was no significant difference for *C. parvum* and *C. muris* capture efficiency but capture of *C. hominis* was significantly lower when IgG3 activated capture surface was used (Appendix C; Table C.7). In case of IgG1, the capture efficiencies varied largely among three *Cryptosporidium* species ranging from ~54 - ~74%. According to ANOVA analysis, all these three species binds significantly differently with IgG1 (P value =

0.000). Analysis from SNK method also supported this claim stating that oocyst recovery capacity was significantly different in all three cases (Appendix C; Table C.8).

From Table 2.2 a general conclusion that the performance of IgG3 was better than IgG1 for all three *Cryptosporidium* species can be drawn. To prove this assumption statistically, a t-test was done between IgG3 & IgG1 for each of *Cryptosporidium* species separately and the result of the t-test showed there were significant differences (P value = 0.000) between the mean capture efficiencies of IgG3 and IgG1 for *C. parvum*, *C. muris* and *C. hominis* (Appendix C; Table C.9, C.10, C.11).

2.4 Antibody cross reactivity determination with other genera

2.4.1 Methods

The cross-reactivity of the capture surface with other microorganisms was verified by testing the unit against another test strain, *Escherichia coli*. *E. coli* ATCC 11775 strain was inoculated into full strength Luria-Bertani medium and incubated at 37°C. The optical density (OD₆₀₀) was measured every 2 hours using a spectrophotometer (Spectronic 20D+ model, Thermo Fisher Scientific Inc., USA) until the reading reached 1.0 which corresponds to 3×10^8 cells/ml (Sutton, 2011). The fresh culture was then serially diluted to 10^{-5} dilution to prepare a working dilution of 3×10^3 cells/ml by adding 1 ml of cell suspension into 9 ml of PBS (pH 7.0) in each dilution step. Ten ml of the working dilution was transferred and centrifuged at 3600g for 10 minutes to concentrate the cells. After centrifugation, the supernatant was discarded and the pellet was dissolved in 1 ml crystal violet stain. The stain was allowed to stand for 1 min, then the sample was centrifuged again at 3600g for 10 minutes. The crystal violet supernatant was discarded and the cell pellet was dissolved in 10 ml PBS solution (pH 7.0). This solution was again centrifuged and the process was repeated 5 times to remove excess crystal violet stain. This resulted in 10 ml stained *E. coli* cell suspension for use as a working dilution (3×10^3

cells/ml) which was then recounted using light microscope to ensure the final cell number. To perform the cell count, 20 μ l of stained *E. coli* cell suspension was placed on a Poly L lysine coated sticky microscope slide (Azer Scientific, US) and air dried. The process was repeated for 3 replicates and the slides were overserved under Zeiss Axioimager M1 microscope with bright field optics using 100x objective lens to determine the cell count. Then 20 μ l of stained and enumerated *E. coli* cell suspension was transferred to each of the three anti-Cryptosporidium IgG3 activated (5 mm diameter) capture spots (spot 1-3) on a gold slide and allowed to stand for 1 hour at 4°C and then gently rinsed with PBS and Type 1 water. As positive and negative control, 20 μ l of Crypt-a-Glo stained *C. parvum* (5.5×10^3 oocysts/ ml) was added on each of the anti-Cryptosporidium IgG3 activated spots (spot 4-6) and each of the IgG3 isotype control (non-specific for *Cryptosporidium*) activated spots (Spot 7-9) respectively. As isotype control, IgG3 isotype control murine (clone PPV-07) (Sigma-Aldrich, USA) specific for plum pox virus was used at a concentration of 100 μ g/ml to determine non-specific background signal. Then all 9 spots were observed using bright field (*E. coli*) or fluorescence (*C. parvum*) microscopy to determine whether the anti-Cryptosporidium antibodies immobilized on the thiolated gold surfaces were capturing cells other than the target organism *Cryptosporidium*.

2.4.2 Results

Figure 2.4 shows the typical morphological characteristics and size of the *E. coli* cells used in this experiment on a sticky slide. Crystal violet stained purple cells appeared rod shaped and approximately 2 μ m size in length. Figure 2.5 represents a microscopic field of a gold slide activated with anti-Cryptosporidium IgG3 antibody under bright field microscope. After scanning the anti-Cryptosporidium IgG3 antibody activated spots loaded with *E. coli* cells under the bright field microscope, no *E. coli* cells were found on

the surface (Figure 2.5) indicating the antibodies specific for *Cryptosporidium* failed to bind with *E. coli* cells. *C. parvum* oocysts were found to bind to the positive control spots showing the capture surface was working properly (Figure 2.6a). Absence of *C. parvum* oocysts on the negative control spots activated with IgG3 isotype control indicated non-specific binding was not taking place and binding of *C. parvum* oocyst with anti-*Cryptosporidium* IgG3 was responsible for generating *Cryptosporidium* specific signal (Figure 2.6b).

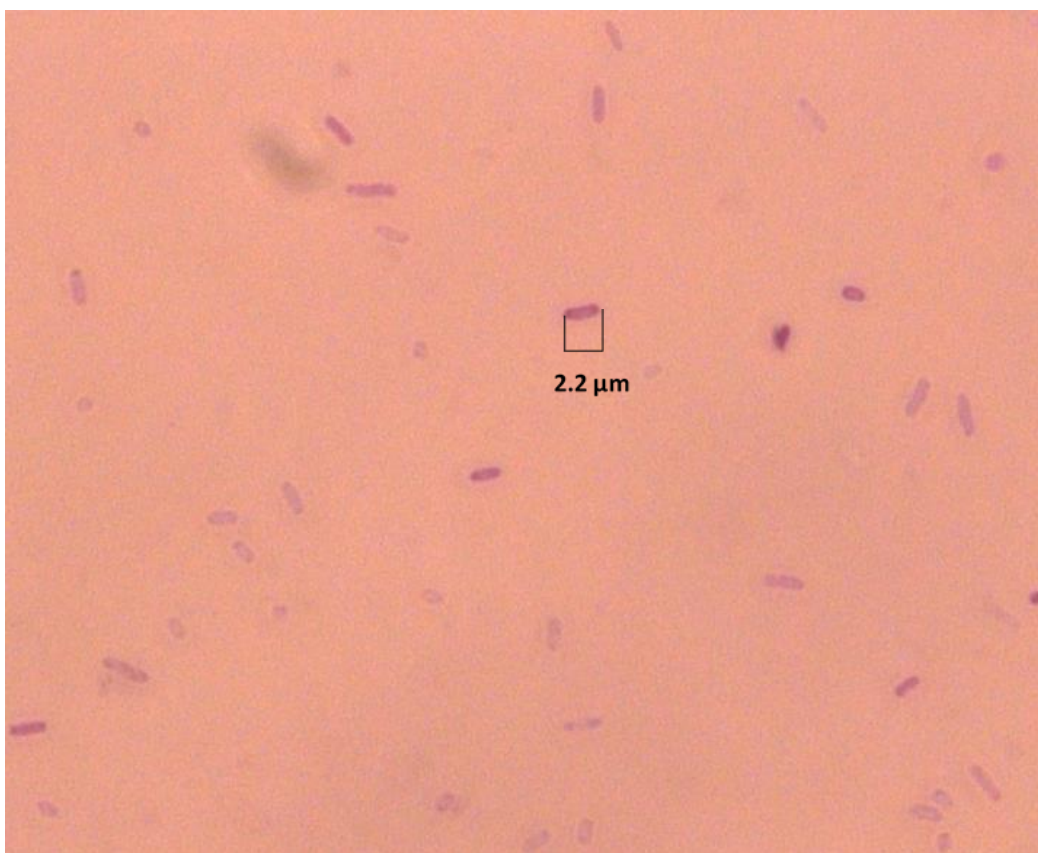


Figure 2.4: Bright field microscopy images of *E. coli* cells on a poly L lysine coated sticky slide showing typical morphology (rod shaped) and size ($\sim 2 \mu\text{m}$ in length). *E. coli* cells were stained using crystal violet and placed on a Poly L lysine coated sticky microscope slide and air dried. The slide was overserved under Zeiss Axioimager M1 microscope with bright field optics using 100x oil immersion objective lens.

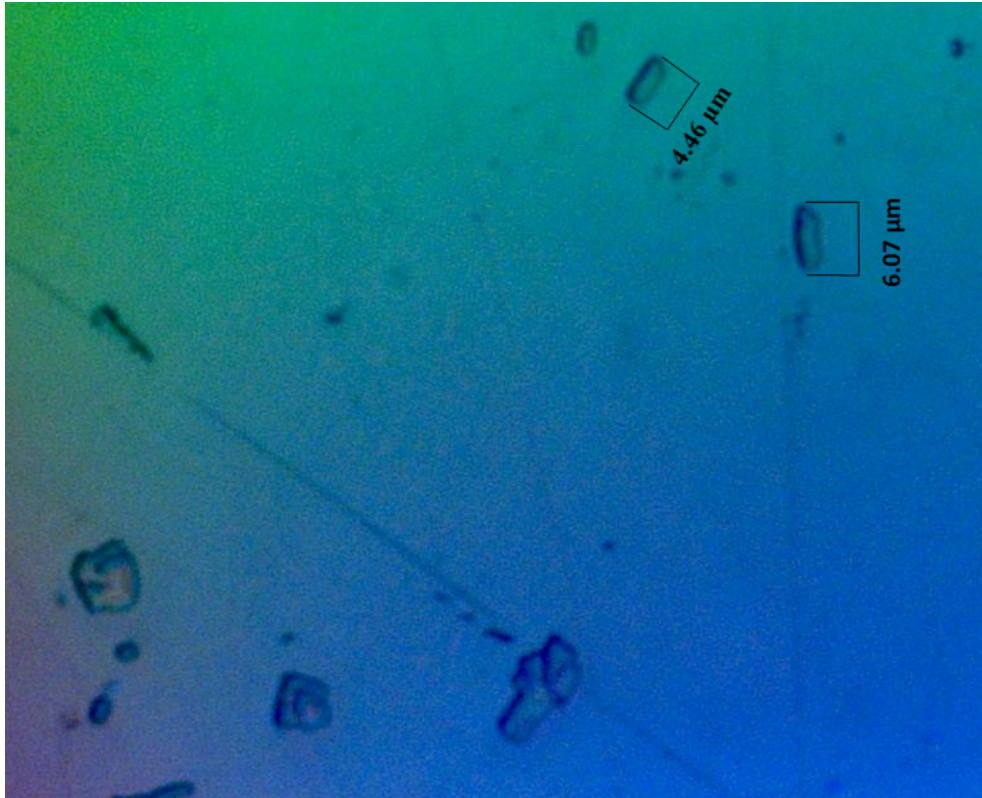
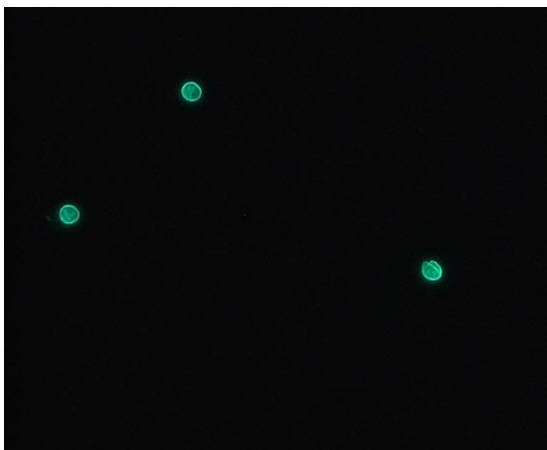


Figure 2.5: Bright field microscopy images of a microscopic field of a gold slide activated with anti-Cryptosporidium IgG3 antibody. The slide was overserved under Zeiss Axioimager M1 microscope with bright field optics using 100x objective lens. Crystal violet stained *E. coli* cells were placed on this antibody activated spot but no *E. coli* cell found on the surface. Rod shaped structures shown in the picture are too large (~5-6 μm in length) to be *E. coli* cell and not purple in color.



(a) Positive control



(b) Negative control

Figure 2.6: Fluorescence microscopy images of positive and negative control of anti-Cryptosporidium antibody cross reactivity experiment. Crypt-a-Glo stained *Cryptosporidium* oocysts were placed on both spots and observed under 100x oil immersion objective lenses. Figure 2.6a represents capture surface activated with anti-Cryptosporidium IgG3, hence successfully captured *Cryptosporidium* oocysts. Figure 2.6b represents capture surface activated with IgG3 isotype control and failed to capture any *Cryptosporidium* oocyst.

2.5 Antibody concentration determination

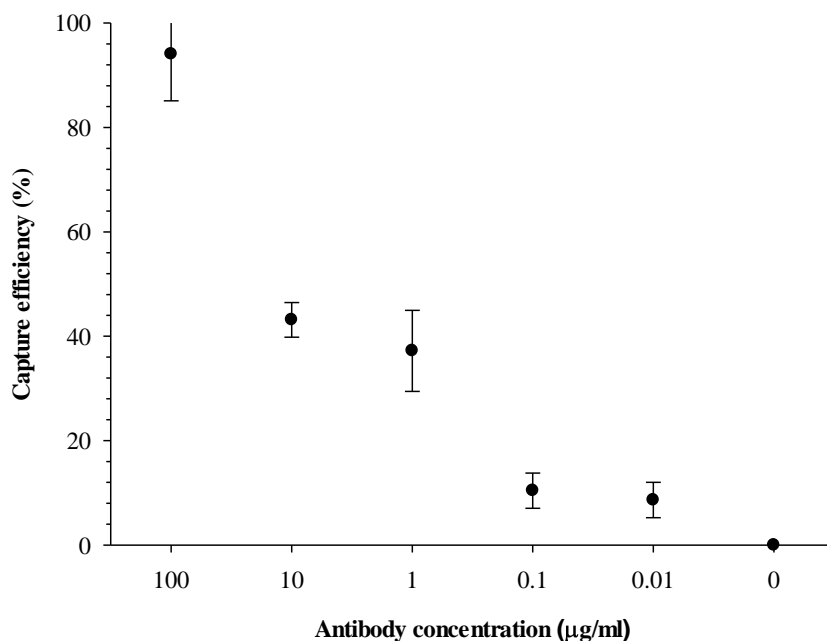
2.5.1 Methods

To determine the optimum antibody concentration that would ensure the maximum capture efficiency, the gold surface was loaded with anti-*Cryptosporidium* antibody ranging from 100 µg/ml to 0.01 µg/ml concentration. At first, three drops of 20 µl of 100 µg/ml IgG3 were placed on 3 different 5 mm diameter gold spots (coated with thiolated protein G) on a slide and incubated at 4°C for 48 hours. Similarly, 5 more slides (with 3 spots in each) were activated with IgG3 at a concentration of 10, 1, 0.1 & 0.01 µg/ml. Before loading *Cryptosporidium* oocysts on the antibody activated surfaces, slides were washed with PBS buffer & deionized water to remove unbound antibodies and air dried. Then, 20 µl of *C. parvum* (5.5×10^3 oocysts/ml) oocysts were added on each of these spots with varying antibody concentration. After 1 hour, the capture surface was washed again and stained with Crypt-a-Glo in order to enumerate the captured oocysts directly under the fluorescence microscope (as described in Section 2.2.2). From this wide range of antibody concentration, a comparatively narrow limit was figured out which indicated better capture ability. Then this narrow range was furthered explored following the same procedure to determine the optimum antibody concentration for the highest *Cryptosporidium* capture. During both experiments, a thiol linked BSA blocked gold spot not activated with IgG3 was used as a negative control. ANOVA was used to statistically analyze the effect of different IgG3 concentration on capture efficiency.

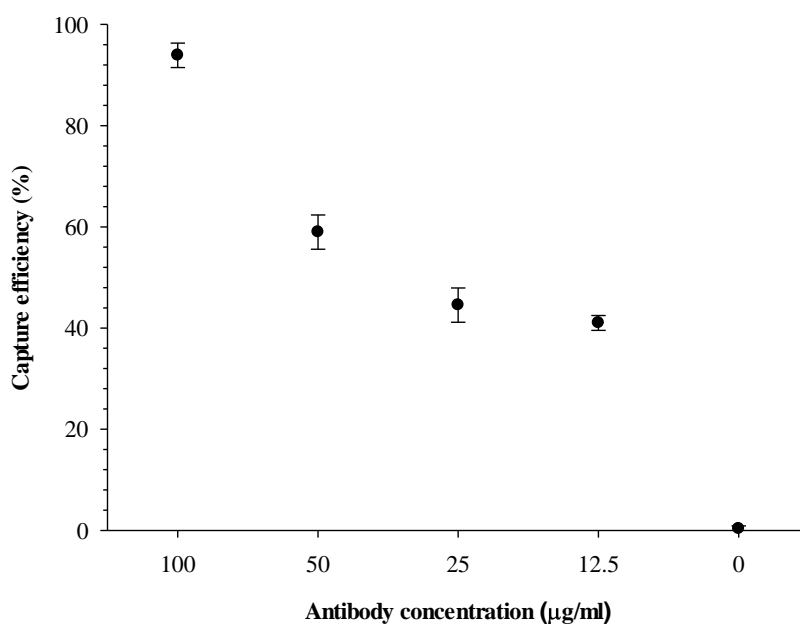
2.5.2 Results

The capture tests were initially performed using a wide range of IgG3 concentrations varying from 100 to 0.01 µg/ml. The trend in the change of *Cryptosporidium* capture efficiency with respect to decreasing antibody concentration is presented in Figure 2.7 (a) (Appendix B; Table B.3). It is evident from the figure that the

capture surface failed to recover more than 50% oocysts below 10 µg/ml antibody concentration. As 95% capture was possible with 100 µg/ml antibody concentration, these findings led to the next experiment where this range (100-10 µg/ml) was further explored to determine a more precise optimal antibody concentration. Figure 2.7 (b) illustrates the changes in capture efficiency with the antibody concentration varying from 100 to 12.5 µg/ml (Appendix B; Table B.4). Again the maximum average capture efficiency was observed at 100 µg/ml (94%), after which the capture ability dropped drastically to 59% at 50 µg/ml suggesting 100 µg/ml as the optimum concentration for maximum capture. One-way ANOVA analysis also supported that different antibody concentration significantly changed the capture efficiency (P value = 0.000) (Appendix C; Table C.12). Post hoc comparisons using SNK test indicated that antibody concentration 100 µg/ml which exhibited maximum recovery of *Cryptosporidium* oocysts was significantly different from 50 µg/ml IgG3. Similarly capture efficiency at lower antibody concentration such as 25 µg/ml & 12.5 µg/ml varied significantly from 50 µg/ml. However, there was no significant difference using 12.5 µg/ml and 25 µg/ml and these showed the lowest performance compared to others.



(a)



(b)

Figure 2.7: Capture efficiency of IgG3 activated capture surfaces in respect to different antibody concentrations. Figure 2.7a & 2.7b represents capture efficiency of surfaces activated with antibodies ranging from 100-0.001 µg/ml and 100-12.5 µg/ml respectively. Data points represent the average and error bars the standard deviation of three replicates. 20 µl of antibody of different concentrations were placed on gold spots coated with thiolated protein G and incubated at 4°C for 48 hours. After washing excess free antibodies with PBS, known number of *Cryptosporidium* oocysts were added on the antibody activated slides. Spots were then stained with Crypt-a-Glo and captured oocysts were enumerated directly under the fluorescence microscope to determine the capture efficiency.

2.6 pH dependent release mechanism

2.6.1 Methods

Different ranges of pH solutions were introduced on the antibody activated capture surface containing *Cryptosporidium*. The target was to release *Cryptosporidium* from antibody without destroying the protein G-antibody interaction, thereby leaving the surface active for subsequent capture. The binding between antigen-antibody and protein G-antibody are affinity based and pH dependent conformational changes can occur due to chemical shifts which could reverse the binding (Kato et al., 1995; Reverberi & Reverberi, 2007).

A pH range between 5.0 to 6.0 was explored to determine if *Cryptosporidium* oocysts could be released. The pH range was chosen based on two factors: (i) favorable pH range for antigen (*Cryptosporidium*) -antibody interaction which is between pH 6.5 & 8.4 and (ii) the Protein G-antibody interaction dissociates below pH 4.5. PBS solutions of pH 5.0, 5.5 and 6.0 were prepared (Reverberi & Reverberi, 2007). For the pH 5.0 PBS solution, 50 µl of PBS solution was placed on each of the three spots pre-loaded with a known number of Crypt-a-Glo stained *Cryptosporidium* (100-120 oocysts/spot) and the solution was allowed to sit for 15 minutes. Then the solution from each spot was aspirated into a micro-centrifuge tube using small tips and the spots were rinsed with PBS buffer (pH 7.0) and type 1 water to remove any free *Cryptosporidium*. The same method was carried out with pH 5.5 & pH 6.0 PBS buffer solutions and all these slides were then examined under epifluorescence microscope (as described in Section 2.2.2) to count the remaining oocysts (if any) on the surface to determine the release efficiency. PBS solution with pH 6.5 was added on a spot loaded with stained *Cryptosporidium* to use as negative control.

2.6.2 Results

The target for the release experiment was to achieve 100% release of captured oocysts and to leave the protein G-antibody binding on the gold surface intact for the next capture step. Figure 2.8 summarizes the increasing tendency of oocyst release from the capture surface in response to decreasing pH with no release at pH 6.5 (negative control) (Appendix B; Table B.5). The highest number of oocysts released at a pH which would still be favorable for retaining protein G-antibody interaction was pH 5.0, still ~40% oocysts from the first capture remained on the spot. This interfered with the process of collecting released oocysts required for the following/subsequent experiments as well as restricted the use of this surface for recapture. Trends in release indicated if more acidic solutions could be used, the release efficiency might get better. As the prime concern was ensuring 100% release, more acidic pH solutions (pH 4.0 & pH 4.5) were used at the risk of losing antibody from the surface thereby losing reusability of the surface. An interesting morphological alteration was observed when oocysts had been exposed to pH 4.0 & pH 4.5 solutions. The oocysts became so severely damaged that they could hardly be recognized as individual structures and counting was not possible. The damaged cell debris were all over the capture surface making the surface not fit for reuse. Surprisingly when the same experiment was repeated at pH 1, ~100% release was achieved at the expense of damaging proteinG-antibody interaction thereby losing antibody and making the device unfit for reuse. The oocysts released at pH 1 were undamaged when observed under microscope.

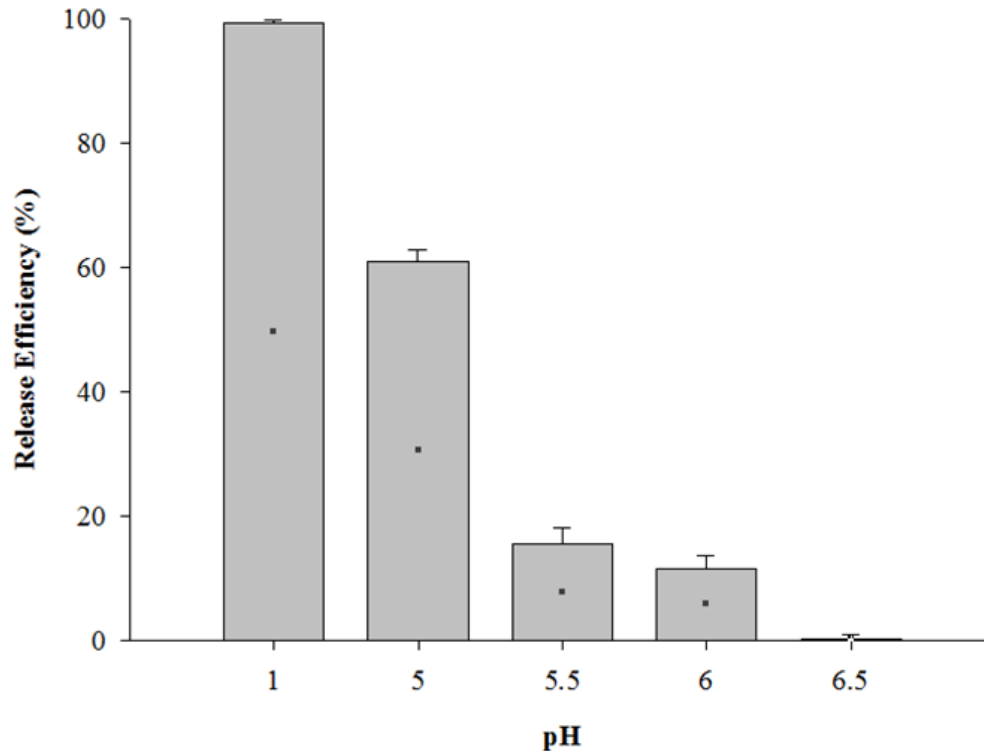


Figure 2.8: The changes in the oocyst release efficiencies with respect to different pH solutions. Bar heights represent the average and error bars the standard deviation of three replicates. For each pH range, 50 μ l of pH adjusted PBS solution was placed on each of the three spots pre-loaded with a known number of Crypt-a-Glo stained *Cryptosporidium* (100-120 oocysts/spot) for 15 minutes. After aspirating the solution from each spot, the spots were rinsed with PBS buffer (pH 7.0) and type 1 water observed under fluorescence microscope for the presence of oocysts.

2.6.3 Facilitating pH dependent release mechanism with extended time exposure and shaking

To determine whether it is possible to increase the release efficiency at the desired pH (pH 5.0) to ensure the antibodies would still be retained on the surface, other experimental parameters were also taken into account. To do this, the method was repeated at pH 5.0 with varying time of exposure and also introducing shaking during the release process to facilitate the release step.

In order to determine the effect of extended treatment period, 9 IgG3 activated gold spots were loaded with 20 μ l of *C. parvum* (5.5×10^3 oocysts/ml) oocysts. After staining and counting oocysts on the spots, 20 μ l of pH 5.0 PBS solution was placed on

these 9 spots and allowed to stand for 15 minutes on spot 1, 2 & 3; for 30 minutes on spot 4, 5 & 6; for 60 minutes on spot 7, 8 & 9. After the designated time period, the solution from each spot was transferred into a micro-centrifuge tube and the spots were rinsed with PBS (pH 7.0) and type 1 water. The *C. parvum* oocysts on the spots were then counted to determine the remaining oocysts on the surface under epifluorescence microscope to determine the effect of increasing time length on the pH dependent release efficiency. An increase in the release efficiency was also encouraged by introducing shaking as a mean of physical force during the release step. For this, four antibody activated slides were prepared with 3 spots on each and loaded with known number (100-120 oocysts/spot) of Crypt-a-Glo stained *Cryptosporidium*. Each of the slides were submerged in four petridishes containing pH 5.0 PBS solution. These petridishes were then placed on an automated orbital shaker (Thermo Scientific MaxQ 2000 model, USA) and shaken at 75 rpm for 15, 30, 45 and 60 mins respectively. Slide-1 was taken out from the solution after 15 minute, washed with pH 7.0 PBS solution & Type 1 water & air dried before counting the remaining oocysts on the spots under epifluorescence microscope. The rest of the slides were also observed after the designated time periods to find out the effect of shaking on *Cryptosporidium* release.

The release efficiency did not improve much when the treatment period was extended. The release capacity increased slightly from 59.76% to 62.78% after increasing the treatment period from 15 min to 60 min, still leaving 38-40% oocysts on the surface from the previous capture (Appendix B; Table B.6). Similar results were also observed for the slides that had been introduced to shaking for different time periods. The release efficiency after 15 minutes of shaking was 61.3% which merely increased to 61.7%, 63.5% and 62.9% when shaking treatment was increased at 15 minute intervals.

2.6.4 Effect of pH on the structure of *Cryptosporidium* oocysts

As *Cryptosporidium* oocysts were found to be damaged at pH 4.0 and 4.5 after going through the pH dependent release step, the question was raised whether the damage was caused due to the pH change only or other factors such as antigen-antibody binding, presence of chemicals such as phosphate, salts were also contributing in the damage process. To answer that, type 1 water in four tubes was adjusted to pH 6.0, 5.0, 4.0, & 1.0 respectively instead of PBS solution. In order to rule out the possible effect of antibodies on the oocyst structure, *Cryptosporidium* oocysts were fixed on Poly L lysine coated sticky microscope slides (Azer Scientific, US) instead of the antibody activated capture surface. Each of the twelve spots on 6 different sticky slides was loaded with 20 μ l of *C. parvum* (5.5×10^3 oocysts/ml) and air dried. The spots were then stained with Crypt-a-Glo according to the above mentioned procedure (Section 2.2.2) and were observed under epifluorescence microscope at 1000x magnification to examine the initial structure of the oocysts without exposure to any kind of treatment. Then 50 μ l of type 1 water with different pH (6.0, 5.0, 4.0 & 1.0) were placed on these 12 *Cryptosporidium* loaded spots (3 replicates for each pH solution) for 15 minutes. A spot with same volume of *C. parvum* was used as a control by placing pH 7.0 type 1 water on it. After 15 minutes, all spots were washed with pH 7.0 type 1 water and the slides were observed again under epifluorescence microscope at 1000x magnification to determine the effect of varying pH on the structure of oocysts. As can be seen in Figure 2.9 oocysts could withstand changes until the pH reached 5.0, after that the oocysts start becoming distorted. At pH 4.0 the oocysts were damaged the most, leaving cell debris on the surface. Cells in clusters were more damaged than the single ones. But the oocysts treated with pH 1.0 solution were intact suggesting that this is the suitable pH that should be used during the release step not only to ensure the highest release but also to recover them in a healthy state.

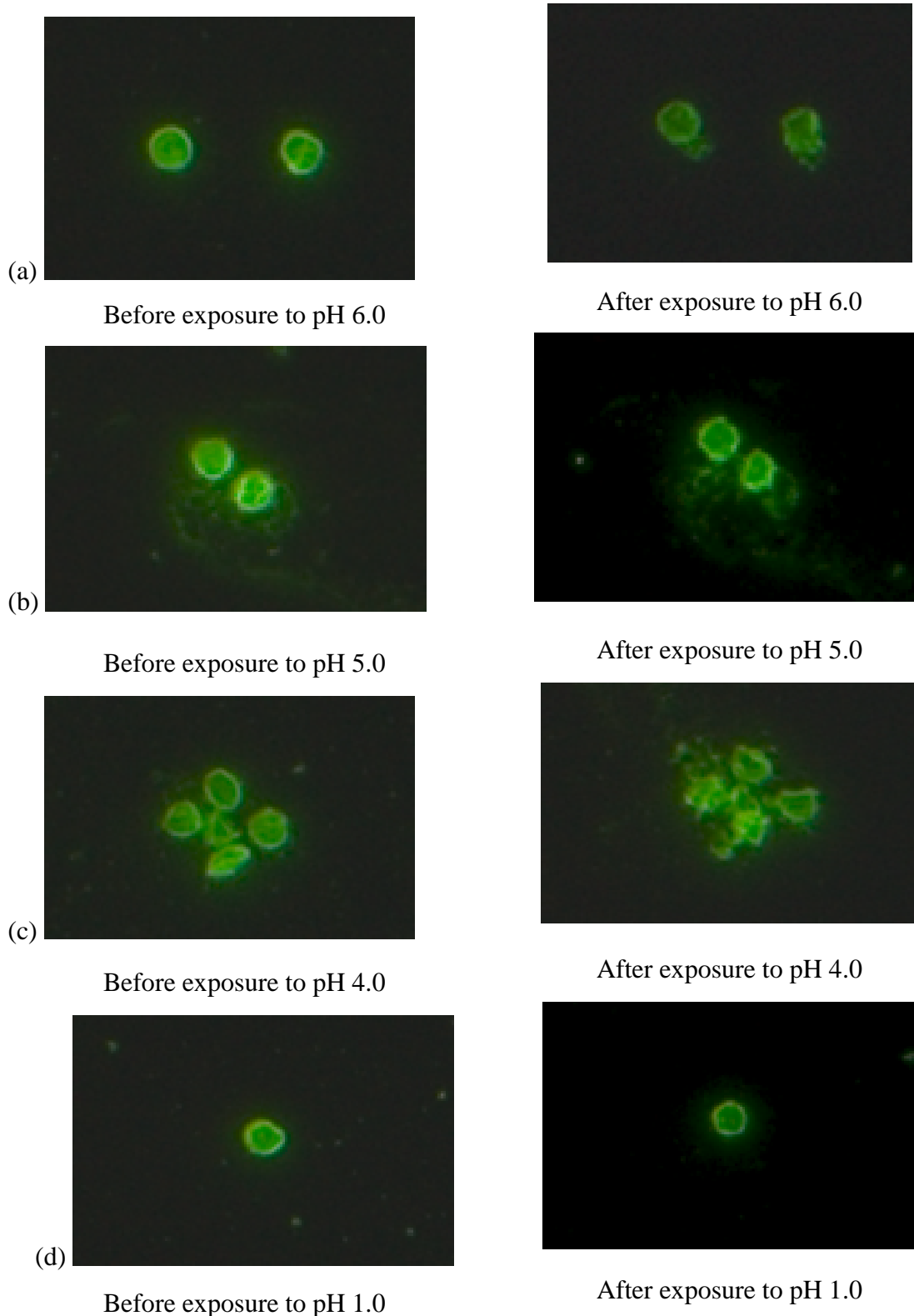


Figure 2.9: Morphological changes in *Cryptosporidium* oocysts due to exposure to different pH solutions observed under epifluorescence microscope. *Cryptosporidium* oocysts were fixed on Poly L lysine coated sticky microscope slides and stained using Crypt-a-Glo, a fluorescein-labeled mouse monoclonal antibody (mAb) agent which is responsible for green fluorescence. Figure 2.9 a, b, c, and d represents the same microscopic fields with oocysts before and after the exposure to pH 6.0, 5.0, 4.0 and 1.0 solutions respectively. Oocysts were observed under 100x oil immersion objective lens.

2.7 Capture surface reusability

2.7.1 Methods

As the ability to reuse the same antibody activated surface for successive *Cryptosporidium* capture could be an important factor in terms of labor and cost, the used capture surface was checked again for reusability. During this experiment, the release steps were always conducted at pH 5.0 to ensure that antibodies remain on the gold surface bound to the thiolated protein G linker molecules. Following the initial capture and release step, each of the three IgG3 activated spots (5 mm diameter size) was loaded with 20 μ l of *C. parvum* (5.5×10^3 oocysts/ml) for the second time. Using the same above mentioned capture procedure, the spots were allowed to stand for 1 hour at 4°C with the *C. parvum* solution on top of that followed by a gentle rinsing with PBS and type 1 water. Then 20 μ l of Crypt-a-Glo (fluorescent stain) was placed on each of the three spots to stain the newly added *C. parvum* and the slides were observed under fluorescence microscope to recount (as described in Section 2.2.2). Then the spots were exposed to pH 5.0 PBS solution to initiate the release of second time captured oocysts from the capture surface. The same process was repeated several times until the capture ability decreased to an insignificant level. The recapture experiment was also repeated with the capture surface exposed to pH 1 during pH dependent release experiment as 100% release was achieved at this pH. During this experiment beside *C. parvum*, *E. coli* cells were also added on one of the pH 1 treated spot to ensure the recapturing is not occurring due to non-specific binding to the surface as BSA was also expected to be damaged during exposure to pH 1.

2.7.2 Results

As the release step was carried out at pH 5.0, it was expected that 35%-40% oocysts from the last capture would be present on the surface which may hinder the

subsequent captures. Figure 2.10 illustrates that the average capture efficiency of the same capture surface decreased with subsequent use (Appendix B; Table B.7). It can be seen from Figure 2.10, the efficiency of first capture reduced from 92% to 72% during second round of capture. Similar results observed during third and fourth round of capture dropping to 43% and 28% respectively suggesting that it was not feasible to repeatedly use the same surface for capturing *Cryptosporidium* oocysts.

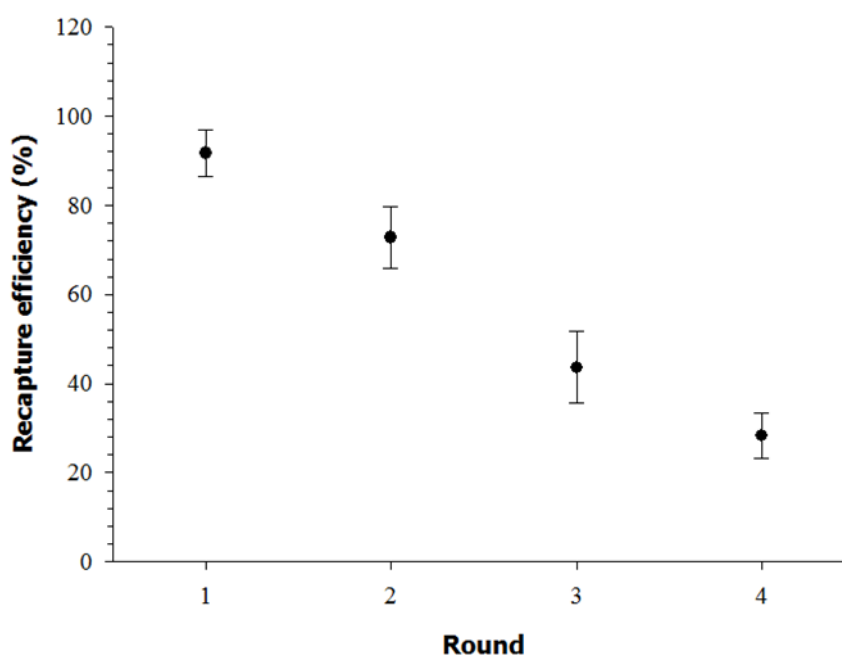


Figure 2.10: Recapture efficiency of an IgG3 activated capture surface during multiple attempts. Data points represent the average and error bars the standard deviation of three replicates. During each round of capture, each of the three IgG3 activated spots (5 mm diameter size) was loaded with 20 μ l of *C. parvum* (5.5×10^3 oocysts/ml) followed by exposure to pH 5.0 PBS solution to initiate the release of captured oocysts from the capture surface. Crypt-a-Glo stained oocysts were counted under fluorescence microscope after every capture and release step to determine the capture surface reusability.

A few *Cryptosporidium* oocysts were found on the capture surface that has undergone pH 1 release step after 1st recapture trial, but the capture efficiency was less than 20% indicating that the capture may not occur due to supposedly present antibodies on the surface. The spot loaded with *E. coli* also showed the presence of some cells on the surface under the microscope indicating that not only antibodies were released from protein G during this pH dependent release step decreasing the recapture efficiency

drastically, but also BSA coating was damaged making the surface non-specific for *Cryptosporidium* capture.

2.8 Discussion

The development of antibody activated capture surfaces specific for *Cryptosporidium* was initiated via selection of the antibody with maximum capture efficiency. During the assembly of the components of the capture surface, the antibodies were immobilized in oriented fashion on the surface using a binding protein, protein G, because oriented immobilization of antibodies improves binding capacity by using Fc portion for attachment leaving Fab site free for antigen interaction (Huy et al., 2011; Ryu et al., 2011; Shen et al., 2011). Thiolated protein G was selected as the linker between the antibody and the metal (gold) surface because thiolation ensures stronger immobilization of protein G on metal surface and protein G ensures tail-on orientation of antibodies (Liu et al., 2012). Protein G was used as the intermediate protein due to its higher affinity to the type of antibody (mouse IgG subclass) used in this research compared to protein A (Akerstrom and Bjorck, 1986; Akerstrom, 1985; Bjorck and Kronvall, 1984; Eliasson et al., 1988). The gold was coated on the glass substrate to generate the metal surface because it is easy to generate thiolated self-assembled monolayers on the gold surface due to its high affinity for sulphur-containing molecules (Xue et al., 2014). Self-assembled monolayers formed from thiols on gold are stable for periods of days to weeks when in contact with the complex liquid media required for cell studies (Love et al., 2005).

During selecting antibodies for *Cryptosporidium* capture, IgG and IgM antibody classes were considered because the oocyst wall stimulates the production of these two antibodies (Weir et al., 2000). IgM was screened out during the selection process as it is a pentamer and lacks free Fc part which was a requirement for the capture surface development (Elgert, 1996). The two commercially available subclasses of IgG anti-

Cryptosporidium antibodies ie. IgG1 and IgG3 were then tested for capture efficiency. Both IgG1 and IgG3 were able to capture three different species of *Cryptosporidium* oocysts indicating these antibodies are genus specific, though the capture efficiency varied significantly (P value= 0.000). The capture surface activated with IgG3 was able to capture more than 90% *C. parvum* and *C. muris* oocysts but the capture efficiency decreased to ~84% in case of *C. hominis*. Still the capture efficiency of IgG3 was significantly higher (P value= 0.000) compared to that of IgG1 which was able to recover at best ~74% *Cryptosporidium* oocysts (*C. parvum*) from the spiked sample. The capture efficiency dropped to ~65% and ~54% for *C. muris* and *C. hominis* respectively. This analysis helped to reach the conclusion that IgG3 would be the ideal candidate for the capture surface development to ensure maximum recovery of the *Cryptosporidium* oocysts. This finding could be supported by the fact that there is a structural difference in the hinge region of IgG1 and IgG3 antibodies (Vidarsson et al., 2014). The hinge region of IgG3 is composed of 62 amino acids which much longer than that of IgG1 (15 amino acids) (Roux et al., 1997). This longer hinge in IgG3 increases distance between Fab arms and Fc tail giving IgG3 more flexibility compared to other subclasses which in turn influences its antigen binding efficiency (Vidarsson et al., 2014). As the capture surface was designed specifically to detect and capture *Cryptosporidium* from water, cross-reactivity of the capture surface with other microbial genera was verified by testing the unit against *E. coli*. Absence of crystal violet stained purple rod shaped cells on the antibody activated slide proved that this capture surface was specific for *Cryptosporidium*, thereby suggesting the chances of capturing microorganisms other than *Cryptosporidium* from water are low.

To make the process cost effective, one of the key step is using minimum antibody concentration for maximum oocyst recovery. It is well established from the

experiment that the capture surface was able to recover the highest number of oocysts (>90%) at 100 µg/ml antibody concentration. Though the concentration range between 50-100 µg/ml was not checked further, 100 µg/ml was selected as optimum antibody concentration. As the difference in price between adding 90 µg/ml or 80 µg/ml instead of 100 µg/ml will not differ much at this point in terms of time and effort, it was decided to proceed forward using 100 µg/ml as optimum antibody concentration.

Attempts were made to recover the capture surface by releasing *Cryptosporidium* oocysts in order to use the setup for subsequent capture. It was expected to get satisfactory release below pH 6.0, as the optimum pH for antigen-antibody binding is between 6.5 to 8.4 and changes in pH would cause conformational modifications in the antibody resulting in loss of compatibility with the antigen (Reverberi & Reverberi, 2007; Devanaboyina et al., 2013). Yet at pH 5.0 not more than 60% release was achieved leaving many oocysts from the previous capture on the slide limiting the use of this surface for recapture. The capture surface was then introduced to more acidic environment to increase the release efficiency. But several drawbacks were associated with exposing the capture surface to such acidic environment. According to the manufacturer, the antibodies are supposed to dissociate from protein G below pH 4.5. Also such harsh acidic conditions induce conformational modifications in the antibodies causing aggregation (Ejima et al., 2007; Welfle et al., 1999). The oocysts were also found to be severely damaged when exposed to pH 4.0 & pH 4.5 solutions causing the cells to crack open and leaving cell debris on the capture surface. The release of *Cryptosporidium* oocysts in intact form was crucial for the next objective in order to extract DNA to detect DNA damage. When the capture surface was treated with pH 1.0 solutions 100% release of the oocysts was achieved at the expense of losing antibodies from the surface but the oocysts were intact. This finding is also supported by the currently in use

Cryptosporidium detection method (EPA 1623.1) where acidic dissociation of *Cryptosporidium* oocysts are carried out at pH 1 to release them from IMS beads (USEPA, 2012). In order to retain the antibody-protein G interaction, the capture slides were also exposed to pH 5.0 for extended time period and with shaking. But the release efficiency did not improve with these treatments leaving no other option than to use pH 1.0 for the release treatment.

Even though the release efficiency did not reach satisfactory level at pH 5.0, the capture surface was checked for reusability. With every recapture and following release step, the oocysts from the last capture piled up on the capture surface. This blocked the antigen binding sites of the antibodies which resulted in inefficient *Cryptosporidium* capture. It was also observed that cells that remained on the slide became more and more damaged with every pH dependent release treatment step. During the 4th round of capture there were so many damaged oocysts on the surface which made the counting process quite difficult, error prone and made the capture surface unfit to use. The recapture test was also repeated with the capture surface exposed to pH 1.0. It was found that along with antibodies BSA (Bovine Serum Albumine) coating of the surface was also damaged due to acidic treatment. Below pH 4.0 Bovine Serum Albumin undergoes pH dependent conformational changes from normal form (N-state) to fast migrating (F-state) form which causes partial unfolding of the protein structure (Barbosa et al., 2010; El Kadi et al., 2006; Michnik et al., 2005). This could be responsible for losing the functionality making the capture surface non-specific and captured cells other than the target one, thereby unsuitable for further use.

Chapter 3 Detection of damaged DNA in UV treated *Cryptosporidium*

The goal of this task was to develop a simple and inexpensive immunoassay for water industries using the principles of Enzyme-linked Immunosorbent Assay (ELISA) to detect CPD in UV irradiated *Cryptosporidium* oocysts with minimum resources. This chapter discusses the selection of the most effective DNA extraction method; optimization of parameters for the ELISA technique, the process of developing a protocol for detection of DNA damage in UV treated *Cryptosporidium* through indirect ELISA in a cuvette and the validation of this method via microscopy.

The rationale for this research was to provide the water suppliers and analysis service labs a simple and direct assay to ensure that the organism present in the water supply have been damaged by the UV light. Though immunofluorescence microscopy (IFM) was considered to be a useful tool for estimating UV photoproducts, IFM has its own drawbacks including being laborious, time-intensive and expensive which limit the implementation of this procedure in non-specialized laboratories or industrial settings. Alternative faster detection methods involving immunochromatographic assays or vital dyes have been explored to detect pathogen viability, but these methods currently lack the accuracy observed when using IFM. Al-Adhami et al. (2007) proposed a method to detect UV damaged DNA in *Cryptosporidium* oocysts based on the microscopic imaging of stained cells. However, this technique is expensive, laborious, requires special setup, skills and is subjective in interpretation. An alternative method substitutes cells with the use of whole extracted DNA by using CPD-antibody binding reaction through ELISA microplate reader, originally conceived from the human cancer research studies (Mori et al., 1991). However, microtiter plate/strips could be expensive and non-feasible for the water industries due to low numbers of samples as compared to clinical samples. There are also very few (if any) other standard water assays that would use a microtiter plate

and reader, while there are many assays requiring a spectrophotometer and cuvette indicating most water industries possess this facility. It would be more convenient for them to conduct UV damage detection tests with the set-up already in use. Considering this, microtitre plate and plate reader were replaced with cuvette and spectrophotometer respectively for this research.

During the development of this cuvette based ELISA protocol several parameters were optimized to ensure good signal with low background. These include selection of the most efficient DNA extraction method to ensure maximum DNA recovery to facilitate DNA damage detection as well as optimizing ELISA components such as primary & secondary antibodies, cuvette size, incubation time & period. The protocol was based on the indirect ELISA method where anti CPD primary antibody was exposed to DNA coated on the cuvette wall followed by exposure to an enzyme (horseradish peroxidase) linked secondary antibody. The signal from the reaction was detected by measuring the absorbance of the influent light signal using a spectrophotometer at 450nm wavelength. Signal from cells irradiated with different doses of UV light was compared with the signal from non-irradiated cells. The color intensity is proportional to the number CPDs present in the DNA. The signal of both non-irradiated cells and those irradiated for different time periods (3, 6, 10, 40 mJ/cm²) were measured to determine the response curve and detection limit. This result was validated by observing the UV irradiated oocysts using epifluorescence microscopy according to the protocol established by Al-Adhami et al. (2007).

3.1 Selection of DNA extraction method for environmental samples

This task was carried out to select an ideal DNA extraction method for *Cryptosporidium* that efficiently recovers clean DNA from environmental samples. Five commercially available DNA extraction kits from different manufacturers and based on

different principles were selected. In order to evaluate the recovery efficiency of the selected kits, the extraction procedure was performed on spiked samples with known concentration of *Cryptosporidium* that ranged between 0-1000 oocysts per ml. The spiking process was carried out in water collected from local creeks (Vernon creek and Duteau creek) that are local drinking water sources.

The actual sample (tested by end user) may contain various types of environmental components in addition to *Cryptosporidium* which can interfere with the downstream procedures. Although PCR is not required in the ELISA assay, it was used during Kit selection as an indicator of clean DNA since the PCR reaction is sensitive to the inhibitors present in the sample. The kits were selected based on the ability to produce clean DNA as well as the lowest detection limit.

The sampling site was selected based on two parameters, a) typically free of *Cryptosporidium*, b) representing the condition of actual sample which may contain inhibitors. This experiment was designed in a way that the whole procedure (including sampling collection) was repeated on three samples in order to check the reproducibility of the extraction results of each kit. To observe the impact of the freeze thaw, each kit was tested using samples spiked with three different dilutions of oocysts, with and without freeze thaw. Creek water without spiking was used as a negative control.

3.1.1 Sample preparation for DNA extraction

In order to evaluate the efficiency of kits in terms of DNA recovery from environmental samples, known concentration of *Cryptosporidium* oocysts were spiked in the filtrate of creek water. To collect the filtrate, initially a sampling unit consisting pump and filter (Pall Envirochek) was set close to the creek. Then, 40L water was pumped in and passed through the filter. In this process water was pumped out leaving solids in the filter. The filter was brought back to the laboratory and eluted by elution buffer (Appendix A)

then centrifuged eventually to produce a pellet. The volume of pellet was recorded, supernatant fluid was discarded and the pellet was re-suspended using 30 ml 1x PBS buffer (Appendix A). This protocol was performed according to EPA Method 1623 which was developed for the screening of water to detection *Cryptosporidium* in the water sample.

Half of the filtrate (15 ml) was used to measure total solids, volatile solids, pH and conductivity, and half of it was utilized as samples for DNA extraction. To measure the solids in the water, an aliquot of 5 ml filtrate was distributed into 3 pre-weighed empty dishes (made of aluminum foil) and incubated at 94°C overnight ensuring the evaporation of liquids. The plates were cooled, weighed and total solids in the water were calculated by subtracting the value of pre-weight from the value of post weight. To measure the total volatile solids, dishes were then heated at 550°C in a muffle furnace for 1 hour. The dishes were weighed again and the total volatile solids in the water were measured by subtracting the value of post weight after muffle furnace from the value of total solids.

Of the remaining filtrate, 10 ml were aliquoted in to 4 tubes (2.5 ml each) which was later spiked with *C. parvum* oocysts at concentration of 1000, 100, 10 and 0 oocysts/ml individually. Vigorous mixing with a vortex mixer was applied to ensure homogeneous distribution of oocysts in the solution during the spiking procedure. The number of oocysts in each dilution was confirmed by microscopy (see Section 2.2.2).

3.1.2 DNA extraction

A list of commercially available kits was prepared through a literature review and after reading the protocol and MSDS of the kits. Five of them were selected including the one used in the EPA protocol for further comparison (Table 3.1). This selection was done based on several parameters found in the literature, protocols and MSDS which included cost, time, easiness and effectiveness in terms of DNA extraction and PCR inhibitor removal. Although the UV inactivation of *Cryptosporidium* oocyst is irreversible despite

the presence of UV repair gene (Rochelle et al., 2004), precaution was taken to avoid photo-reactivation in order to retain the status of UV products by limiting light exposure to the DNA products all through the process.

Table-3.1: Properties of selected commercially available DNA extraction kits

Product name (Manufacturer)	Format	Lysis Process	Chemical used for lysis and purification	Additional requirement	Protocol time (Kit cost per reaction)
PowerSoil® DNA Isolation Kit (MoBio)	Silica Spin Filter Tubes	Physical & Chemical	IRT technology Guanidine HCl, ethanol	None	40-60 mins (\$4.94)
PowerFecal™ DNA Isolation Kit (Moio)	Silica Spin Filter Tubes	Physical & Chemical	IRT technology Guanidine HCl, ethanol	None	40-60 mins (\$4.74)
E.Z.N.A.® Stool DNA Kit (Omega)	Column	Physical & Chemical	HTR (Guanidine HCl), ethanol	Ethanol, tubes	90-120 mins (\$2.33)
DNeasy Blood & Tissue Kit (Qiagen)	Column	Chemical	Proteinase-k, Ethanol	Ethanol, tube	50-70 mins (\$3.24)
TRI Reagent (Sigma)	Liquid phase extraction	Chemical	Phenol, chloroform, ethanol	Chloroform, ethanol, NaOH, EDTA, Trisodium citrate, tubes	~150 mins (\$3.12)

As the hardy oocyst structure of *Cryptosporidium* makes the DNA extraction process difficult, many studies incorporated supplementary treatment procedures prior to DNA extraction to crack the hard shell (Belli et al., 2006). One of the common methods was applying freeze thaw technique. The necessity of conducting this additional step prior to DNA extraction was also verified during this task. In order to execute this, 10 aliquots of 250 µl eluate was prepared in micro centrifuge tube from each sample (2.5 ml eluate)

containing three different concentrations of oocysts to compare between freeze thaw vs no freeze thaw. For Qiagen, the comparison was done between freeze thaw with liquid nitrogen vs in the -80°C freezer.

- a) Freeze thaw vs no Freeze thaw: One set of samples went through freeze thaw processing before DNA extraction (excluding Qiagen). To do so, 250 µl samples containing oocysts (between 0-1000/ml) were lysed using 5 cycles (approx. 10 min each) of freezing in -80°C and thawing at 75°C. One set of samples was kept at -20°C until DNA extraction without doing any pre-treatment.
- b) Freeze thaw with liquid nitrogen vs without liquid nitrogen (only for Qiagen): Initially 250 µl of 1:1 Chelex/molecular grade water was vortexed and added to each sample (250 µl) containing oocysts (between 0-1000/ml) using a large bore tip. One set of samples went through freeze thaw processing with liquid N₂ before DNA extraction (only Qiagen). The oocysts were lysed using 8 cycles (approx. 1 min each) of freezing in liquid nitrogen and thawing at 95°C with shaking the sample down after thaw step. Other set of samples went through freeze thaw processing without using liquid N₂. To do so, oocysts were lysed using 5 cycles (approx. 10 min each) of freezing in -80°C and thawing at 75°C with shaking the sample down after the thaw step. After rapid spinning, the sample including Chelex and foam was transferred to a 0.45 µm cellulose acetate microfuge spin filter (Corning Spin-X #8162, VWR # 29442-756). With the spin filter hinge in the 12 o'clock position, the sample was centrifuged at high speed for 30 seconds. The spin filter insert containing the Chelex resin was discarded. The sample volume was 250µl which further used as template in DNA extraction. The DNA extraction was done for each aliquot of samples (250 µl) using 5 different kits according to the manufacturer's instruction (MoBio, 2013; MoBio, 2016; Omega Bio-tek, 2015; Qiagen, 2006; Sigma-Aldrich, 2016).

3.1.3 Polymerase Chain Reaction (PCR)

To determine the ability of extraction kits to produce clean DNA from environmental sample, nested PCR was performed. Nested PCR consists of two PCR runs, the external PCR using the external primers selected to amplify an extended gene target and the internal PCR using internal primers selected to amplify a specific 18S rRNA gene segment in *Cryptosporidium spp.* as described by Yu et al., 2009 (Table 3.2). The external PCR was performed in 50 μ L reaction volume comprised of 20 μ L of 5-Prime™ MasterMix, 200 μ g/mL Bovine Serum Albumin (BSA), 200 nM of each primer, 4 mM MgCl₂ and 5 μ L sample DNA as template (Table 3.3). The reaction volume was eventually adjusted with diethylpyrocarbonate (DEPC)-treated PCR grade water. The amplification was run in a thermal cycler (Eppendorf AG 22331 model, Germany) using a temperature program set for 10 minutes at 94°C followed by 35 cycles of 94°C (45 seconds), 55°C (45 seconds), and 72°C (60 seconds). The thermocycler parameter for internal PCR was the same except 25 cycles were used instead of 35. Similarly, identical reaction components in a 50 μ L reaction volume were used to perform internal PCR except the primers, DNA template and BSA (Table 3.4). In the reaction volume for internal PCR, 1 μ L of the external PCR product was used as template and with the internal primers without adding BSA (Yu et al., 2009). PCR grade water instead of DNA template was used as negative control in both PCR runs. DNA of positive amplification result and previously amplified product were used as positive control for external and internal PCR.

Table 3.2: The primer sequences for the 18S rRNA gene external and internal PCR runs

Primer name	Sequence
External Forward Primer (EF)	5'-TTCTAGAGCTAATACATGCG-3'
External Reverse Primer (ER)	5'-CCCATTTCTTCGAAACAGGA-3'
Internal Forward Primer (IF)	5'-GGAAGGGTTGTATTTATTAGATA-3'
Internal Reverse Primer (IR)	5'-AAGGAGTAAGGAACAACCTCCA-3'

Table 3.3: Reaction composition for external PCR (single reaction)

Ingredients	Stock concentration	Final concentration	Volume (μ l)
DEPC treated PCR grade water			19
5-Prime™ Master Mix	2.5X	1X	20
BSA	2500 μ g/ml	200 μ g/ml	4
Primer EF	10,000 nM	200 nM	1
Primer ER	10,000 nM	200 nM	1
DNA			5
Total PCR volume			50

Table 3.4: Reaction composition for internal PCR (single reaction)

Ingredients	Stock concentration	Final concentration	Volume (μ l)
DEPC treated PCR grade water			27
5-Prime™ Master Mix	2.5X	1X	20
Primer IF	10,000 nM	200 nM	1
Primer IR	10,000 nM	200 nM	1
Primary PCR product			1
Total PCR volume			50

3.1.4 Gel electrophoresis

An agarose gel (1% w/v) was prepared by suspending dry 1.1 g agarose in 110 ml of 1X Tris buffered saline (TBE) (Appendix A) with 2 μ l syber safe DNA stain (Thermo Fisher Scientific, USA). Initially a low heat setting was used, later the mixture was boiled (up to 160°C) until the solution became clear to avoid the agarose clumps. A magnetic stirrer (speed 125 rpm) was used to mix the solution while heating. The solution was cooled down to 50-60°C before pouring into the casting tray. After cooling, the solution was cast in Fisher BioTech Electrophoresis System Midi-Horizontal FB-SB-1316 using

two 20-well combs. After solidification, the comb was carefully pulled out and the gel was submerged in a chamber containing 0.5X TBE buffer as well as positive and negative electrode. Then, 2 μ l of 5x bromophenol blue loading dye was added to 18 μ L of each nested PCR product, mixed with pipette and loaded in the well. The gel was run at 110 volts for 70 mins in 0.5X TBE buffer. Band sizes were estimated using 1kb plus ladder reference (Invitrogen, Lot No. 1513825). After the run, the gel was visualized in an AlphaImager EC light cabinet at 365nm.

3.1.5 Results

Positive results from PCR indicated the kits were able to recover clean DNA from environmental water samples which was confirmed by visualizing 850 bp PCR product on gel electrophoresis. Result showed that DNA recovery was dependent on the removal of the PCR inhibitors presented in the environmental water samples which were spiked with different concentration of oocysts. Concentrations of 2.40, 1.80 and 0.09 μ g/ml of solids were present in sample 1, 2 and 3 respectively. The overall performance of five different kits with/without freeze-thaw treatment was compared in terms of DNA recovery from three water samples spiked with 10, 100, 1000 oocysts/ ml. DNA extracted by Power Soil, Power Fecal, ENZA Fecal, Qiagen and TRI reagent yielded 94% (17/18), 78% (14/18), 72% (13/18), 33%(6/18) and 17% (3/18) PCR positive results respectively. Both the presence of higher amounts of solids and lower concentration of oocysts were responsible for reduction in DNA recovery. Unlike other kits, only Power Soil was able to recover DNA from the samples containing 10 oocysts/ml in the presence of 2.40 μ g/ml of solids in the water. Moreover, the freeze thaw method did not show any impact on PCR result.

3.2 DNA damage detection using ELISA

The irradiated *C. parvum* oocysts (5×10^6 cells in 10ml PBS) used in this research were provided by Hyperion Research Ltd. (Alberta, Canada). The number of irradiated oocysts was confirmed by counting under microscope (see Section 2.2.2) and preserved in 4°C in a dark environment until DNA extraction. Before irradiation these oocysts were purified from calf feces through water-ether concentration and sucrose floatation. The viability of the original oocysts was determined using fluorogenic vital dye assay and more than 90% were found viable. *C. parvum* oocysts suspended in PBS buffer were exposed to a low-pressure UV lamp at 254 nm. To obtain different UV dosages (mJ/cm^2), oocysts were placed in a biohazard hood and irradiated using UV lamp directly from the top for different periods of time using constant distance (10 cm) and the constant intensity UV source ($1 \text{ mJ}/\text{sec}.\text{cm}^2$ at 254 nm). Control oocysts were exposed likewise without irradiation. Although *Cryptosporidium* is sensitive to low doses of irradiation (6-10 mJ/cm^2) compared to the standard dose ($40 \text{ mJ}/\text{cm}^2$) demanded for disinfectant system by standard UV protocol (USEPA 2006; DVGW 2006). CPDs remained undetectable at $<10 \text{ mJ}/\text{cm}^2$ dose (Al-Adhami et al., 2007). In order to determine the discriminatory power of the current method in terms of detecting increasing DNA damage with increasing UV doses, *Cryptosporidium* oocysts were irradiated at 0, 3, 6, 10 and $40 \text{ mJ}/\text{cm}^2$ UV doses. The irradiated oocysts were stored in PBS buffer at the concentration of 5×10^5 oocysts/ml.

From each UV dose, 250 μl from the stock solution (5×10^5 oocysts/ml) was added to the PowerBead tubes provided with PowerSoil® DNA Isolation Kit (MO Bio Laboratories, USA) and the DNA extraction was done according to the manufacturer's instructions (MoBio, 2016). Finally, 100 μl eluate containing purified DNA was recovered and preserved at -20°C. As the DNA concentration less than 100 $\mu\text{g}/\text{ml}$ is not

feasible to measure using spectrophotometer due to the chances of not getting reproducible results (Shim et al., 2010), the DNA concentration in this eluate was measured as mentioned in Coupe et al. (2005). The DNA concentration was approximated to 0.06 µg/ml as 5×10^{-5} ng DNA corresponds to a single oocyst (Coupe et al., 2005). DNA was denatured by heating the solution in the thermocycler (Eppendorf AG 22331 model, Germany) at 100 °C for 10 minutes and was chilled rapidly in an ice bath for 15 minutes to generate single-stranded DNA for ELISA.

3.2.1 Steps of ELISA procedure

The original procedure for the ELISA method was conceived from the protocol used by Cosmo Bio Co. Ltd. (2017) which was developed based on microtiter plate to detect CPDs in cancer patients. During this research, this protocol was adapted for a cuvette and environmental samples. Indirect ELISA was conducted to detect CPDs in UV damaged DNA of *Cryptosporidium* oocysts. In the indirect ELISA method, antigens are absorbed on the surface wall instead of antibody. Single stranded purified *Cryptosporidium* DNA was used as antigen during this ELISA. The following steps were followed:

- a) Coating of cuvette wall by protamine sulfate: Protamine sulfate (0.003%) solution was prepared in distilled water and stirred for 1 hour to achieve a homogeneous suspension. After complete mixing, 200 µl of the solution was transferred in each cuvette (Eppendorf, Germany). Each cuvette was incubated at 37°C overnight to completely dry. Cuvettes were washed three times with 400 µl/tube of Type 1 water. The tubes were used immediately or stored in dark at room temperature.
- b) DNA sample adhesion: DNA solutions were prepared in PBS at the concentration of 0.06 µg/ml was denatured by heating the solution in the thermocycler (Eppendorf AG 22331 model, Germany) at 100 °C for 10 minutes and was chilled rapidly in an ice

bath for 15 minutes. Then, 200 µl of single stranded DNA solution was distributed in each of the protamine sulfate pre-coated cuvettes. Each cuvette was incubated at 37°C overnight to completely dry.

c) Signal detection by Spectrophotometer: Each DNA-coated cuvette was washed for 5 mins for 5 times with 400 µl of PBS-T (0.05% Tween-20 in PBS). To prevent non-specific antibody binding, 400 µl of 2% BSA in PBS was distributed in each cuvette. Cuvettes were incubated at 37°C for 30 mins. Each cuvette was washed 5 mins X 5 times with with 400 µl of PBS-T (0.05% Tween-20 in 1X PBS) and 200 µl of anti-CPD TDM-2 mouse monoclonal antibodies (2 µg/ml) (Cosmo Bio Co., Japan) was added. Following incubation at 37°C for 30 mins, each cuvette was washed 5 mins X 5times with 400 µl of PBS-T (0.05% Tween-20 in 1X PBS). Then 200 µl of Anti-Mouse IgG (whole molecule)–Peroxidase antibody (0.375 µg/ml) (Sigma Aldrich, USA) was distributed in each cuvette. After 30 minutes of incubation at 37°C, each cuvette was washed 5 mins X 5 times with 400 µl of PBS-T (0.05% Tween-20 in 1X PBS). Then, once again washed with 400 µl of Citrate-phosphate buffer (Appendix A). The buffer solution was kept in the cuvette until the next substrate solution was ready to add. After throwing the buffer away, 200 µl of 1-Step™ Ultra TMB-ELISA (Thermo Fisher Scientific, USA) was distributed as the substrate in each cuvette and incubated for 30 minutes at 37°C. To stop enzyme reaction, 100 µl of 2M H₂SO₄ was distributed in each cuvette. After gentle mixing, the absorbance was determined at 450 nm by a spectrophotometer (Evolution™ 60S UV-Visible Spectrophotometer, Thermo Fisher Scientific, USA).

3.2.2 Parameter optimization for ELISA method

Several factors including cuvette size, antibody concentrations, incubation time and temperature were optimized during developing this ELISA technique in cuvette to get

best results. Substrate was separately incubated with DNA, primary antibody, secondary antibody, wash buffer (0.05% Tween-20 in 1X PBS) and 2% BSA in protamine sulfate coated cuvette (small) at 37°C for 30 mins to rule out the possibility of the substrate's cross-reactivity with any other reagent which might give false positive result. As none of them gave signal it was shown that the reagents were incapable of producing signal without complete assembly of the components. The following key components were then optimized to establish the protocols for this method. In the following section, all other factors were held constant as described in Section 3.2.1 during one single factor was being optimized.

3.2.2.1 Selection of cuvette

As a spectrophotometer was used during this research to measure the signal of antigen antibody reaction, microtiter plate was replaced with a cuvette to determine if it could be used as the test vessel. Three different sizes of cuvettes, i.e small (50 μ l), medium (400 μ l) and large (800 μ l) cuvettes were selected for the evaluation process (Figure 3.1). All these cuvettes are made of polystyrene which makes them suitable for coating with protamine sulphate. In order to conduct this evaluation process, small, medium and large cuvettes were coated with protamine sulfate then 50, 200 and 400 μ l of ssDNA (0.06 μ g/ml) respectively. The volume of primary antibody (2 μ g/ml) and secondary antibody (0.375 μ g/ml) used for small medium and large cuvettes was also 50, 200 and 400 μ l respectively. The volume of blocking agent and washing buffer was 150, 600 and 1200 μ l used for small, medium and large cuvettes respectively. Then 100, 400 and 800 μ l of substrate and stop solution were added in small, medium and large cuvettes respectively. After adding stop solution, the absorbance was measured at 450nm wavelength. Cuvettes of three different sizes were evaluated using both irradiated (40 mJ/cm²) and non-irradiated (0 mJ/cm²) oocysts.

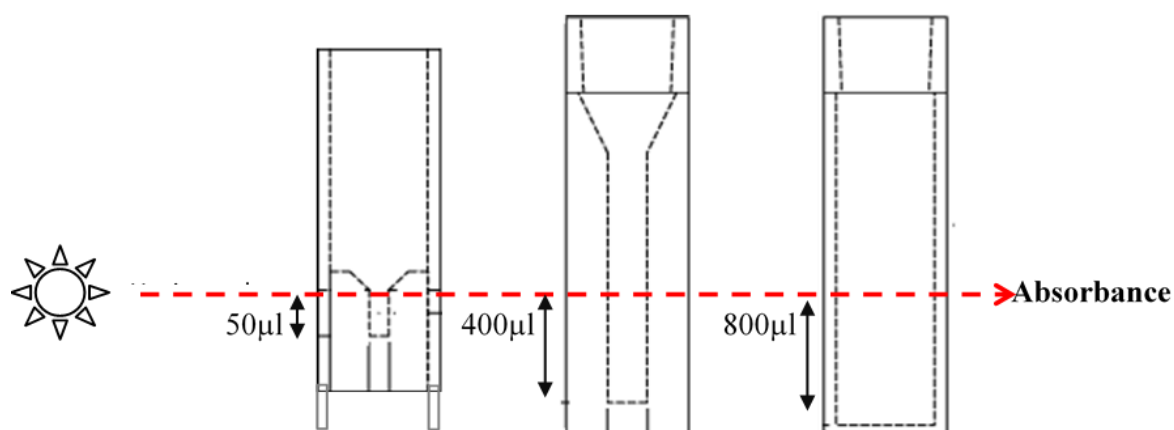


Figure 3.1: Different sizes of cuvettes used during the optimization step. Minimum 50, 200 and 400 μl of samples are required for small, medium and large cuvettes respectively to get accurate absorbance readings.

3.2.2.2 Antibody concentration optimization

The most vital step during developing the ELISA is the optimization of the concentration of antibodies. The optimization was assessed based on obtaining better signal with low background noise using *Cryptosporidium* oocysts irradiated with 40 and 0 mJ/cm^2 UV light.

Anti cyclobutane pyrimidine dimers (CPDs) TDM-2 mouse IgG2 κ (Cosmo Bio CO., Japan) monoclonal antibodies produced in mouse myeloma cell were used as primary antibodies. It arrived in a lyophilized form and was reconstituted with PCR grade water as per manufacturer's instruction. It was preserved at -20°C into small aliquots of 5 μl . AntiCPD-TDM2 reacts with ssDNA and stably binds to CPD formed in oligonucleotides consisting of more than 8 bases as well as every dipyrimidine sequence (TT, TC, CT and CC). The manufacturer recommended concentration was 2 $\mu\text{g}/\text{ml}$ for ELISA, which was further evaluated by comparing the reaction signal obtained when 1 $\mu\text{g}/\text{ml}$ and 4 $\mu\text{g}/\text{ml}$ concentrations were also used.

Anti-Mouse IgG (whole molecule)–Peroxidase antibody (Cat no. A9044, Sigma-Aldrich, USA) labeled with HRP was selected as the secondary antibody that binds with Fc portion of the primary antibody. This secondary antibody was produced in rabbit and

arrived in a lyophilized form which was further reconstituted at 10-20 mg/ml concentration using PCR grade water. The antibody was stored at -20°C in small aliquot. For ELISA, the manufacturer recommended concentration was 0.375 µg/ml for secondary antibody to give absorbance of 1.0 at 450nm. To evaluate this concentration, two other concentrations of 0.3 µg/ml and 0.5 µg/ml were also used in the optimization process.

The concentrations of both primary and secondary antibodies were optimized simultaneously in single cuvette using each of the three different concentrations (1 µg/ml, 2 µg/ml, 4 µg/ml) of primary antibodies with three different concentrations of secondary antibodies (0.5 µg/ml, 0.375 µg/ml, 0.3 µg/ml) resulting in 9 primary-secondary antibody concentration combinations. For each combination, 3 cuvettes were treated with irradiated oocysts and 3 cuvettes with non-irradiated oocysts.

3.2.2.3 Incubation time & temperature

The rate of antigen-antibody reactions can also be affected by the incubation temperature. Both primary and secondary antibodies were evaluated for three different incubation times (30, 60 and 90 mins) at two different temperatures (37°C and 4°C). For each antibody, 6 different combinations of incubation time and temperature were used in the evaluation process. For each combination, three cuvettes were used to capture data reproducibility. In both cases the parameter of the evaluated antibody was changed but the other antibody was incubated at 30 min at 37°C.

As substrate, 1-Step™ Ultra TMB-ELISA (Thermo Fisher Scientific, USA) was selected which is very sensitive and develops a blue color. The blue color was changed into yellow upon addition of H₂SO₄. During each optimization step, the signal: noise ratio was measured by comparing the signal obtained with the sample containing irradiated DNA vs. the sample containing non-irradiated DNA. Increased signal-noise ratio would indicate the higher possibility of detecting CPDs in the test sample.

3.2.2.4 Results

Cuvette size: The average absorbance values of 50 μ l, 400 μ l and 800 μ l cuvettes treated with irradiated oocysts were recorded as 0.65, 1.12 and 1.44 with the standard deviation of 0.057, 0.035 and 0.160 respectively (Figure 3.2). When the absorbance values of these cuvettes were compared with those containing non-irradiated DNA, the signal: noise ratio was found to reduce with cuvette size increase (Figure 3.3) indicating the highest background in the large cuvette.

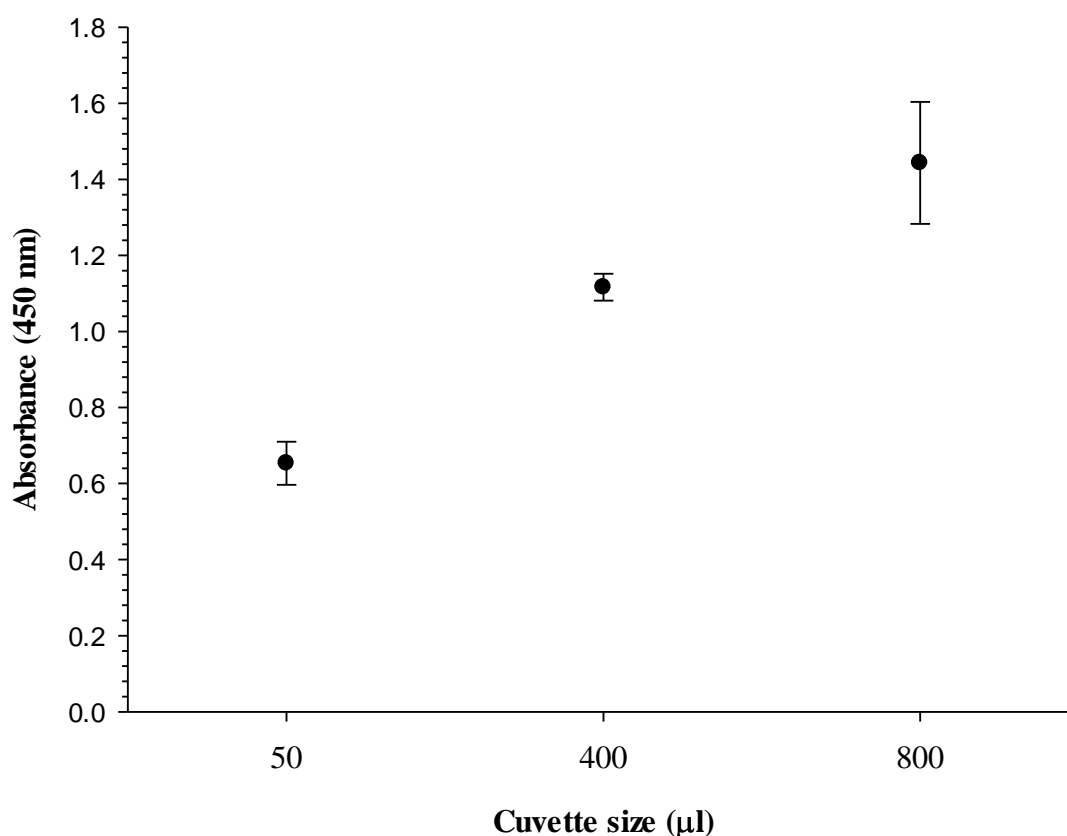


Figure 3.2: Absorbance of CPD-antibody reaction in different sizes of cuvettes against *Cryptosporidium* oocysts irradiated at 40 mJ/cm². Data points represent the average and error bars the standard deviation of three replicates. DNA extracted from 40 mJ/cm² irradiated oocysts was added into different sizes of cuvettes coated with protamine sulfate. Upon addition of primary antibody (2 μ g/ml) and secondary antibody (0.375 μ g/ml), substrate (color changed to blue) and stop solution (color changed to yellow) were added in the cuvettes and the absorbance was measured at 450nm wavelength. The incubation period of 30 minutes and incubation temperature of 37°C were used for both primary and secondary antibodies.

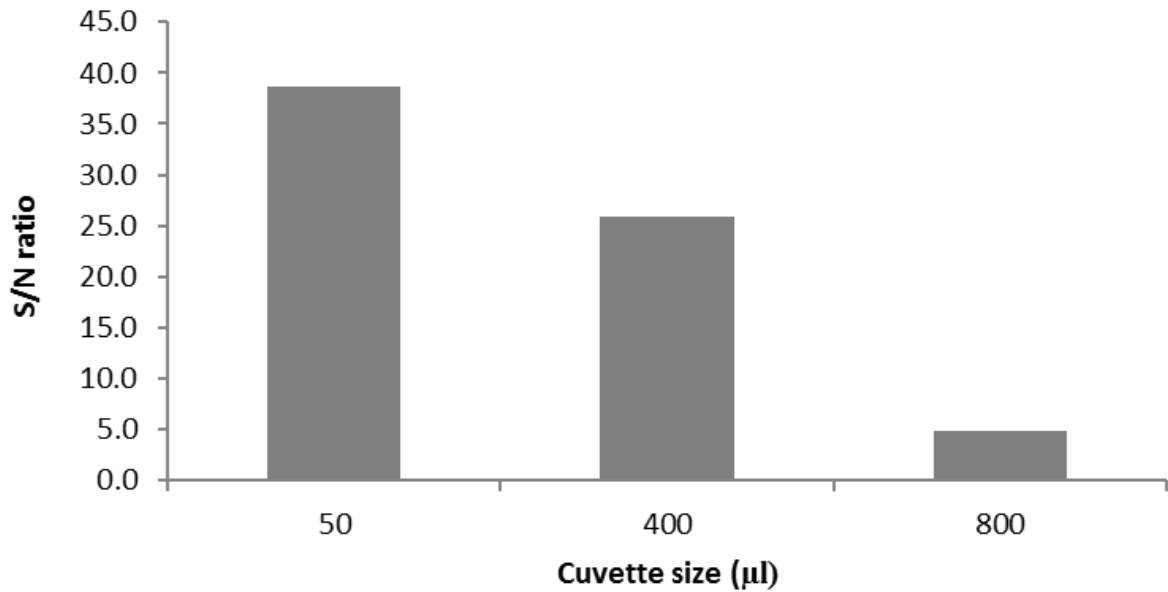


Figure 3.3: Signal to noise ratio in different sizes of cuvettes. The signal-to-noise ratio was calculated by dividing the absorbance of test sample (40 mJ/cm² irradiated oocysts) by the absorbance of negative control (non- irradiated oocysts).

The smaller the size of the cuvette, the minimum the volume of DNA and antibodies would be required to conduct the ELISA test. The target was to find out the cuvette size which would give the best absorbance value. The 50 µl cuvette was not selected as it gave poor signal and the 800 µl one gave high background. So the 400 µl cuvette was selected as it provided satisfactory absorbance with minimal requirement of DNA and antibody.

Antibody concentration: For each combination of primary-secondary antibody, the average absorbance of three cuvettes containing irradiated DNA were measured and plotted in the graph (Figure 3.4). All cuvettes using 1 µg/ml primary antibody incubated with three different secondary antibody dilutions yielded low signal (<0.65) with higher standard deviations. The other two primary antibody concentrations 2 µg/ml and 4 µg/ml gave comparatively similar absorbance values except for the cases when 0.3 µg/ml secondary antibody was used. As better results were found with both 2 µg/ml and 4 µg/ml

primary antibody concentrations against both 0.5 $\mu\text{g/ml}$ and 0.375 $\mu\text{g/ml}$ secondary antibody concentrations, the lowest antibody concentration combination that is 2 $\mu\text{g/ml}$ for primary and 0.375 $\mu\text{g/ml}$ for secondary was selected as the optimum combination which was also suggested by the manufacturers. The signal: noise ratio as shown in Figure 3.5 supported this decision as higher background noise was found with 0.5 $\mu\text{g/ml}$ compared to 0.375 $\mu\text{g/ml}$ secondary antibody concentration.

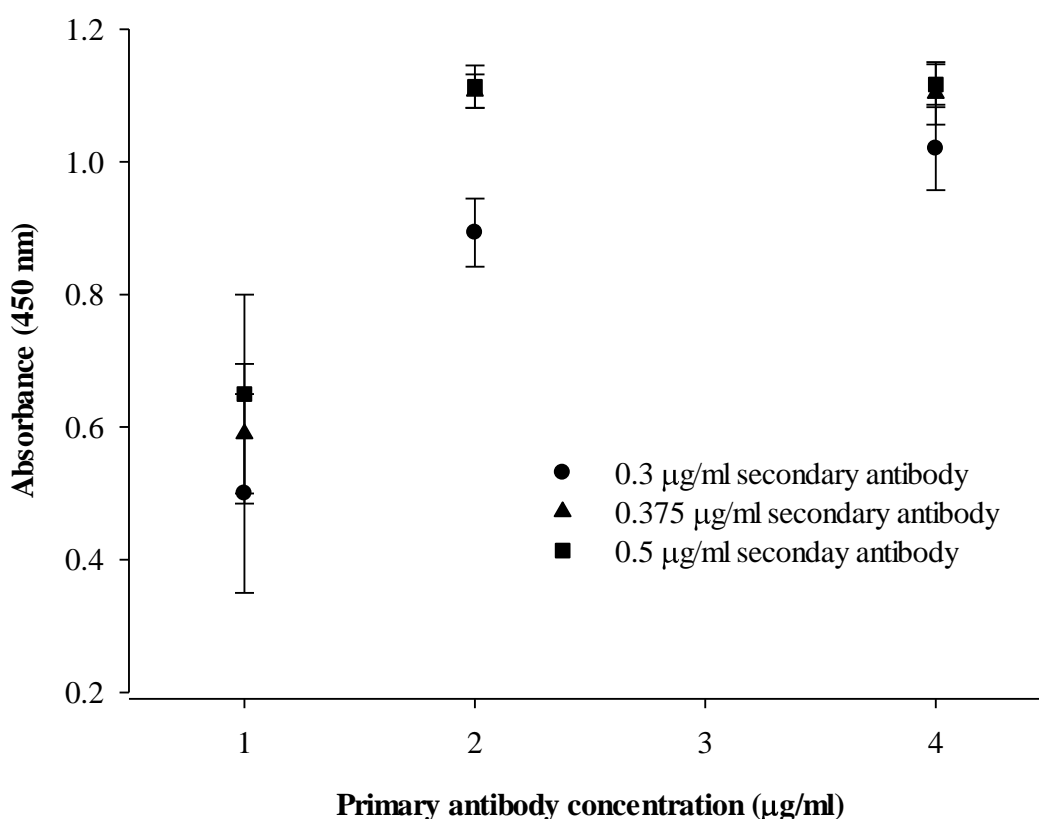


Figure 3.4: Changes in absorbance in response to different combination of primary (1 $\mu\text{g/ml}$, 2 $\mu\text{g/ml}$, 4 $\mu\text{g/ml}$) & secondary antibody (0.3 $\mu\text{g/ml}$, 0.375 $\mu\text{g/ml}$, 0.5 $\mu\text{g/ml}$) concentrations against *Cryptosporidium* oocysts irradiated at 40 mJ/cm^2 . Data points represent the average and error bars the standard deviation of three replicates. DNA extracted from 40 mJ/cm^2 irradiated oocysts was added into 400 μl size cuvettes coated with protamine sulfate. Each of the three different concentrations (1 $\mu\text{g/ml}$, 2 $\mu\text{g/ml}$, 4 $\mu\text{g/ml}$) of primary antibodies with three different concentrations of secondary antibodies (0.5 $\mu\text{g/ml}$, 0.375 $\mu\text{g/ml}$, 0.3 $\mu\text{g/ml}$) resulting in 9 primary-secondary antibody concentration combinations were added in 9 cuvettes. Upon addition of substrate (color changed to blue) and stop solution (color changed to yellow) in the cuvettes, the absorbance was measured at 450nm wavelength. The incubation period of 30 minutes and incubation temperature of 37°C were used for every primary and secondary antibody combination.

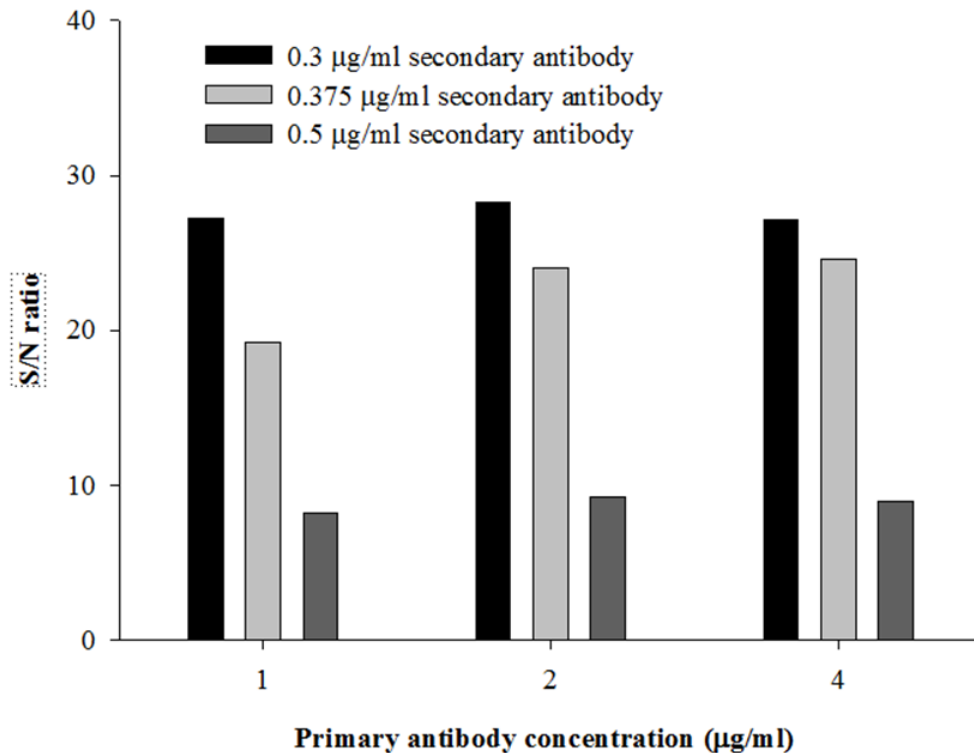


Figure 3.5: Signal to noise ratio over different combination of primary (1 µg/ml, 2 µg/ml, 4 µg/ml) & secondary antibody(0.3 µg/ml, 0.375 µg/ml, 0.5 µg/ml) concentrations. The signal-to-noise ratio was calculated by dividing the absorbance of test sample (40 mJ/cm² irradiated oocysts) by the absorbance of negative control (non- irradiated oocysts).

Incubation time and temperature: The average absorbance of antibodies vs. incubation time for irradiated oocysts at 37°C & 4°C were plotted in Figure 3.6. As can be seen from Figure 3.6, the responses of CPD-antibody reaction were similar over 3 different time periods for both primary and secondary antibodies. Also there was not any differences in responses at 4°C to at 37°C. According to the signal noise ratio (Figure 3.7) the chances of false positive result increased when the secondary antibody incubated for over 30 mins. So for both primary and secondary antibodies 30-minute incubation was selected as the optimum incubation period at 37°C which was also suggested by the manufacturers.

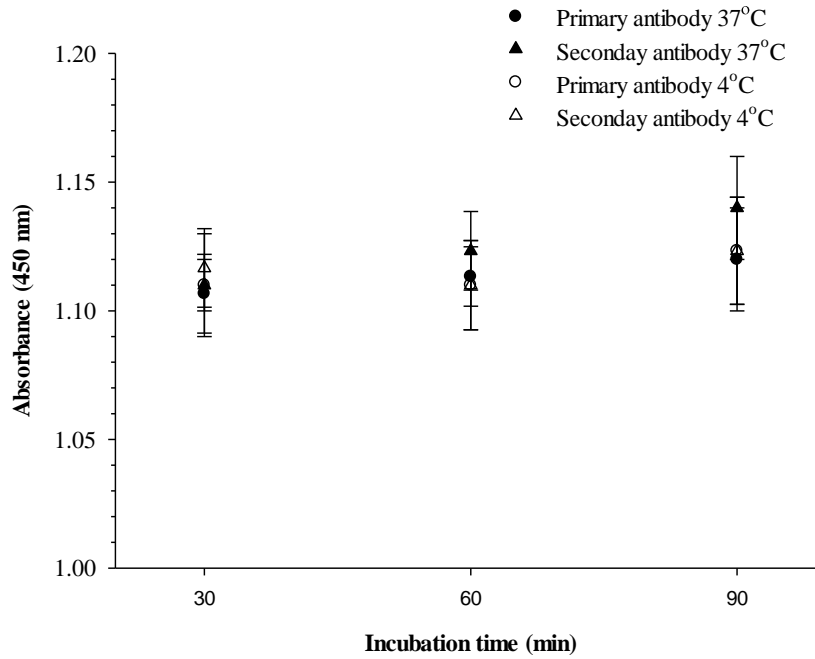


Figure 3.6: Changes in absorbance in response to different incubation period of primary & secondary antibodies at 37°C and 4°C with *Cryptosporidium* oocysts irradiated at 40 mJ/cm². Data points represent the average and error bars the standard deviation of three replicates. DNA extracted from 40 mJ/cm² irradiated oocysts was added into 400 µl size cuvettes coated with protamine sulfate. Both primary antibody (2 µg/ml) and secondary antibody (0.375 µg/ml) were evaluated for three different incubation times (30, 60 and 90 mins) at two different temperatures (37°C and 4°C). For each antibody, 6 different combinations of incubation time and temperature were used in the evaluation process. Upon addition of substrate (color changed to blue) and stop solution (color changed to yellow) in the cuvettes, the absorbance was measured at 450nm wavelength.

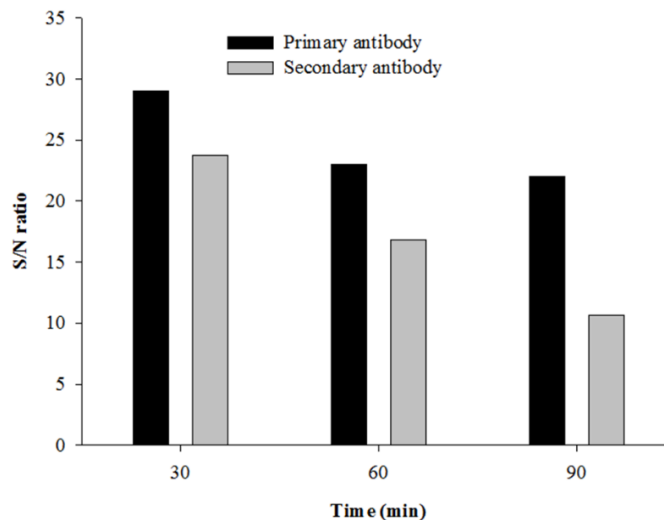


Figure 3.7: Signal to noise ratio over different incubation period of primary and secondary antibodies at 37°C. The signal-to-noise ratio was calculated by dividing the absorbance of test sample (40 mJ/cm² irradiated oocysts) by the absorbance of negative control (non-irradiated oocysts).

3.2.3 Indirect ELISA to detect UV photoproducts in DNA

Based on the results obtained from the optimization steps, the following parameters were selected: (i) Cuvette size: 400 μl ; (ii) primary antibody concentration: 2 $\mu\text{g/ml}$; (iii) secondary antibody concentration: 0.375 $\mu\text{g/ml}$; (iv) incubation period: 30 minutes; (v) incubation temperature: 37°C. Using these parameters as optimum, the protocol of ELISA was used to detect whether the absorbance can be correlated with the degree of damage in *Cryptosporidium* oocysts after UV treatment. In order to run the experiment, *Cryptosporidium* oocysts were treated with 40, 10, 6, 3 and 0 mJ/cm^2 UV doses before DNA extraction. The extracted ssDNA of irradiated oocysts tested by indirect ELISA method and the absorbance were detected by spectrophotometer (as described in Section 3.2.1). For statistical analysis, three trials of ELISA test were done for each irradiated oocysts.

3.2.4 Results

The average absorbances revealed from the test were 1.127, 0.600, 0.580, 0.185 and 0.098 for 40, 10, 6, 3 and 0 mJ/cm^2 UV irradiated oocysts respectively. The standard deviation was calculated 0.021, 0.010, 0.010, 0.003 and 0.010 for 0 mJ/cm^2 UV irradiated oocysts respectively. In order to observe the correlation between UV damage and the signal obtained from CPD-antibody reaction, the absorbance of each UV dose was plotted and fit with an exponentially rise curve in Figure 3.8. As increase in absorbance represents more CPDs are present, Figure 3.8 showed a significant exponential rise to maximum (slope 0.084, R^2 0.95, intercept 1.16) of absorbance with the increase of UV doses indicating more DNA damage and the plateau was reached before 40 mJ/cm^2 which agrees well with current regulations.

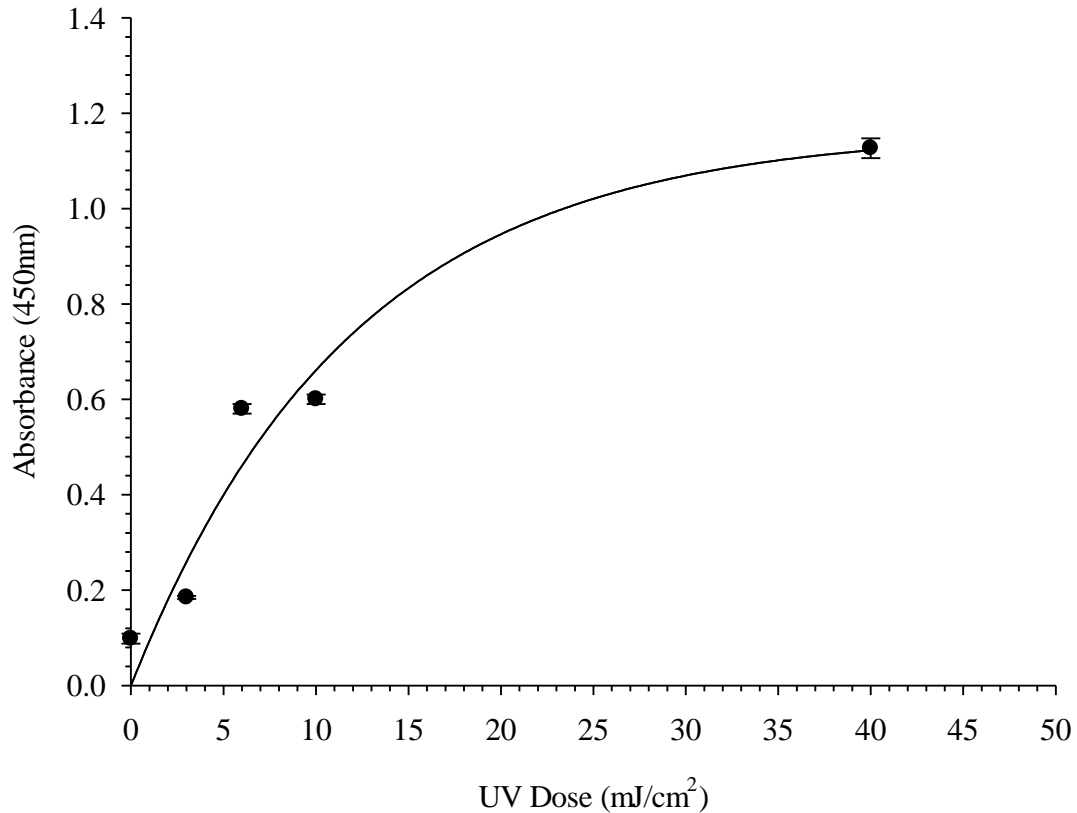


Figure 3.8: Dose response curve to detect CPDs in *Cryptosporidium* oocysts irradiated with different doses of UV light. Symbols represent the average of 3 analyses, error bars are one standard deviation. The line represents the fit to an exponential curve. DNA extracted from 0, 3, 6, 10 & 40 mJ/cm² irradiated oocysts were added into 400 μ l size cuvettes coated with protamine sulfate. For each cuvettes 2 μ g/ml primary antibody and 0.375 μ g/ml of secondary antibody were added. The incubation period of 30 minutes and incubation temperature of 37°C were used for both antibody incubation. Upon addition of substrate (color changed to blue) and stop solution (color changed to yellow) in the cuvettes, the absorbance was measured at 450nm wavelength

3.3 Validating ELISA results via microscopy

To validate the results obtained from ELISA technique, the UV irradiated oocysts were examined using epifluorescence microscopy according to the protocol established by Al-Adhami et al. (2007).

3.3.1 Methods

From the samples spiked with oocysts (10⁵/ml) irradiated at 40 mJ/cm² UV doses, 30 μ l of each were individually pipetted onto two wells of sticky slides and air dried for 1 hour at 37°C in a slide moat microscope slide incubator. The slides were treated with freeze-thaw method to facilitate the localization of the antibody in the nuclei of UV

exposed sporozoites within intact oocysts. The air dried slides were exposed to 3 cycles of freezing and thawing for 10 min at -80°C and 75°C respectively. After freeze thaw, slides were fixed with absolute methanol and subsequently washed and blocked with blocking solution (HBSS containing 0.2% Triton X-100 and 5% dried skim milk) for one hour at room temperature. Then washed again in wash solution (1% dried skim milk in HBSS) followed by incubation at 37°C for 30 min and then overnight at 4°C with anti-CPD TDM-2 mouse monoclonal antibodies (Cosmo Bio CO., Japan). After incubation, slides were washed 3 times for 5 min and drained followed by incubation with anti-Mouse IgG Alexa Flour 555 labelled antibodies (Thermo Fisher Scientific, USA) at 37°C for an hour. After incubation with secondary antibody slides were washed 3 times for 5 min with wash solution and twice for 5 mins in HBSS (Appendix A). Slides were counterstained with DAPI (1: 5,000 dilution; Waterborne™ Inc., USA) at room temperature for 5 min with subsequent washing in HBSS. Then air dried and mounted with fluorescence No-Fade™ mounting medium (Waterborne™ Inc., USA).

Slides were analyzed by epifluorescence microscopy (see Section 2.2.2) to observe the presence of CPDs (red fluorescence due to Alexa Flour 555) in the DNA (blue fluorescence due to DAPI). A black and white camera (AxioCam MRm) was used to collect the images because this camera has increased sensitivity to allow the visualization of fluorescence due to the binding of Alexa Flour with the CPD positive DNA.

3.3.2 Results

Using fluorescence excitation/emission filters of the microscope, the presence of CPDs in the DNA of the UV irradiated oocysts was observed. Figure 3.9 represents an example image of a microscopic field of a slide containing 40 mJ/cm² UV irradiated oocysts. Images were taken using a black and white camera where the white areas in

Figure 3.9a corresponded to CPD positive DNA excited with Alexa Flour 555 fluorescence excitation/emission and in Figure 3.9b corresponded to DAPI stained DNA excited with DAPI fluorescence excitation/emission. No white area was found in case of the microscopic field with DNA from non-irradiated oocysts when image was taken with Alexa Flour excitation (Figure 3.10 a) indicating the absence of the UV photoproducts. The presence of DAPI stained DNA is evident from Figure 3.10 b presenting the same microscopic field. Table 3.5 was generated by analyzing 10 random microscopic fields for both non-irradiated and irradiated *Cryptosporidium* oocysts (Appendix B, Table B.8) where it was found that in case of 40 mJ/cm² irradiated oocysts, the presence of CPD was detected in 63% of the total areas indicating DNA. Areas corresponding to DNA with CDPs were absent in non-irradiated oocysts.

Table 3.5: Presence of CPD in the DNA of non-irradiated and irradiated *Cryptosporidium* oocysts

UV exposure	% CPD indicating areas in the microscopic field
0 mJ/cm ²	0%
40 mJ/cm ²	63%

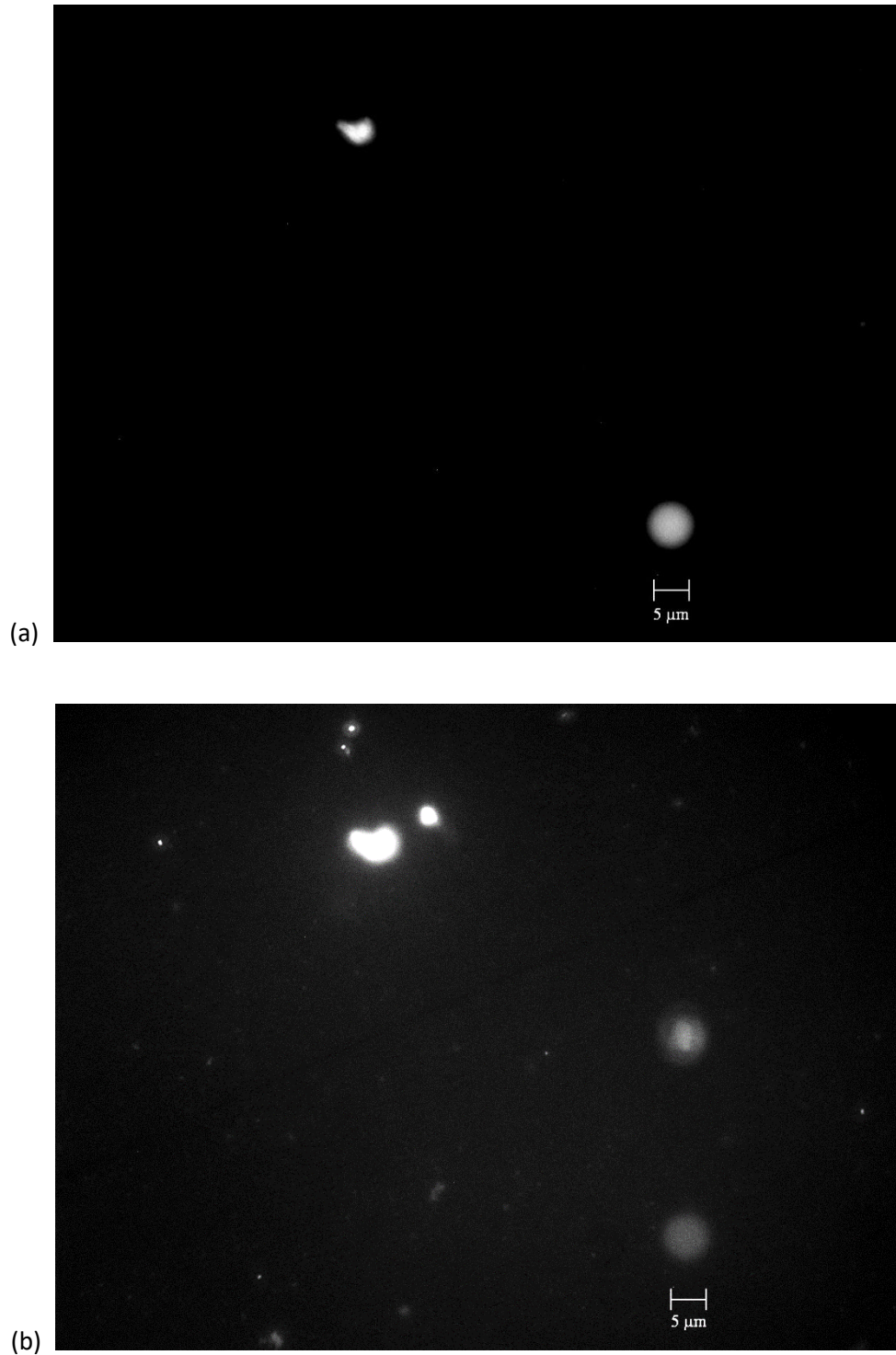


Figure 3.9: Black and white images of 40 mJ/cm² UV radiation treated *Cryptosporidium* DNA taken with (a) Alexa fluorescence excitation and (b) DAPI fluorescence excitation using epifluorescence microscope. Irradiated oocysts were fixed on glass slides and had undergone freeze-thaw process to facilitate the localization of antibodies. Slides were incubated with anti-CPD primary antibodies for 24 hours and Alexa fluor 555 labelled secondary antibody for 1 hour. Slides were then stained with DAPI and observed under epifluorescence microscope using 100x oil immersion objective lens.

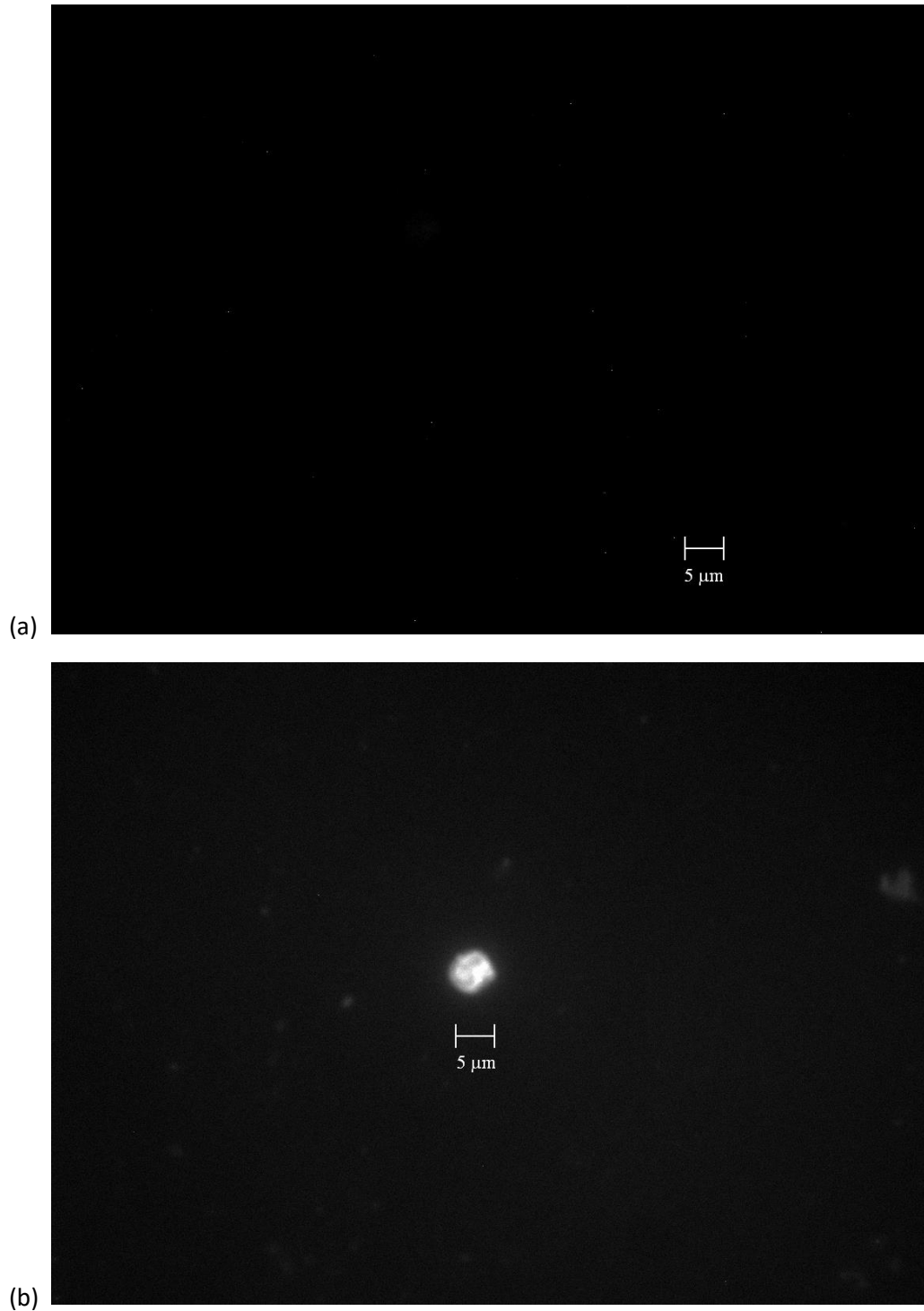


Figure 3.10: Black and white images of UV non-irradiated *Cryptosporidium* DNA taken with (a) Alexa fluorescence excitation and (b) DAPI fluorescence excitation using epifluorescence microscope. Non-irradiated oocysts were fixed on glass slides and had undergone freeze-thaw process to facilitate the localization of antibodies. Slides were incubated with anti-CPD primary antibodies for 24 hours and Alexa fluor 555 labelled secondary antibody for 1 hour. Slides were then stained with DAPI and observed under epifluorescence microscope using 100x oil immersion objective lens.

It can be seen from Figure 3.11 DNA was not necessarily confined within the oocyst during this experiment, where the oocysts stained with Crypt-a-Glo appeared green and DNA stained with DAPI appeared blue under fluorescence excitation/emission. This may have occurred due to the damage of the oocysts that happened during conducting freeze-thaw step of the experiment resulting in the leakage of DNA from the cyst structure. This was taken into account during detecting the presence of UV photoproducts (CPD) in DNA. For each microscopic field only the white spots corresponding to CPD positive DNA and the white spots presenting DAPI stained DNA were counted as an indicator of damage, ignoring the Crypt-a-Glo stained areas. The presence of Crypt-a-Glo generated fluorescence is associated with the presence of the oocyst structure. As the main concern was the detection of DNA not the oocyst itself, the white areas corresponding to Crypt-a-Glo fluorescence excitation were not included in the analysis.

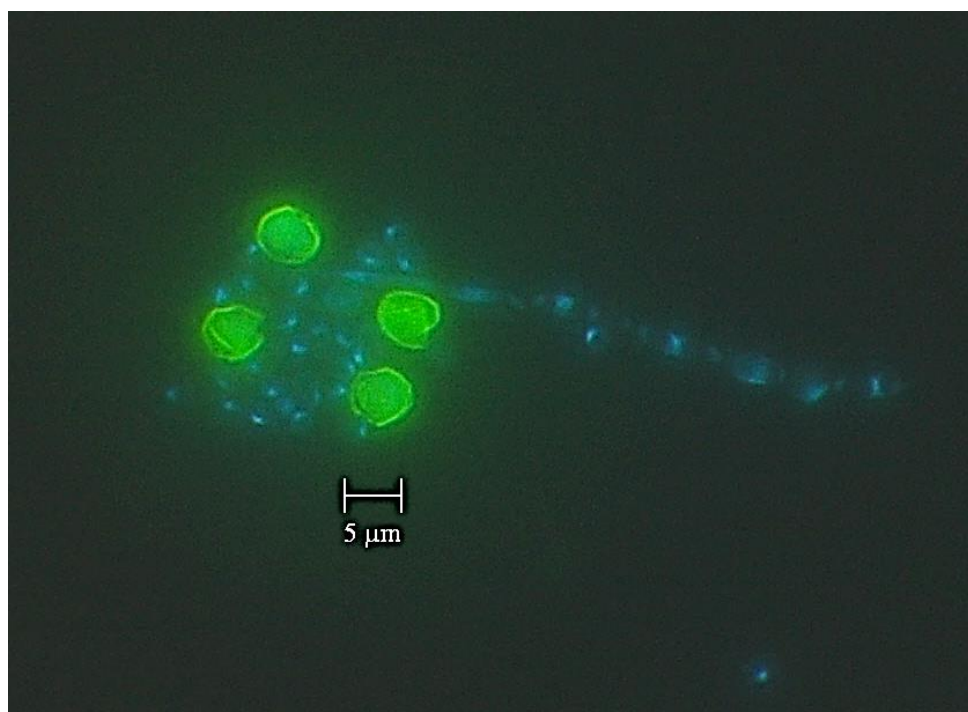


Figure 3.11: Crypt-a-Glo stained *Cryptosporidium* oocysts with DAPI stained DNA under epifluorescence microscope. Blue fluorescence due to DAPI indicated non-damaged DNA. Crypto-glow stain bound with oocyst cell wall and the oocysts appeared green. Oocysts were observed under 100x oil immersion objective lens.

3.4 Discussion

The detection of DNA damage in UV irradiated *Cryptosporidium* oocysts involved identification of CPD photoproducts within *Cryptosporidium* DNA. ELISA technique was used in this research to detect CPDs by using antibodies specific for these UV induced photoproducts. ELISA technique is a commonly used immunological assay for diagnostics and clinical research with limited application in case of environmental samples (Tighe et al., 2015). Following the basic principles, an ELISA was developed to meet the needs of this specific research for the environmental samples. Before developing ELISA an ideal DNA extraction method was selected which would ensure maximum DNA recovery. This optimization step was required as environment samples, unlike clinical samples, contain low number of oocysts and good number of solids which could cause low DNA recovery upon extraction (Guy et al., 2003; Adamska et al., 2010). In addition, chemically resistant oocyst wall of *Cryptosporidium* complicates the extraction procedure (Belli, 2006).

Five commercially available DNA extraction kits selected through literature review were compared to overcome these barriers. The evaluation process was done by comparing the efficiency in terms of recovering DNA from minimum concentration of oocysts and removing solids in water sample. Among the five kits, only PowerSoil DNA isolation kit efficiently recovered DNA from the sample containing as low as 10 oocysts/ml in the presence of high amount of solids (2.40 µg/ml). Results also showed that freeze thaw treatment was not necessary when extracting DNA using this kit. In some cases, freeze thaw actually worked adversely for the kit. This may be due to the loss of DNA from very low concentration of oocysts during this additional physical treatment step (Brunstein et al., 2015). One of the major reasons of getting better performance using PowerSoil DNA isolation kit was the lysis mechanism used by the kit. It included both

physical (bead bashing) and chemical (SDS) treatment to facilitate the recovery from low number of oocysts. The other reason was incorporation of better PCR inhibitor removal technology which yielded clean DNA through efficient removal of solids from the sample.

Although ELISA is a well established method for immunoassay, protocol optimization for specific study is essential to get optimal result. The basic procedure of ELISA for this study was conceived from the protocol given by anti-CPD antibody manufacturer Cosmo Bio Co. where indirect ELISA technique was followed (Cosmo Bio Co. Ltd., Japan). This was developed for clinical sample on an ELISA 96 well plate. During this research a cuvette was used instead of ELISA plate to perform the ELISA reaction and the signal was measured by the spectrophotometer. The reasons for selecting spectrophotometer has been described earlier in the introduction chapter. As cuvettes are not common for ELISA, at first the cuvette of appropriate size was selected before optimizing other parameters. To do so, ELISA was done in three different size of cuvettes and evaluated in terms of signal intensity and signal to noise ratio. The bottom of large cuvette was wide open and other two (medium and small) was narrow, requires at least 800, 400 and 50 μ l of reaction volume for being detectable by spectrophotometer respectively. The original protocol given by the manufacturer (other than DNA concentration) was used for 50 μ l cuvette where 50 μ l of extracted DNA was used in contrast to 4X or 8X more (in volume) with 400 μ l and 800 μ l cuvette respectively. However, ELISA conducted in 50 μ l cuvette revealed <0.6 absorbance compared to the value (>1.2) revealed with 400 μ l and 800 μ l cuvettes. According to the manufacturer protocol, the optimum signal should be >1.5 when 40UV irradiated oocysts with 0.2 μ g/ml DNA used for ELISA. In this study, the initial volume of sample for DNA extraction was 250 μ l containing 5X10⁵ oocysts/ml which approximately yielded 0.06 μ g/ml DNA in 100

μl eluate. As comparatively low amount of DNA was used during ELISA, this could be the one possible reason to get low signal all through the study compared to the referred value. But it would not be rational to expect more DNA in environmental sample due to low microbial load. On the other hand, 50 μl and 400 μl cuvettes produced high signal to noise ratio compare to 800 μl cuvette. Considering low sensitivity of 50 μl cuvette and low signal noise ratio of 800 μl cuvette, 400 μl cuvette was selected for this study.

Appropriate dilution of antibodies is very important as it determines the sensitivity and signal noise ratio of the ELISA test (Kuen et al., 1993). According to the manufacturers instruction the working dilution for ELISA was 1:1000 (2 $\mu\text{g/ml}$) and 1:40,000 (0.375 $\mu\text{g/ml}$) for primary and secondary antibody respectively. In order to optimize the dilution for this study, both primary and secondary antibodies were evaluated together in single cuvettes with nine different combinations of antibody concentration. The combinations were made of three different concentrations of primary (1, 2 and 4 $\mu\text{g/ml}$) and secondary antibody (0.3, 0.375 and 0.5 $\mu\text{g/ml}$). Absorbance was less than 0.6 when 1 $\mu\text{g/ml}$ of primary antibody was used with any concentration of secondary antibody. The absorbance remained mostly around 1.0 when the concentration of primary antibody was increased up to 2 or 4 $\mu\text{g/ml}$ with the any combination of secondary antibody concentration. In order to save reagent, 2 $\mu\text{g/ml}$ concentration of primary antibody was selected for this study which represents 1:1000 dilution in the manufacturer instruction. The concentration of secondary antibody was selected based on the signal-noise ratio from the ELISA. According to the result, the signal-noise ratio was revealed to be 25 when the concentration used for secondary antibody between 0.3-0.375 $\mu\text{g/ml}$ which dropped below 6 when the concentration increased up to 0.5 $\mu\text{g/ml}$. From these concentrations, secondary antibody 0.375 $\mu\text{g/ml}$ (1: 40,000) was selected because this combined with any combination of primary antibody gave better signal with high

signal to noise ratio. As the results coincided with the manufacturer's recommendation, 2 µg/ml for primary antibody and 0.375 µg/ml for secondary antibody were selected as an optimized concentration for the ELISA in this study.

The duration of antigen-antibody or antibody-antibody reaction time influences the result of ELISA (Shah and Maghsoudlou, 2016). Both primary and secondary antibody were evaluated for three different incubation periods (30, 60 and 90 mins). No impact was observed with the primary antibody but for the secondary antibody the signal-noise ratio decreased with the increase in incubation time. The best signal with high ratio was found with 30 minutes of incubation. No significance differences were found with the change in incubation temperatures (37°C vs 4°C). From these findings 30 mins and 37°C were selected as optimum incubation period and incubation temperature.

Using the optimized protocol, DNA extracted from *Cryptosporidium* oocysts irradiated at 0, 3, 6, 10 and 40 mJ/cm² UV doses were tested to detect the presence of CPDs by using ELISA in cuvette technique. The value of UV dose increases with the duration of exposure of the light from same light source and distance which hypothesized the statement that the longer the duration will generate larger the number of CPDs in DNA. An exponential rise to maximum curve constructed using the data points from ELISA results clearly showed that the increase in UV doses was responsible for the increased level of damage in DNA. The higher the absorbance value, the higher the amount of photoproducts present in the DNA (Matsunaga et al., 1993).

The result obtained from this customized ELISA protocol was validated by conducting microscopy of the irradiated oocysts. The microscopic experiment for DNA damage detection was done following the protocol established by Al-Adhami et al. (2007). The microscopic observation indicated the presence of photoproducts in UV irradiated oocysts whereas absence in non-irradiated ones thereby supporting the ELISA

experiment. These findings suggest that UV treatment is responsible for causing DNA damage within *Cryptosporidium* oocysts and it is possible to detect this DNA damage using the ELISA protocol developed during this research. This could replace the laborious, expensive as well as subjective microscopic procedure. Al-Adhami (2007) also showed that UV irradiated oocysts did not cause any infection when injected in the mouse compared to non-irradiated oocysts suggesting the efficiency of UV treatment in terms of disinfection. As it is not feasible for the water treatment companies to carry out infectivity assays, this ELISA would allow the process operators to determine the efficiency of UV treatment system by detecting DNA damage in the oocysts following the treatment.

Chapter 4 Conclusions

4.1 Concluding remarks

The first objective of this research work was to develop an antibody based capture surface to detect *Cryptosporidium* oocysts in treated water with increased capture capability and specificity. The antibody activated surface developed during this research was able to capture three different species of *Cryptosporidium*: *C. parvum*; *C. muris*; *C. hominis*. This finding shows that these anti-*Cryptosporidium* antibodies are genus specific rather than species specific though they have been raised against intact oocysts of *C. parvum*. Cross reactivity test with *E. coli* proved that the capture surface was specific for *Cryptosporidium* oocysts, thereby suggesting the chances of capturing microorganisms other than *Cryptosporidium* from water are low. The capture efficiency of IgG3 (~84%-90%) was higher than that of IgG1 (~54%-74%) for all three *Cryptosporidium* species suggesting that IgG3 would be the ideal candidate for the capture surface development to ensure maximum recovery of *Cryptosporidium* oocysts. Another important finding is the effect of pH on the captured oocysts release process. It was observed that oocysts were released successfully from the capture surface when exposed to pH 1.0, thereby losing antibodies from the surface as well making the surface unfit for reuse.

The second objective described an opportunity for water research companies to expand its service with the ability to detect DNA damage in *Cryptosporidium* after UV treatment in water purification plant. This study optimized an indirect ELISA protocol in cuvette for water samples to detect the UV induced photoproducts (CPDs) in the DNA of *Cryptosporidium* oocysts using spectrophotometer. During the optimization process, Power soil kit was selected as a DNA extraction kit because of its high recovery from low concentration of *Cryptosporidium* and high concentration of solids. The key parameters of ELISA were optimized based on the higher signal intensity and S/N ratio. The

optimized ELISA protocol was applied on the samples spiked with *Cryptosporidium* oocysts irradiated at different doses (0, 3, 6, 10 and 40 mJ/cm²) of UV light. The signal generated from DNA-antibody reaction was plotted which resulted in an exponentially rise to maximum curve. The curve showed that the absorbance which indicated the presence of DNA damage increased with the increase of UV doses. Microscopy result from this study and other studies (Al-Adhami et al., 2007) also supported the ELISA results. This is a proof of concept which indicates that the optimized ELISA protocol is capable to measure the degree of damage which is correlated with UV doses.

4.2 Limitations of the study

1. Cross reactivity of the capture surface was done only with *E. coli*. There are many waterborne pathogens against which this device should be tested.
2. The capture test was carried out in static conditions.
3. During developing the ELISA protocol, extracted DNA concentration could not be measured using a spectrophotometer due to low oocyst concentrations in environmental samples.
4. The DNA damage induced by UV treatment was not validated in vivo to ensure the loss of infectivity of *Cryptosporidium* oocysts due to complexity of handling animal models and time constraints.

4.3 Future recommendations

1. During this research the capture experiment was carried out with oocysts in static water to determine the capture ability & specificity of the selected antibodies. The next step could be implementation of this technique with oocysts in flowing water to determine the effect of flow rate on the oocysts capture to mimic the actual capture condition.

2. As it was not possible to regenerate the capture surface using pH dependent release mechanism, the future work would be to look into other properties of antigen-antibody bindings such as conformational changes based on hydrophobic-hydrophilic interactions rather than ionic changes in order to reuse the surface. It would also be wise to perform an economic analysis to determine whether the analysis would be commercially acceptable without the reusability.
3. Completion of the development of electrical sensing technology to replace the microscopy based detection step. This could be done by incorporating this antibody based capture surface into a biosensor using gold interdigitated electrodes capacitor arrays. This step is under development in the School of Engineering of the University of British Columbia (Okanagan).
4. For DNA damage detection, the ELISA protocol optimized for environmental samples was carried out in a cuvette but was not compared with a microtiter plate. In the future this ELISA in cuvette should be compared with ELISA in plate to validate the findings.
5. The overall absorbance was not as high as clinical samples due to low DNA concentration (0.06 $\mu\text{g/ml}$) in the environmental samples. In fact, in actual environmental samples the concentration of DNA might be lower than the concentration used in this experiment. This might cause very low signal even with 40 mJ/cm^2 UV irradiated *Cryptosporidium* oocysts. In the future, the study should be designed to determine the DNA detection limit of this ELISA technique designed for environmental samples.
6. The analysis of UV treatment efficiency should be expressed as the ratio of damaged DNA to total DNA instead of presence of damaged DNA only.

7. The dose response curve was explored for the following UV doses 0, 3, 6, 10 & 40 mJ/cm². UV doses between 10 to 40 mJ/cm² should be checked in the future as well to fully determine the shape of the curve and the true signal threshold level vs. DNA damage.
8. Though the literature supports that the UV irradiated oocysts failed to cause infection in mice models, this ELISA result should be confirmed in the future by using animal models.

References

- Abe, N., Sawano, Y., Yamada, K., Kimata, I., & Iseki, M. (2002). *Cryptosporidium* infection in dogs in Osaka, Japan. *Veterinary Parasitology*, 108(3), 185-193.
- Abrahamsen, M. S., Templeton, T. J., Enomoto, S., Abrahante, J. E., Zhu, G., Lancto, C. A., . . . Kapur, V. (2004). Complete genome sequence of the apicomplexan, *Cryptosporidium parvum*. *Science*, 304(5669), 441-445.
- Adamska, M., Leonska-Duniec, A., Maciejewska, A., Sawczuk, M., & Skotarczak, B. (2010). Comparison of efficiency of various DNA extraction methods from cysts of *Giardia intestinalis* measured by PCR and taqman real time PCR. *Parasite-Journal De La Societe Francaise De Parasitologie*, 17(4), 299-305.
- Akerstrom, B., & Bjorck, L. (1986). A physicochemical study of protein-G, a molecule with unique immunoglobulin-G-binding properties. *Journal of Biological Chemistry*, 261(22), 240-247.
- Akerstrom, B., Brodin, T., Reis, K., & Bjorck, L. (1985). Protein-G - a powerful tool for binding and detection of monoclonal and polyclonal antibodies. *Journal of Immunology*, 135(4), 2589-2592.
- Akerstrom, B., Nielsen, E., & Bjorck, L. (1987). Definition of IgG-binding and albumin-binding regions of streptococcal protein-G. *Journal of Biological Chemistry*, 262(28), 13388-13391.
- Al-Adhami, B. H., Nichols, R. A. B., Kusel, J. R., O'Grady, J., & Smith, H. V. (2007). Detection of UV-induced thymine dimers in individual *Cryptosporidium parvum* and *Cryptosporidium hominis* oocysts by immunofluorescence microscopy. *Applied and Environmental Microbiology*, 73(3), 947-955.
- Alves, N. J., Kiziltepe, T., & Bilgicer, B. (2012). Oriented surface immobilization of antibodies at the conserved nucleotide binding site for enhanced antigen detection. *Langmuir*, 28(25), 9640-9648.
- ASTM (1991). American Society for Testing and Materials. *Annual Book of ASTM Standards*. Philadelphia: ASTM.
- Avrameas, S. (1969). Coupling of enzymes to proteins with glutaraldehyde: Use of conjugates for detection of antigens and antibodies. *Immunochemistry*, 6(1), 43-52.
- Bae, Y. M., Oh, B., Lee, W. H., Lee, W., & Choi, J. (2005). Study on orientation of immunoglobulin G on protein G layer. *Biosensors and Bioelectronics*, 21(1), 103-110.
- Baio, J. E., Cheng, F., Ratner, D. M., Stayton, P. S., & Castner, D. G. (2011). Probing orientation of immobilized humanized anti-lysozyme variable fragment by time-of-flight secondary-ion mass spectrometry. *Journal of Biomedical Materials Research Part a*, 97A(1), 1-7.

- Baker, J., Muller, R., & Rollinson, D. (2005). *Advances in Parasitology* (1st ed.). USA: Academic Press.
- Balajee, A., May, A., & Bohr, V. (1999). DNA repair of pyrimidine dimers and 6-4 photoproducts in the ribosomal DNA. *Nucleic Acids Research*, 27(12), 2511-2520.
- Baldursson, S., & Karanis, P. (2011). Waterborne transmission of protozoan parasites: Review of worldwide outbreaks - an update 2004-2010. *Water Research*, 45(20), 6603-6614.
- Balevicius, Z., Ramanaviciene, A., Baleviciute, I., Makaraviciute, A., Mikoliunaite, L., & Ramanavicius, A. (2011). Evaluation of intact- and fragmented-antibody based immunosensors by total internal reflection ellipsometry. *Sensors and Actuators B-Chemical*, 160(1), 555-562.
- Bankier, A., Spriggs, H., Fartmann, B., Konfortov, B., Madera, M., Vogel, C., . . . Dear, P. (2003). Integrated mapping, chromosomal sequencing and sequence analysis of *Cryptosporidium parvum*. *Genome Research*, 13(8), 1787-1799.
- Barbosa, L. R. S., Ortore, M. G., Spinozzi, F., Mariani, P., Bernstorff, S., & Itri, R. (2010). The importance of protein-protein interactions on the pH-induced conformational changes of bovine serum albumin: A small-angle X-ray scattering study. *Biophysical Journal*, 98(1), 147-157.
- Baxter, H. C., Richardson, P. R., Campbell, G. A., Kovalev, V. I., Maier, R., Barton, J. S., . . . Baxter, R. L. (2009). Application of epifluorescence scanning for monitoring the efficacy of protein removal by RF gas-plasma decontamination. *New Journal of Physics*, 11, 115028.
- Belli, S. I., Smith, N. C., & Ferguson, D. J. P. (2006). The coccidian oocyst: A tough nut to crack! *Trends in Parasitology*, 22(9), 416-423.
- Belosevic, M., Guy, R. A., Taghi-Kilani, R., Neumann, N. F., Gyürék, L. L., Liyanage, L. R. J., . . . Finch, G. R. (1997a). Nucleic acid stains as indicators of *Cryptosporidium parvum* oocyst viability. *International Journal for Parasitology*, 27(7), 787-798.
- Belosevic, M., Taghi-Kilani, R., Guy, R. A., Neumann, N. F., Finch, G. R., Gyürék, L. L., Liyanage, L. R. J. (1997b). *Vital Dye Staining of Giardia and Cryptosporidium*. Denver: AWWA Research Foundation and American Water Works Association.
- Bereli, N., Sener, G., Yavuz, H., & Denizli, A. (2011). Oriented immobilized anti-LDL antibody carrying poly (hydroxyethyl methacrylate) cryogel for cholesterol removal from human plasma. *Materials Science & Engineering C-Materials for Biological Applications*, 31(5), 1078-1083.
- Bjorck, L., & Kronvall, G. (1984). Purification and some properties of streptococcal protein-G, protein-a novel IgG-binding reagent. *Journal of Immunology*, 133(2), 969-974.

- Black, E., Finch, G., TaghiKilani, R., & Belosevic, M. (1996). Comparison of assays for *Cryptosporidium parvum* oocysts viability after chemical disinfection. *FEMS Microbiology Letters*, 135(2-3), 187-189.
- Blunt, D., Khramtsov, N., Upton, S., & Montelone, B. (1997). Molecular karyotype analysis of *Cryptosporidium parvum*: Evidence for eight chromosomes and a low-molecular-size molecule. *Clinical and Diagnostic Laboratory Immunology*, 4(1), 11-13.
- Bolton, J. R. (2001). *Ultraviolet Applications Handbook* (2nd ed.). Ontario: Bolton Photosciences Inc.
- Bolton, J. R., Cotton, C. A. (2008). Knovel, Academic, Environment & Environmental Engineering, & Ebrary Academic Complete (Canada) Subscription Collection. *The ultraviolet disinfection handbook* (1st ed.). Denver, CO: American Water Works Association.
- Bonnin, A., Gut, J., Dubremetz, J., Nelson, R., & Camerlynck, P. (1995). Monoclonal-antibodies identify a subset of dense granules in *Cryptosporidium parvum* zoites and gamonts. *Journal of Eukaryotic Microbiology*, 42(4), 395-401.
- Borrebaeck, C. (2000). Antibodies in diagnostics - from immunoassays to protein chips. *Immunology Today*, 21(8), 379-382.
- Brash, D. (1988). UV mutagenic photoproducts in *Escherichia coli* and human cells - a molecular genetics perspective on human skin cancer. *Photochemistry and Photobiology*, 48(1), 59-66.
- Bridle, H., Kersaudy-Kerhoas, M., Miller, B., Gavriilidou, D., Katzer, F., Innes, E. A., & Desmulliez, M. P. Y. (2012). Detection of *Cryptosporidium* in miniaturized fluidic devices. *Water Research*, 46(6), 1641-1661.
- Brunstein, J. (2015). *Freeze-thaw cycles and nucleic acid stability: What's safe for your samples?*. United States: NP Communications, LLC.
- Bukhari, Z., McCuin, R., Fricker, C., & Clancy, J. (1998). Immunomagnetic separation of *Cryptosporidium parvum* from source water samples of various turbidities. *Applied and Environmental Microbiology*, 64(11), 4495-4499.
- Buret, A., Chin, A., & Scott, K. (2003). Infection of human and bovine epithelial cells with *Cryptosporidium andersoni* induces apoptosis and disrupts tight junctional ZO-1: Effects of epidermal growth factor. *International Journal for Parasitology*, 33(12), 1363-1371.
- Bushkin, G. G., Motari, E., Carpentieri, A., Dubey, J. P., Costello, C. E., Robbins, P. W., & Samuelson, J. (2013). Evidence for a structural role for acid-fast lipids in oocyst walls of *Cryptosporidium*, *Toxoplasma*, and *Eimeria*. *Mbio*, 4(5), e00387-13.
- Cacciò, S. M., Thompson, R. C. A., McLauchlin, J., & Smith, H. V. (2005). Unravelling *Cryptosporidium* and *Giardia* epidemiology. *Trends in Parasitology*, 21(9), 430-437.

- Campbell, A., Robertson, L., & Smith, H. (1992). Viability of *Cryptosporidium parvum* oocysts - correlation of invitro excystation with inclusion or exclusion of fluorogenic vital dyes. *Applied and Environmental Microbiology*, 58(11), 3488-3493.
- Carey, C., Lee, H., & Trevors, J. (2004). Biology, persistence and detection of *Cryptosporidium parvum* and *Cryptosporidium hominis* oocyst. *Water Research*, 38(4), 818-862.
- CDC (USA) (2016). Centers for Disease Control and Prevention. Cryptosporidiosis. DPDx-Laboratory identification of parasitic diseases of public health concern. Retrieved March 16, 2017, from <https://www.cdc.gov/dpdx/cryptosporidiosis/>
- Chalmers, R., Elwin, K., Thomas, A., Guy, E., & Mason, B. (2009). Long-term *Cryptosporidium* typing reveals the aetiology and species-specific epidemiology of human cryptosporidiosis in England and Wales, 2000 to 2003. *Eurosurveillance*, 14(2), 6-14.
- Chatterjee, A., Banerjee, S., Steffen, M., O'Connor, R. M., Ward, H. D., Robbins, P. W., & Samuelson, J. (2010). Evidence for mucin-like glycoproteins that tether sporozoites of *Cryptosporidium parvum* to the inner surface of the oocyst wall. *Eukaryotic Cell*, 9(1), 84-96.
- Chauret, C., Radziminski, C., Lepuil, M., Creason, R., & Andrews, R. (2001). Chlorine dioxide inactivation of *Cryptosporidium parvum* oocysts and bacterial spore indicators. *Applied and Environmental Microbiology*, 67(7), 2993-3001.
- Chen, X., Keithly, J. S., Paya, C. V., & LaRusso, N. F. (2002). Cryptosporidiosis. *The New England Journal of Medicine*, 346(22), 1723-1731.
- Cho, I., Park, J., Lee, T. G., Lee, H., & Paek, S. (2011). Biophysical characterization of the molecular orientation of an antibody-immobilized layer using secondary ion mass spectrometry. *Analyst*, 136(7), 1412-1419.
- Chung, E., Aldom, J., Carreno, R., Chagla, A., Kostrzynska, M., Lee, H., . . . De Grandis, S. (1999). PCR-based quantitation of *Cryptosporidium parvum* in municipal water samples. *Journal of Microbiological Methods*, 38(1-2), 119-130.
- Clancy, J., Hargy, T., Marshall, M., & Dyksen, J. (1998). UV light inactivation of *Cryptosporidium* oocysts. *Journal American Water Works Association*, 90(9), 92-102.
- Cleaver, J., Cortes, F., Lutze, L., Morgan, W., Player, A., & Mitchell, D. (1987). Unique DNA repair properties of a xeroderma-pigmentosum revertant. *Molecular and Cellular Biology*, 7(9), 3353-3357.
- Cleaver, J., Cortes, F., Karentz, D., Lutze, L., Morgan, W., Player, A., . . . Mitchell, D. (1988). The relative biological importance of cyclobutane and (6-4) pyrimidine-pyrimidone dimer photoproducts in human cells - evidence from a xeroderma pigmentosum revertant. *Photochemistry and Photobiology*, 48(1), 41-49.

- Corso, P., Kramer, M., Blair, K., Addiss, D., Davis, J., & Haddix, A. (2003). Cost of illness in the 1993 waterborne *Cryptosporidium* outbreak, Milwaukee, Wisconsin. *Emerging Infectious Diseases*, 9(4), 426-431.
- Cosmo Bio Co. Ltd., Japan. Retrieved January 18, 2017, from http://search.cosmobio.co.jp/cosmo_search_p/search_gate2/docs/CAC_/NMDND001.20161130.pdf
- Coupe, S., Sarfati, C., Hamane, S., & Derouin, F. (2005). Detection of *Cryptosporidium* and identification to the species level by nested PCR and restriction fragment length polymorphism. *Journal of Clinical Microbiology*, 43(3), 1017-1023.
- Current, W. L. (1990). Techniques and laboratory maintenance of *Cryptosporidium*. In J. P. Dubey, C. A. Speer & R. Fayer (Eds), *Cryptosporidiosis of man and animals* (pp. 31-49). Boca Raton, FL: CRC Press.
- D' Antonio, R., Winn, R., Taylor, J., Gustafson, T., Current, W., Rhodes, M., . . . Zajac, R. (1985). A waterborne outbreak of cryptosporidiosis in normal hosts. *Annals of Internal Medicine*, 103(6), 886-888.
- Das, R. (2010). *Cryptosporidium* detection through antibody immobilization on a solid surface University of British Columbia.
- Devanaboyina, S. C., Lynch, S. M., Ober, R. J., Ram, S., Kim, D., Puig-Canto, A., . . . Gao, C. (2013). The effect of pH dependence of antibody-antigen interactions on subcellular trafficking dynamics. *Mabs*, 5(6), 851-859.
- Di Giovanni, G., Hashemi, F., Shaw, N., Abrams, F., LeChevallier, M., & Abbaszadegan, M. (1999). Detection of infectious *Cryptosporidium parvum* oocysts in surface and filter backwash water samples by immunomagnetic separation and integrated cell culture-PCR. *Applied and Environmental Microbiology*, 65(8), 3427-3432.
- DVGW German Technical and Scientific Association for Gas and Water (1997). UV systems for disinfection in drinking water supplies—requirements and testing. In *DVGW Standards and Guidelines*. Bonn, Germany.
- DVGW German Technical and Scientific Association for Gas and Water (2006). *UV devices for the disinfection for drinking water supply – Parts 1, 2 and 3*. Bonn, Germany.
- Ejima, D., Tsumoto, K., Fukada, H., Yumioka, R., Nagase, K., Arakawa, T., & Philo, J. S. (2007). Effects of acid exposure on the conformation, stability, and aggregation of monoclonal antibodies. *Proteins-Structure Function and Bioinformatics*, 66(4), 954-962.
- El Kadi, N., Taulier, N., Le Huerou, J. Y., Gindre, M., Urbach, W., Nwigwe, I., . . . Waks, M. (2006). Unfolding and refolding of bovine serum albumin at acid pH: Ultrasound and structural studies. *Biophysical Journal*, 91(9), 3397-3404.

- Elgert, K. D. (1996). Antibody Structure and Function. In *Immunology: Understanding the immune system*. New York: Wiley-Liss.
- Eliasson, M., Olsson, A., Palmcrantz, E., Wiberg, K., Inganas, M., Guss, B., . . . Uhlen, M. (1988). Chimeric IgG-binding receptors engineered from staphylococcal protein-A and streptococcal protein-G. *Journal of Biological Chemistry*, 263(9), 4323-4327.
- Engvall, E., & Perlmann, P. (1971). Enzyme-linked immunosorbent assay (elisa) quantitative assay of immunoglobulin-G. *Immunochemistry*, 8(9), 871-&.
- Entrala, E., Sbihi, Y., Sanchez-Moreno, M., & Mascaro, C. (2001). Antigen incorporation on *Cryptosporidium parvum* oocyst walls. *Memorias do Instituto Oswaldo Cruz*, 96(2), 233-235.
- Fahnestock, S., Alexander, P., Nagle, J., & Filpula, D. (1986). Gene for an immunoglobulin-binding protein from a group-G streptococcus. *Journal of Bacteriology*, 167(3), 870-880.
- Fahnestock, S. (1987). Cloned streptococcal protein-G genes. *Trends in Biotechnology*, 5(3), 79-83.
- Fairley, C. K., Sinclair, M. I., & Rizak, S. (1999). Monitoring not the answer to *Cryptosporidium* in water. *The Lancet*, 354(9183), 967-969.
- Farthing, M. J. (2000). Clinical aspects of human cryptosporidiosis. *Contributions to Microbiology*, 6, 50.
- Fayer, R. (1997). *Cryptosporidium and cryptosporidiosis*. Boca Raton: CRC Press.
- Fayer, R. (2010). Taxonomy and species delimitation in *Cryptosporidium*. *Experimental Parasitology*, 124(1), 90-97.
- Franco, E. J., Hofstetter, H., & Hofstetter, O. (2006). A comparative evaluation of random and site-specific immobilization techniques for the preparation of antibody-based chiral stationary phases. *Journal of Separation Science*, 29(10), 1458-1469.
- Friedberg, E. C., Walker, G. C., & Siede, W. (1995). *DNA repair and mutagenesis*. Washington, D.C: ASM Press.
- Gasser, R., & O'Donoghue, P. (1999). Isolation, propagation and characterization of *Cryptosporidium*. *International Journal for Parasitology*, 29(9), 1379-1413.
- Gentil, A., LePage, F., Margot, A., Lawrence, C., Borden, A., & Sarasin, A. (1996). Mutagenicity of a unique thymine-thymine dimer or thymine-thymine pyrimidine pyrimidone (6-4) photoproduct in mammalian cells. *Nucleic Acids Research*, 24(10), 1837-1840.
- Ghazy, A. A., Shafy, S. A., & Shaapan, R. M. (2015). Cryptosporidiosis in animals and man: 1. taxonomic classification, life cycle, epidemiology and zoonotic importance. *Asian Journal of Epidemiology*, 8(3), 48-63.

- Goh, S., Reacher, M., Casemore, D., Verlander, N., Chalmers, R., Knowles, M., . . . Richards, S. (2004). Sporadic cryptosporidiosis, North Cumbria, England, 1996-2000. *Emerging Infectious Diseases*, 10(6), 1007-1015.
- Guss, B., Eliasson, M., Olsson, A., Uhlen, M., Frej, A., Jornvall, H., . . . Lindberg, M. (1986). Structure of the IgG-binding regions of streptococcal protein-G. *Embo Journal*, 5(7), 1567-1575.
- Guy, R. A., Payment, P., Krull, U. J., & Horgen, P. A. (2003). Real-time PCR for quantification of *Giardia* and *Cryptosporidium* in environmental water samples and sewage. *Applied and Environmental Microbiology*, 69(9), 5178-5185.
- Haas, C. N., Rose, J. B., & Gerba, C. P. (1999). Analytical methods for developing occurrence and exposure databases. In C.N. Hass, J.B. Rose & C.P. Gerba (Eds.), *Quantitative microbial risk assessment* (pp. 137-161). New York: Wiley.
- Hallier-Soulier, S., & Guillot, E. (1999). An immunomagnetic separation polymerase chain reaction assay for rapid and ultra-sensitive detection of *Cryptosporidium parvum* in drinking water. *FEMS Microbiology Letters*, 176(2), 285-289.
- Han, H. J., Kannan, R. M., Wang, S., Mao, G., Kusanovic, J. P., & Romero, R. (2010). Multifunctional dendrimer-templated antibody presentation on biosensor surfaces for improved biomarker detection. *Advanced Functional Materials*, 20(3), 409-421.
- Hijnen, W., Beerendonk, E., & Medema, G. (2006). Inactivation credit of UV radiation for viruses, bacteria and protozoan (oo)cysts in water: A review. *Water Research*, 40(1), 3-22.
- Hjelm, H., Sjodahl, J., & Sjoquist, J. (1975). Immunologically active and structurally similar fragments of protein-A from *Staphylococcus aureus*. *European Journal of Biochemistry*, 57(2), 395-403.
- Ho, J. A., Hsu, W., Liao, W., Chiu, J., Chen, M., Chang, H., & Li, C. (2010). Ultrasensitive electrochemical detection of biotin using electrically addressable site-oriented antibody immobilization approach via aminophenyl boronic acid. *Biosensors & Bioelectronics*, 26(3), 1021-1027.
- Hoyer, O. (2004). Water disinfection with UV radiation—requirements and realization. In *Proceedings of the European Conference UV Karlsruhe, UV radiation. Effects and Technologies*, September 22–24, 2003, Karlsruhe, pp. 22-24.
- Huffman, D., Slifko, T., Salisbury, K., & Rose, J. (2000). Inactivation of bacteria, virus and *Cryptosporidium* by a point-of-use device using pulsed broad spectrum white light. *Water Research*, 34(9), 2491-2498.
- Hunter, P., Hughes, S., Woodhouse, S., Syed, Q., Verlander, N., Chalmers, R., . . . Osborn, K. (2004). Sporadic cryptosporidiosis case-control study with genotyping. *Emerging Infectious Diseases*, 10(7), 1241-1249.

- Huy, T. Q., Hanh, N. T. H., Chung, P. V., Anh, D. D., Nga, P. T., & Tuan. M. A. (2011). Characterization of immobilization methods of antiviral antibodies in serum for electrochemical biosensors. *Applied Surface Science*, 257(16), 7090-7095.
- Jaidi, K., Barbeau, B., Carriere, A., Desjardins, R., & Prevost, M. (2009). Including operational data in QMRA model: Development and impact of model inputs. *Journal of Water and Health*, 7(1), 77-95.
- Jakubowski, W., Boutros, S., Faber, W., Fayer, R., Ghiorse, W., LeChevallier, M., . . . Stewart, M. (1996). Environmental methods for *Cryptosporidium*. *Journal American Water Works Association*, 88(9), 107-121.
- Janeway, C. A. (2001). *Immunobiology: The immune system in health and disease* (5th ed.). New York: Garland Publ.
- Jenkins, M., Trout, J., Abrahamsen, M., Lancto, C., Higgins, J., & Fayer, R. (2000). Estimating viability of *Cryptosporidium parvum* oocysts using reverse transcriptase-polymerase chain reaction (RT-PCR) directed at mRNA encoding amyloglucosidase. *Journal of Microbiological Methods*, 43(2), 97-106.
- Jomeh, S. (2013). *Development of a microfluidic capture device for the manipulation and concentration of waterborne pathogens* University of British Columbia.
- Jomeh, S., Hoorfar, M. (2012). Study of the effect of electric field and electroneutrality on transport of biomolecules in microreactors. *Microfluidics and Nanofluidics*, 12 (1), 279–294.
- Joshi, A., Prasad, S., Kasav, J. B., Segan, M., & Singh, A. K. (2013). Water and sanitation hygiene knowledge attitude practice in urban slum settings. *Global Journal of Health Science*, 6(2), 23.
- Jung, Y., Kang, H. J., Lee, J. M., Jung, S. O., Yun, W. S., Chung, S. J., & Chung, B. H. (2008). Controlled antibody immobilization onto immunoanalytical platforms by synthetic peptide. *Analytical Biochemistry*, 374(1), 99-105.
- Kang, J. H., Choi, H. J., Hwang, S. Y., Han, S. H., Jeon, J. Y., & Lee, E. K. (2007). Improving immunobinding using oriented immobilization of an oxidized antibody. *Journal of Chromatography a*, 1161(1-2), 9-14.
- Karanis, P., Kourenti, C., & Smith, H. (2007). Waterborne transmission of protozoan parasites: A worldwide review of outbreaks and lessons learnt. *Journal of Water and Health*, 5(1), 1-38.
- Kato, K., Lian, L., Barsukov, I., Derrick, J., Kim, H., Tanaka, R., . . . Roberts, G. (1995). Model for the complex between protein-G and an antibody Fc fragment in solution. *Structure*, 3(1), 79-85.
- Kaucner, C. & Stinear, T. (1998). Sensitive and Rapid Detection of Viable *Giardia* Cysts and *Cryptosporidium parvum* oocysts in large-volume water samples with wound

- fiberglass cartridge filters and reverse transcription-PCR. *Applied and Environmental Microbiology*, 64(5), 1743–1749.
- Ko, S., Kim, A. R., Kim, C., & Kwon, D. (2010). Detection of aflatoxin B1 by SPR biosensor using fusion proteins as a linker. *NSTI-Nanotech*, 3, 129-132.
- Kohler, G., & Milstein, C. (1975). Continuous cultures of fused cells secreting antibody of predefined specificity. *Nature*, 256(5517), 495-497.
- Komatsu, Y., Tsujino, T., Suzuki, T., Nikaido, O., & Ohtsuka, E. (1997). Antigen structural requirements for recognition by a cyclobutane thymine dimer-specific monoclonal antibody. *Nucleic Acids Research*, 25(19), 3889-3894.
- Korich, D., Mead, J., Madore, M., Sinclair, N., & Sterling, C. (1990). Effects of ozone, chlorine dioxide, chlorine, and monochloramine on *Cryptosporidium parvum* oocyst viability. *Applied and Environmental Microbiology*, 56(5), 1423-1428.
- Kozwicz, D., Johansen, K., Landau, K., Roehl, C., Woronoff, S., & Roehl, P. (2000). Development of a novel, rapid integrated *Cryptosporidium parvum* detection assay. *Applied and Environmental Microbiology*, 66(7), 2711-2717.
- Kronvall, G., Grey, H., & Williams, R. (1970). Protein-a reactivity with mouse immunoglobulins - structural relationship between some mouse and human immunoglobulins. *Journal of Immunology*, 105(5), 1116-23.
- Kronvall, G., & Williams, R. (1969). Differences in anti-protein A activity among IgG subgroups. *Journal of Immunology*, 103(4), 828-833.
- Kruithof, J., van der Leer, R., & Hijnen, W. (1992). Practical experiences with UV disinfection in the Netherlands. *Aqua-Journal of Water Supply Research and Technology*, 41(2), 88-88.
- Kuen, L. S., Ming, C. H., & Fan, Y. S. (1993). Background noise in ELISA procedures influence of the pH of the coating buffer and correlations with serum IgM concentration. *Journal of Immunological Methods*, 163(2), 277-278.
- Kumari, S., Rastogi, R. P., Singh, K. L., Singh, S. P., & Sinha, R. P. (2008). DNA damage: Detection strategies. *Excli Journal*, 7, 44-62.
- Le Blancq, S., Khramtsov, N., Zamani, F., Upton, S., & Wu, T. (1997). Ribosomal RNA gene organization in *Cryptosporidium parvum*. *Molecular and Biochemical Parasitology*, 90(2), 463-478.
- Le Brun, A. P., Holt, S. A., Shah, D. S. H., Majkrzak, C. F., & Lakey, J. H. (2011). The structural orientation of antibody layers bound to engineered biosensor surfaces. *Biomaterials*, 32(12), 3303-3311.
- Lechevallier, M., Norton, W., & Lee, R. (1991). Occurrence of *Giardia* and *Cryptosporidium* spp. in surface-water supplies. *Applied and Environmental Microbiology*, 57(9), 2610-2616.

- Lechevallier, M., Norton, W., Siegel, J., & Abbaszadegan, M. (1995). Evaluation of the immunofluorescence procedure for detection of *Giardia* cysts and *Cryptosporidium* oocysts in water. *Applied and Environmental Microbiology*, 61(2), 690-697.
- Leclerc, H., Schwartzbrod, L., & Dei-Cas, E. (2002). Microbial agents associated with waterborne diseases. *Critical Reviews in Microbiology*, 28(4), 371-409.
- Lee, N., Yang, Y., Kim, Y., & Park, S. (2006). Microfluidic immunoassay platform using antibody-immobilized glass beads and its application for detection of *Escherichia coli* O157: H7. *Bulletin of the Korean Chemical Society*, 27(4), 479-483.
- Lee, J. H., Choi, H. K., Lee, S. Y., Lim, M., & Chang, J. H. (2011). Enhancing immunoassay detection of antigens with multimeric protein Gs. *Biosensors & Bioelectronics*, 28(1), 146-151.
- Lee, J. E., Seo, J. H., Kim, C. S., Kwon, Y., Ha, J. H., Choi, S. S., & Cha, H. J. (2013). A comparative study on antibody immobilization strategies onto solid surface. *Korean Journal of Chemical Engineering*, 30(10), 1934-1938.
- Li, Y., Schluesener, H. J., & Xu, S. (2010). Gold nanoparticle-based biosensors. *Gold Bulletin*, 43(1), 29-41.
- Ligon, G., & Bartram, J. (2016). Literature review of associations among attributes of reported drinking water disease outbreaks. *International Journal of Environmental Research and Public Health*, 13(6), 527.
- Linden KG, Mofidi AA (1999). Measurement of UV irradiance: tools and considerations. In *Proceedings of the AWWA's Water Quality Technology Conference*. Washington, DC: American Water Works Association.
- Liu, Y., Guo, C. X., Hu, W., Lu, Z., & Li, C. M. (2011). Sensitive protein microarray synergistically amplified by polymer brush-enhanced immobilizations of both probe and reporter. *Journal of Colloid and Interface Science*, 360(2), 593-599.
- Liu, X., Wang, X., Zhang, J., Feng, H., Liu, X., & Wong, D. K. Y. (2012). Detection of estradiol at an electrochemical immunosensor with a Cu UPD vertical bar DTBP-protein G scaffold. *Biosensors & Bioelectronics*, 35(1), 56-62.
- Love, J., Estroff, L., Kriebel, J., Nuzzo, R., & Whitesides, G. (2005). Self-assembled monolayers of thiolates on metals as a form of nanotechnology. *Chemical Reviews*, 105(4), 1103-1169.
- Lu, B., Smyth, M., & O'Kennedy, R. (1996). Oriented immobilization of antibodies and its applications in immunoassays and immunosensors. *Analyst*, 121(3), R29-R32.
- Macey, J., Lior, L., Johnston, A., Elliott, L., Krahn, D., Nowicki, D. & Wylie, J. (2002). Outbreak of diarrheal illness in attendees at a Ukrainian dance festival, Dauphin, Manitoba - May 2001. *Canada Communicable Disease Report*, 28(17), 141-145.

- Mackenzie, W., Hoxie, N., Proctor, M., Gradus, M., Blair, K., Peterson, D., . . . Davis, J. (1994). A massive outbreak in Milwaukee of *Cryptosporidium* infection transmitted through the public water-supply. *New England Journal of Medicine*, 331(3), 161-167.
- Maher, V., Rowan, L., Silinskas, K., Kateley, S., & McCormick, J. (1982). Frequency of UV-induced neoplastic transformation of diploid human-fibroblasts is higher in xeroderma pigmentosum-cells than in normal-cells. *Proceedings of the National Academy of Sciences of the United States of America-Biological Sciences*, 79(8), 2613-2617.
- Malinsky, P., Slepicka, P., Hnatowicz, V., & Svorcik, V. (2012). Early stages of growth of gold layers sputter deposited on glass and silicon substrates. *Nanoscale Research Letters*, 7, 241.
- Malley, J., et al. (2004). *Inactivation of pathogens with innovative UV technologies*. Portland: American Water Work Associations.
- Matsunaga, T., Hatakeyama, Y., Ohta, M., Mori, T., & Nikaido, O. (1993). Establishment and characterization of a monoclonal-antibody recognizing the dewar isomers of (6-4) photoproducts. *Photochemistry and Photobiology*, 57(6), 934-940.
- Matsunaga, T., Mori, T., & Nikaido, O. (1990). Base sequence specificity of a monoclonal-antibody binding to (6-4) photoproducts. *Mutation Research*, 235(3), 187-194.
- Medema, G. J., Payment, P., Dufour, A., Robertson, W., Waite, M., Hunter, P., Kirby, R. & Andersson, Y. (2003). Safe drinking water: An ongoing challenge. In Dufour, A., Snozzi, M., Koster, W., Bartram, J., Ronchi, E. & Fewtrell, L. (Eds) *Assessing microbial safety of drinking water improving approaches and methods: Improving approaches and methods* (pp. 11- 45) Paris, France: WHO-OECD.
- McGlade, T., Robertson, I., Elliot, A., & Thompson, R. (2003). High prevalence of *Giardia* detected in cats by PCR. *Veterinary Parasitology*, 110(3-4), 197-205.
- Michnik, A., Michalik, K., & Drzazga, Z. (2005). Stability of bovine serum albumin at different pH. *Journal of Thermal Analysis and Calorimetry*, 80(2), 399-406.
- Mitchell, D. L. (1988). The relative cytotoxicity of (6-4) photoproducts and cyclobutane dimers in mammalian cells. *Photochemistry and Photobiology*, 48(1), 51-57.
- MoBio (2013). *PowerFecal DNA Isolation Kit*. Retrieved Jan 16, 2017, from <https://mobio.com/media/wysiwyg/pdfs/protocols/12830.pdf>
- MoBio (2016). *PowerSoil DNA Isolation Kit*. Retrieved Jan 16, 2017, from <https://mobio.com/media/wysiwyg/pdfs/protocols/12888.pdf>
- Morgan, G., & Levinsky, R. (1985). Monoclonal-antibodies in diagnosis and treatment. *Archives of Disease in Childhood*, 60(2), 96-98.

- Morgan, U., Pallant, L., Dwyer, B., Forbes, D., Rich, G., & Thompson, R. (1998). Comparison of PCR and microscopy for detection of *Cryptosporidium parvum* in human fecal specimens: Clinical trial. *Journal of Clinical Microbiology*, 36(4), 995-998.
- Mori, T., Nakane, M., Hattori, T., Matsunaga, T., Ihara, M., & Nikaido, O. (1991). Simultaneous establishment of monoclonal-antibodies specific for either cyclobutane pyrimidine dimer or (6-4) photoproduct from the same mouse immunized with ultraviolet-irradiated DNA. *Photochemistry and Photobiology*, 54(2), 225-232.
- Morita, S., Namikoshi, A., Hirata, T., Oguma, K., Katayama, H., Ohgaki, S., . . . Fujiwara, M. (2002). Efficacy of UV irradiation in inactivating *Cryptosporidium parvum* oocysts. *Applied and Environmental Microbiology*, 68(11), 5387-5393.
- Musial, C. E., Arrowood, M. J., Sterling, C. R., & Gerba, C. P. (1987). Detection of *Cryptosporidium* in water by using polypropylene cartridge filters. *Applied and Environmental Microbiology*, 53(4), 687-692.
- Naghavi, M., Wang, H., Lozano, R., Davis, A., Liang, X., Zhou, M., . . . GBD Mortal 2013 Causes Death Colla. (2015). Global, regional, and national age-sex specific all-cause and cause-specific mortality for 240 causes of death, 1990-2013: A systematic analysis for the global burden of disease study 2013. *Lancet*, 385(9963), 117-171.
- Nakane, P. K., & Pierce, G. B. (1967). Enzyme-labeled antibodies for the light and electron microscopic localization of tissue antigens. *The Journal of Cell Biology*, 33(2), 307-318.
- Neumann, N., Gyurek, L., Gammie, L., Finch, G., & Belosevic, M. (2000). Comparison of animal infectivity and nucleic acid staining for assessment of *Cryptosporidium parvum* viability in water. *Applied and Environmental Microbiology*, 66(1), 406-412.
- Nieminski, E. C., F W Schaefer 3rd, & Ongerth, J. E. (1995). Comparison of two methods for detection of *Giardia* cysts and *Cryptosporidium* oocysts in water. *Applied and Environmental Microbiology*, 61(5), 1714-1719.
- Nime, F. A., Burek, J. D., Page, D. L., Holscher, M. A., & Yardley, J. H. (1976). Acute enterocolitis in a human being infected with the protozoan *Cryptosporidium*. *Gastroenterology*, 70(4), 592.
- Nishiwaki, Y., Kobayashi, N., Imoto, K., Iwamoto, T., Yamamoto, A., Katsumi, S., . . . Mori, T. (2004). Trichothiodystrophy fibroblasts are deficient in the repair of ultraviolet-induced cyclobutane pyrimidine dimers and (6-4) photoproducts. *Journal of Investigative Dermatology*, 122(2), 526-532.
- NIPH (Norwegian Institute of Public Health (Nasjonalt Folkehelseinstitutt) (2002). Retrieved May 13, 2003, from <http://www.fhi.no/tema/drikkevann/uvinfo-en.html>
- Oguma, K., Katayama, H., Mitani, H., Morita, S., Hirata, T., & Ohgaki, S. (2001). Determination of pyrimidine dimers in *Escherichia coli* and *Cryptosporidium*

- parvum* during UV light inactivation, photoreactivation, and dark repair. *Applied and Environmental Microbiology*, 67(10), 4630-4637.
- Olsson, A., Eliasson, M., Guss, B., Nilsson, B., Hellman, U., Lindberg, M., & Uhlen, M. (1987). Structure and evolution of the repetitive gene encoding streptococcal protein-G. *European Journal of Biochemistry*, 168(2), 319-324.
- Omega Bio-tek (2015). *E.Z.N.A Stool DNA kit*. Retrieved Jan 16, 2017, from <http://omegabiotek.com/store/wp-content/uploads/2013/04/D4015-Stool-DNA-Kit-Combo-Online.pdf>
- Ong, C., Eisler, D., Alikhani, A., Fung, V., Tomblin, J., Bowie, W., & Isaac-Renton, J. (2002). Novel *Cryptosporidium* genotypes in sporadic cryptosporidiosis cases: First report of human infections with a cervine genotype. *Emerging Infectious Diseases*, 8(3), 263-268.
- Ongerth, J., & Stibbs, H. (1987). Identification of *Cryptosporidium* oocysts in river water. *Applied and Environmental Microbiology*, 53(4), 672-676.
- Oppenheimer, J. A., Aieta, E. M., Trussell, R. R., Jacangelo, J. G. & Najm, I. S. (2000) *Evaluation of Cryptosporidium Inactivation in Natural Waters*. USA: Awwa Research Foundation and the American Water Works Association.
- Park, J., Cho, I., Moon, D. W., Paek, S., & Lee, T. G. (2011). ToF-SIMS and PCA of surface-immobilized antibodies with different orientations. *Surface and Interface Analysis*, 43(1-2), 285-289.
- Peccia, J., & Hernandez, M. (2002). Rapid immunoassays for detection of UV-induced cyclobutane pyrimidine dimers in whole bacterial cells. *Applied and Environmental Microbiology*, 68(5), 2542-2549.
- Peng, M. M., Freeman, A. R., Escalante, A. A., Weltman, A. C., Ong, C. S., MacKenzie, W. R., Beard, C. B. (1997). Genetic polymorphism among *Cryptosporidium parvum* isolates: Evidence of two distinct human transmission cycles. *Emerging Infectious Diseases*, 3, 567-573.
- Plutzer, J., & Karanis, P. (2009). Genetic polymorphism in *Cryptosporidium* species: An update. *Veterinary Parasitology*, 165(3-4), 187-199.
- Pons, W., Young, I., Truong, J., Jones-Bitton, A., McEwen, S., Pintar, K., & Papadopoulos, A. (2015). A systematic review of waterborne disease outbreaks associated with small non-community drinking water systems in Canada and the United States. *Plos One*, 10(10), e0141646.
- Puiu, D., Enomoto, S., Buck, G., Abrahamsen, M., & Kissinger, J. (2004). CryptoDB: The *Cryptosporidium* genome resource. *Nucleic Acids Research*, 32, D329-D331.
- Putignani, L., & Menichella, D. (2010). Global distribution, public health and clinical impact of the protozoan pathogen *Cryptosporidium*. *Interdisciplinary Perspectives on Infectious Diseases*, 2010

- Qiagen (2006). *DNeasy Blood & Tissue Handbook*. Retrieved Jan 16, 2017, from http://diagnostics1.com/MANUAL/General_Qiagen.pdf
- Quintero-Betancourt, W., Peele, E., & Rose, J. (2002). *Cryptosporidium parvum* and *Cyclospora cayetanensis*: A review of laboratory methods for detection of these waterborne parasites. *Journal of Microbiological Methods*, 49(3), 209-224.
- Ramirez, N. E., Ward, L. A., & Sreevatsan, S. (2004). *A review of the biology and epidemiology of cryptosporidiosis in humans and animals*. France: Elsevier SAS.
- Rao, S. V., Anderson, K. W., & Bachas, L. G. (1998). Oriented immobilization of proteins. *Mikrochimica Acta*, 128(3), 127-143.
- Read, C., Walters, J., Robertson, I., & Thompson, R. (2002). Correlation between genotype of *Giardia duodenalis* and diarrhoea. *International Journal for Parasitology*, 32(2), 229-231.
- Reverberi, R., & Reverberi, L. (2007). Factors affecting the antigen-antibody reaction. *Blood Transfusion = Trasfusione Del Sangue*, 5(4), 227-240.
- Robertson, L., Campbell, A., & Smith, H. (1992). Survival of *Cryptosporidium parvum* oocysts under various environmental pressures. *Applied and Environmental Microbiology*, 58(11), 3494-3500.
- Robertson, L. J., Casaert, S., Valdez-Nava, Y., Ehsan, M. A., & Claerebout, E. (2014). Drying of *Cryptosporidium* oocysts and *Giardia* cysts to slides abrogates use of vital dyes for viability staining. *Journal of Microbiological Methods*, 96, 68-69.
- Rochelle, P., DeLeon, R., Stewart, M., & Wolfe, R. (1997a). Comparison of primers and optimization of PCR conditions for detection of *Cryptosporidium parvum* and *Giardia lamblia* in water. *Applied and Environmental Microbiology*, 63(1), 106-114.
- Rochelle, P., Ferguson, D., Handojo, T., DeLeon, R., Stewart, M., & Wolfe, R. (1997b). An assay combining cell culture with reverse transcriptase PCR to detect and determine the infectivity of waterborne *Cryptosporidium parvum*. *Applied and Environmental Microbiology*, 63(5), 2029-2037.
- Rochelle, P., De Leon, R., Johnson, A., Stewart, M., & Wolfe, R. (1999). Evaluation of immunomagnetic separation for recovery of infectious *Cryptosporidium parvum* oocysts from environmental samples. *Applied and Environmental Microbiology*, 65(2), 841-845.
- Rochelle, P., Fallar, D., Marshall, M., Montelone, B., Upton, S., & Woods, K. (2004). Irreversible UV inactivation of *Cryptosporidium* spp. despite the presence of UV repair genes. *Journal of Eukaryotic Microbiology*, 51(5), 553-562.
- Rochelle, P., Upton, S., Montelone, B., & Woods, K. (2005). The response of *Cryptosporidium parvum* to UV light. *Trends in Parasitology*, 21(2), 81-87.

- Rose, J. (1991). In Hall J. G., Gd (Ed.), *New technology for protozoology - immunofluorescence and gene probe technology for detection of parasites*
- Rose, J., Landeen, L., Riley, K., & Gerba, C. (1989). Evaluation of immunofluorescence techniques for detection of *Cryptosporidium* oocysts and *Giardia* cysts from environmental samples. *Applied and Environmental Microbiology*, 55(12), 3189-3196.
- Roux, K., Strelets, L., & Michaelsen, T. (1997). Flexibility of human IgG subclasses. *Journal of Immunology*, 159(7), 3372-3382.
- Ryu, Y., Jin, Z., Kang, M. S., & Kim, H. (2011). Increase in the detection sensitivity of a lateral flow assay for a cardiac marker by oriented immobilization of antibody. *Biochip Journal*, 5(3), 193-198.
- Samuelson, J., Bushkin, G. G., Chatterjee, A., & Robbins, P. W. (2013). Strategies to discover the structural components of cyst and oocyst walls. *Eukaryotic Cell*, 12(12), 1578-1587.
- Schlesinger, M., Paunovic, M., & Books24x7, I. (2010). *Modern electroplating, fifth edition* (5th ed.). Hoboken, N.J: John Wiley & Sons.
- Scholtyssek, E., Mehlhorn, H., & Friedhoff, K. (1970). The fine structure of the conoid of sporozoa and related organisms. *Zeitschrift für Parasitenkunde*, 34(1), 68-94.
- Setlow, R. (1978). Repair deficient human disorders and cancer. *Nature*, 271(5647), 713-717.
- Shah, K., & Maghsoudlou, P. (2016). Enzyme-linked immunosorbent assay (ELISA): The basics. *British Journal of Hospital Medicine*, 77(7), C98-C101.
- Sharma, S., Byrne, H., & O'Kennedy, R. J. (2016). Antibodies and antibody-derived analytical biosensors. *Essays in Biochemistry*, 60(1), 9-18.
- Shen, G., Cai, C., Wang, K., & Lu, J. (2011). Improvement of antibody immobilization using hyperbranched polymer and protein A. *Analytical Biochemistry*, 409(1), 22-27.
- Shim, S., Kim, J., Jung, S., Kim, D., Oh, J., Han, B., & Jeon, J. (2010). Multilaboratory assessment of variations in spectrophotometry-based DNA quantity and purity indexes. *Biopreservation and Biobanking*, 8(4), 187-192.
- Sibley, L. (2004). Intracellular parasite invasion strategies. *Science*, 304(5668), 248-253.
- Sigma-Aldrich (2016). *TRI Reagent*. Retrieved Jan 16, 2017, from <http://www.sigmaaldrich.com/content/dam/sigma-aldrich/docs/Sigma/Bulletin/t9424bul.pdf>
- Sjoberg, U., Falkenberg, C., Nielsen, E., Akerstrom, B., & Bjorck, L. (1988). Isolation and characterization of a 14-kda albumin-binding fragment of streptococcal protein-G. *Journal of Immunology*, 140(5), 1595-1599.

- Slifko, T., Freidman, D., Rose, J., & Jakubowski, W. (1997). An in vitro method for detecting infectious *Cryptosporidium* oocysts with cell culture. *Applied and Environmental Microbiology*, 63(9), 3669-3675.
- Slifko, T. R., Huffman, D. E., & Rose, J. B. (1999). A most-probable-number assay for enumeration of infectious *Cryptosporidium parvum* oocysts. *Applied and Environmental Microbiology*, 65(9), 3936-3941.
- Slifko, T.R. (2001). *Development and evaluation of an infectivity assay for Cryptosporidium disinfection studies* (Doctoral dissertation). St. Petersburg, FL: University of South Florida.
- Smith, H. V., Caccio, S. M., Cook, N., Nichols, R. A. B., & Tait, A. (2007). *Cryptosporidium* and *Giardia* as foodborne zoonoses. *Veterinary Parasitology*, 149(1-2), 29-40.
- Smith, H. V., & Nichols, R. A. B. (2010). *Cryptosporidium*: Detection in water and food. *Experimental Parasitology*, 124(1), 61-79.
- Smith, H., Grimason, A., Benton, C., & Parker, J. (1991). The occurrence of *Cryptosporidium* spp. oocysts in Scottish waters, and the development of a fluorogenic viability assay for individual *Cryptosporidium* spp. oocysts. *Water Science and Technology*, 24(2), 169-172.
- Smith, H., & Hayes, C. (1997). The status of UK methods for the detection of *Cryptosporidium* spp. oocysts and *Giardia* spp. cysts in water concentrates. *Water Science and Technology*, 35(11-12), 369-376.
- Snelling, W. J., Xiao, L., Ortega-Pierres, G., Lowery, C. J., Moore, J. E., Rao, J. R., . . . Dooley, J. S. G. (2007). Cryptosporidiosis in developing countries. *Journal of Infection in Developing Countries*, 1(3), 242-256.
- Sommer, R., Lhotsky, M., Haider, T., & Cabaj, A. (2000). UV inactivation, liquid-holding recovery, and photoreactivation of *Escherichia coli* O157 and other pathogenic *Escherichia coli* strains in water. *Journal of Food Protection*, 63(8), 1015-1020.
- Song, H. Y., Zhou, X., Hogley, J., & Su, X. (2012). Comparative study of random and oriented antibody immobilization as measured by dual polarization interferometry and surface plasmon resonance spectroscopy. *Langmuir: The ACS Journal of Surfaces and Colloids*, 28(1), 997.
- Stanfield, G., Carrington, E., Albinet, F., Compagnon, B., Dumoutier, N., Hamsch, B., . . . Whitmore, T. (2000). An optimised and standardised test to determine the presence of the protozoa *Cryptosporidium* and *Giardia* in water. *Water Science and Technology*, 41(7), 103-110.

- Sterling, C. R., Adam, R. D. (2004). ebrary eBooks, & SpringerLINK eBooks - English/International Collection (Archive). *The pathogenic enteric protozoa: Giardia, Entamoeba, Cryptosporidium, and Cyclospora*. Boston: Kluwer Academic.
- Stinear, T., Matusan, A., Hines, K., & Sandery, M. (1996). Detection of a single viable *Cryptosporidium parvum* oocyst in environmental water concentrates by reverse transcription-PCR. *Applied and Environmental Microbiology*, 62(9), 3385-3390.
- Stirling, R., Aramini, J., Ellis, A., Lim, G., Meyers, R., Fleury, M., & Werker, D. (2001). Waterborne cryptosporidiosis outbreak, North Battleford, Saskatchewan, spring 2001. *Canada Communicable Disease Report = Relevé Des Maladies Transmissibles Au Canada*, 27(22), 185.
- Sturbaum, G., Reed, C., Hoover, P., Jost, B., Marshall, M., & Sterling, C. (2001). Species-specific, nested PCR-restriction fragment length polymorphism detection of single *Cryptosporidium parvum* oocysts. *Applied and Environmental Microbiology*, 67(6), 2665-2668.
- Sutton, S. (2011). Measurement of microbial cells by optical density. *Journal of Validation Technology*, 17 (1), 46-49.
- Suzuki, F., Han, A., Lankas, G., Utsumi, H. & Elkind, M. (1981). Spectral dependencies of killing, mutation, and transformation in mammalian cells and their relevance to hazards caused by solar ultraviolet radiation. *Cancer Research*, 41(12 Pt 1), 4916-4924.
- Taghi-Kilani, R., Remacha-Moreno, M., & Wenman, W. M. (1994). Three tandemly repeated 5S ribosomal RNA-encoding genes identified, cloned and characterized from *Cryptosporidium parvum*. *Gene*, 142(2), 253-258.
- Tajima, N., Takai, M., & Ishihara, K. (2011). Significance of antibody orientation unraveled: Well-oriented antibodies recorded high binding affinity. *Analytical Chemistry*, 83(6), 1969-1976.
- Tetley, L., Brown, S. M. A., McDonald, V., & Coombs, G. H. (1998). Ultrastructural analysis of the sporozoite of *Cryptosporidium parvum*. *Microbiology*, 144(12), 3249-3255.
- Thompson, R. C. A. (2003). The zoonotic potential of *Cryptosporidium*. In: R. C. A. Thompson, A. Armson & U. M. Morgan Ryan (Eds), *Cryptosporidium: From Molecules to Disease* (pp. 113-119). Amsterdam; New York; London: Elsevier.
- Thoma, F. (1999). Light and dark in chromatin repair: Repair of UV-induced DNA lesions by photolyase and nucleotide excision repair. *The EMBO Journal*, 18(23), 6585-6598.
- Tighe, P. J., Ryder, R. R., Todd, I., & Fairclough, L. C. (2015). ELISA in the multiplex era: Potentials and pitfalls. *PROTEOMICS – Clinical Applications*, 9(3-4), 406-422.

- Tirado, C., & Schmidt, K. (2001). WHO surveillance programme for control of foodborne infections and intoxications: Preliminary results and trends across greater europe. world health organization. *The Journal of Infection*, 43(1), 80-84.
- Torizawa, T., Yamamoto, N., Suzuki, T., Nobuoka, K., Komatsu, Y., Morioka, H., . . . Shimada, I. (2000). DNA binding mode of the Fab fragment of a monoclonal antibody specific for cyclobutane pyrimidine dimer. *Nucleic Acids Research*, 28(4), 944-951.
- Trilling, A. K., Beekwilder, M. J., & Zuilhof, H. (2013a). Antibody orientation on biosensor surfaces: A minireview. *The Analyst*, 138(6), 1619-1627.
- Trilling, A. K., Harmsen, M. M., Ruigrok, V. J., Zuilhof, H., & Beekwilder, J. (2013b). The effect of uniform capture molecule orientation on biosensor sensitivity: Dependence on analyte properties. *Biosensors and Bioelectronics*, 40(1), 219-226.
- Tyzzer, E. E. (1910). An extracellular coccidium, *Cryptosporidium muris* (gen. et sp. nov.), of the gastric glands of the common mouse. *The Journal of Medical Research*, 23(3), 487-510.3.
- Tzipori, S., & Ward, H. (2002). Cryptosporidiosis: Biology, pathogenesis and disease. *Microbes and Infection*, 4(10), 1047-1058.
- Um, H., Kim, Y., Kim, H., Kim, M., Lee, S., Min, J., & Choi, Y. (2011). Electrochemically oriented immobilization of antibody on poly-(2-cyanoethylpyrrole)-coated gold electrode using a cyclic voltammetry. *Talanta*, 84(2), 330-334.
- USEPA (US Environmental Protection Agency) (1999a). Method 1622: *Cryptosporidium* in water by filtration/IMS/FA. *Office of Water*. Washington, DC. EPA-821-R-99-061.
- USEPA (US Environmental Protection Agency) (1999b). Method 1623: *Cryptosporidium* and *Giardia* in water by filtration/IMS/FA. *Office of Water*. Washington, DC. EPA-821-R-99-006.
- USEPA (US Environmental Protection Agency) (2006). Ultraviolet Disinfection Guidance Manual for the Final Long Term 2 Enhanced Surface Water Treatment Rule. *Office of Water*. Washington, DC. EPA 815-R-06-007.
- USEPA (US Environmental Protection Agency) (2012). Method 1623.1: *Cryptosporidium* and *Giardia* in water by filtration/IMS/FA. *Office of Water*. Washington, DC. EPA-816-R-12-001.
- Vashist, S., Dixit, C., MacCraith, B., & O'Kennedy, R. (2011). Effect of antibody immobilization strategies on the analytical performance of a surface plasmon resonance-based immunoassay. *Analyst*, 136(21), 4431-4436.
- Venables, J. (2000). *Introduction to surface and thin film processes*. New York; Cambridge, UK: Cambridge University Press.

- Ventura, B. D., Schiavo, L., Altucci, C., Esposito, R., & Velotta, R. (2011). Light assisted antibody immobilization for bio-sensing. *Biomedical Optics Express*, 2(11), 3223-3231.
- Vesey, G., Ashbolt, N., Wallner, G., Dorsch, M., Williams, K.L. & Veal, D.A. (1995). Assessing *Cryptosporidium parvum* oocysts viability with fluorescent in-situ hybridization using ribosomal RNA probes and flow cytometry. In W.B. Betts, D. Casemore, C. Fricker, H. Smith & J. Watkins (Eds.), *Protozoan Parasites and Water* (pp. 133– 138). Cambridge: Royal Society of Chemistry.
- Vesey, G., Ashbolt, N., Fricker, E., Deere, D., Williams, K., Veal, D., & Dorsch, M. (1998). The use of a ribosomal RNA targeted oligonucleotide probe for fluorescent labelling of viable *Cryptosporidium parvum* oocysts. *Journal of Applied Microbiology*, 85(3), 429-440.
- Vidarsson, G., Dekkers, G., & Rispens, T. (2014). IgG subclasses and allotypes: From structure to effector functions. *Frontiers in Immunology*, 5, 520.
- Vidic, J., Pla-Roca, M., Grosclaude, J., Persuy, M., Monnerie, R., Caballero, D., . . . Samitier, J. (2007). Gold surface functionalization and patterning for specific immobilization of olfactory receptors carried by nanosomes. *Analytical Chemistry*, 79(9), 3280-3290.
- Ward, H., & Cevallos, A. M. (1998). *Cryptosporidium*: Molecular basis of host-parasite interaction. *Advances in Parasitology*, 40, 151.
- Weiner, L. M., Wang, S., & Surana, R. (2010). Monoclonal antibodies: Versatile platforms for cancer immunotherapy. *Nature Reviews Immunology*, 10(5), 317-327.
- Weir, C., Vesey, G., Slade, M., Ferrari, B., Veal, D., & Williams, K. (2000). An immunoglobulin G1 monoclonal antibody highly specific to the wall of *Cryptosporidium* oocysts. *Clinical and Diagnostic Laboratory Immunology*, 7(5), 745-750.
- Welfle, K., Misselwitz, R., Hausdorf, G., Höhne, W., & Welfle, H. (1999). Conformation, pH-induced conformational changes, and thermal unfolding of anti-p24 (HIV-1) monoclonal antibody CB4-1 and its Fab and Fc fragments. *Biochimica Et Biophysica Acta*, 1431(1), 120.
- WHO (2002). Ebrary Academic Complete (Canada) Subscription Collection & World Health Organization Staff. *The world health report 2002: Reducing risks, promoting healthy life (Revis ed.)*. Herndon; Geneva: World Health Organization.
- Widmer, G., Akiyoshi, D., Buckholt, M. A., Feng, X., Rich, S. M., Deary, K. M., . . . Tzipori, S. (2000). Animal propagation and genomic survey of a genotype 1 isolate of *Cryptosporidium parvum*. *Molecular & Biochemical Parasitology*, 108(2), 187-197.

- Wiedenmann, A., Krüger, P., & Botzenhart, K. (1998). PCR detection of *Cryptosporidium parvum* in environmental samples—a review of published protocols and current developments. *Journal of Industrial Microbiology & Biotechnology*, 21(3), 150-166.
- Wiseman, A. (1993). Designer enzyme and cell applications in industry and in environmental monitoring. *Journal of Chemical Technology and Biotechnology*, 56(1), 3-13.
- Wolfe, R. (1990). Ultraviolet disinfection of potable water - current technology and research needs. *Environmental Science & Technology*, 24(6), 768-772.
- Wu, Q., Sun, Y., Zhang, D., Li, S., Wang, X., & Song, D. (2016). Magnetic field-assisted SPR biosensor based on carboxyl-functionalized graphene oxide sensing film and Fe₃O₄-hollow gold nanohybrids probe. *Biosensors & Bioelectronics*, 86, 95-101.
- Xiao, L., Escalante, L., Yang, C., Sulaiman, I., Escalante, A., Montali, R., . . . Lal, A. (1999). Phylogenetic analysis of *Cryptosporidium* parasites based on the small-subunit rRNA gene locus. *Applied and Environmental Microbiology*, 65(4), 1578-1583.
- Xiao, L., Alderisio, K., Limor, J., Royer, M., & Lal, A. A. (2000). Identification of species and sources of *Cryptosporidium* oocysts in storm waters with a small-subunit rRNA-based diagnostic and genotyping tool. *Applied and Environmental Microbiology*, 66(12), 5492–5498.
- Xiao, L., Limor, J., Bern, C., Lal, A., & Epidemic Working Group. (2001a). Tracking *Cryptosporidium parvum* by sequence analysis of small double-stranded RNA. *Emerging Infectious Diseases*, 7(1), 141-145.
- Xiao, L., Singh, A., Limor, J., Graczyk, T., Gradus, S., & Lal, A. (2001b). Molecular characterization of *Cryptosporidium* oocysts in samples of raw surface water and wastewater. *Applied and Environmental Microbiology*, 67(3), 1097-1101.
- Xiao, L., Alderisio, K. A., & Jiang, J. (2006). Detection of *Cryptosporidium* oocysts in water: Effect of the number of samples and analytic replicates on test results. *Applied and Environmental Microbiology*, 72(9), 5942-5947.
- Xiao, Y., & Isaacs, S. (2012). Enzyme-linked immunosorbent assay (ELISA) and blocking with bovine serum albumin (BSA)-not all BSAs are alike. *Journal of Immunological Methods*, 384(1-2), 148-151.
- Xue, Y., Li, X., Li, H., & Zhang, W. (2014). Quantifying thiol-gold interactions towards the efficient strength control. *Nature Communications*, 5, 4348.
- Xu, P., Ozaki, L. S., Kapur, V., Mackey, A. J., Serrano, M. G., Buck, G. A., . . . Akiyoshi, D. (2004). The genome of *Cryptosporidium hominis*. *Nature*, 431(7012), 1107-1112.
- Yoshimoto, K., Nishio, M., Sugawara, H., & Nagasaki, Y. (2010). Direct observation of adsorption-induced inactivation of antibody fragments surrounded by mixed-PEG

layer on a gold surface. *Journal of the American Chemical Society*, 132(23), 7982-7989.

Yu, J., O'Hara, S., Lin, J., Dailey, M., Cain, G., & Lin, J. L. (2002). A common oocyst surface antigen of *Cryptosporidium* recognized by monoclonal antibodies. *Parasitology Research*, 88(5), 412-420.

Yu, X., Van Dyke, M., Portt, A., & Huck, P. (2009). Development of a direct DNA extraction protocol for real-time PCR detection of *Giardia lamblia* from surface water. *Ecotoxicology*, 18(6), 661-668.

Yuan, Y., Yin, M., Qian, J., & Liu, C. (2011). Site-directed immobilization of antibodies onto blood contacting grafts for enhanced endothelial cell adhesion and proliferation. *Soft Matter*, 7(16), 7207-7216.

Zhao, X., Pan, F., Garcia-Gancedo, L., Flewitt, A., Ashley, G., Luo, J., & Lu, J. (2012). Interfacial recognition of human prostate-specific antigen by immobilized monoclonal antibody: Effects of solution conditions and surface chemistry. *Journal of the Royal Society Interface*, 9(75), 2457-2467.

Zimmer, J. L., & Slawson, R. M. (2002). Potential repair of *Escherichia coli* DNA following exposure to UV radiation from both medium- and low-pressure UV sources used in drinking water treatment. *Applied and Environmental Microbiology*, 68(7), 3293-3299.

Zimmer, J. L., Slawson, R. M., & Huck, P. M. (2003). Inactivation and potential repair of *Cryptosporidium parvum* following low- and medium-pressure ultraviolet irradiation. *Water Research*, 37(14), 3517-3523.

Appendices

Appendix A: Chemical composition

1L 1x PBS:

- 8g of NaCl
- 0.2g of KCl
- 1.44g of Na₂HPO₄
- 0.24g of KH₂PO₄
- pH to 7.4
- Up to 1L in RO H₂O
- Autoclaved

1L 1x LB:

- 10 g of Peptone
- 5 g of Yeast Extract
- 10 g of Sodium Chloride
- pH to 7.0
- Up to 1L in RO H₂O
- Autoclaved

1L 1x TBE:

- 10.8 g Tris
- 5.5 g Boric acid
- 4 ml 0.5 M Na₂EDTA (pH 8.0)
- Up to 1L in Type 1 water

1 L Elution buffer:

- 1% v/v Laureth 12
- 0.01% v/v antifoam A
- 0.01% v/v EDTA
- Up to 1L in RO water

1L Citrate-phosphate buffer:

- 4.20 g of Citric acid monohydrate
- 2.82 g of Sodium phosphate dibasic
- pH to 5.6
- Up to 1L in RO H₂O
- Autoclaved

1L HBSS:

- 0.14 g of Calcium Chloride
- 0.40 g of Potassium Chloride
- 0.06 g of Potassium Phosphate Monobasic
- 0.10 g of Magnesium Chloride
- 0.10 g of Magnesium Sulfate
- 8 g of Sodium Chloride

- 0.35 g of Sodium Bicarbonate
- 0.048 g of Sodium Phosphate Dibasic
- 1 g of Glucose 180
- 0.10 g of Phenol Red
- pH to 6.9
- Up to 1L in RO H₂O

Chelex/MGW preparation:

Thirty five ml of molecular grade water (MGW) was added to 10g of Chelex 100 resin (BioRad Cat# 143-2832, pH 10) to make a mixture of a 1:1 volume-to-volume suspension of Chelex resin and MGW, then 3.5 mL of 1.0 N HCl (standard solution, e.g. VWR Cat# VW3202-1) was added and stirred. After stirring, the chelex was allowed to settle by standing for 2 min, and then the supernatant was aspirated without removing the resin, to a total volume of approximately 25 mL of Chelex/MGW. To remove the salts in the resin formed during pH adjustment, 200 mL of MGW was added and stirred for 10 minutes. After stirring, the chelex was allowed to settle by standing for 2 min, and then the supernatant was aspirated without removing the resin, leaving approximately 30 mL Chelex/MGW. Then, again another 200 mL of MGW was added, stirred for 10 minutes. After stirring, the chelex was allowed to settle by standing for 2 min, and then the supernatant was aspirated without removing the leaving approximately 1:1 Chelex/MGW volume-to-volume ratio. Then, it was covered and allowed to settle overnight. After overnight stay, stirred briefly and the chelex/MGW was allowed to settle by standing for 2 min. The pH was kept approximately between 7.0 to 8.0. While stirring, 4 mL aliquots were transferred to graduated 5 mL flat bottom tubes, allowed to sit upright overnight and then adjust the molecular grade water volume was adjusted as necessary to achieve a 1:1 Chelex/MGW volume-to-volume ratio. Chelex/MGW can be stored at room temperature for up to 1 year.

Appendix B: Raw Data

Table B.1: Capture efficiency of the antibody capture surfaces with non-significant differences (P value > 0.05)

Ab	Organism	Given oocysts	Recovered oocysts	Capture efficiency (%)	Mean recovery (%)	Standard deviation	CV
IgG1	<i>C. parvum</i>	105	78	74.29	74.32	3.42	4.61
		105	80	76.19			
		105	73	69.52			
		110	81	73.64			
		110	89	80.91			
		110	82	74.55			
		111	81	72.97			
		111	78	70.27			
		111	85	76.58			
	<i>C. muris</i>	153	100	65.36	65.84	3.35	5.08
		153	95	62.09			
		153	107	69.93			
		147	92	62.59			
		147	91	61.90			
		147	96	65.31			
		149	98	65.77			
		149	105	70.47			
		149	103	69.13			
	<i>C. hominis</i>	79	41	51.90	54.13	3.69	6.82
		79	45	56.96			
		79	46	58.23			
		85	50	58.82			
		85	43	50.59			
		85	42	49.41			
		80	44	55.00			
		80	45	56.25			
		80	40	50.00			
IgG3	<i>C. parvum</i>	110	102	92.73	92.60	2.79	3.02
		110	97	88.18			
		110	100	90.91			
		107	101	94.39			
		107	103	96.26			
		107	96	89.72			
		112	104	92.86			
		112	108	96.43			
		112	103	91.96			

Table B.2: Capture efficiency of the antibody capture surfaces with significant differences (P value< 0.05)

Ab	Organism	Given oocysts	Recovered oocysts	Capture efficiency (%)	Mean recovery (%)	Overall Mean Recovery (%)	Std	CV
IgG3	<i>C. muris</i>	150	144	96.00	94.22	93.59	1.86	1.99
		150	141	94.00				
		150	139	92.67				
		155	149	96.13	95.05			
		155	146	94.19				
		155	147	94.84				
		145	131	90.34	91.49			
		145	135	93.10				
		145	132	91.03				
	<i>C. hominis</i>	82	69	84.15	86.18	84.13	2.92	3.47
		82	70	85.37				
		82	73	89.02				
		85	69	81.18	80.78			
		85	70	82.35				
		85	67	78.82				
		80	67	83.75	85.42			
		80	70	87.50				
		80	68	85.00				

Table B.3: Capture efficiency of IgG3 activated capture surfaces in respect to different antibody concentrations ranging from 100-0.001 µg/ml

Antibody concentration	Oocysts applied	<i>C. parvum</i>			Average	%	Std	CV
		Spot 1	Spot 2	Spot 3				
100 µg/ml	112	109	101	106	105.333	94	4.041	0.038
10 µg/ml	112	47	50	48	48.333	43.2	1.528	0.032
1 µg/ml	112	38	42	45	41.667	37.2	3.512	0.084
0.1 µg/ml	112	12	10	13	11.667	10.4	1.528	0.131
0.01 µg/ml	112	11	8	10	9.667	8.6	1.528	0.158
0 µg/ml	112	0	0	0	0.000	0	0.000	0.000

Table B.4: Capture efficiency of IgG3 activated capture surfaces in respect to different antibody concentrations ranging from 100-12.5 µg/ml

Antibody concentration	Oocysts applied	<i>C. parvum</i>			Average	%	Std	CV
		Spot 1	Spot 2	Spot 3				
100 µg/ml	104	98	100	95	97.667	93.9	2.517	0.026
50 µg/ml	104	65	61	58	61.333	59	3.512	0.057
25 µg/ml	104	46	43	50	46.333	44.6	3.512	0.076
12.5 µg/ml	104	43	44	41	42.667	41	1.528	0.036
0 µg/ml	104	0	0	1	0.333	0.30	0.577	1.732

Table B.5: Effect of different pH on the release of *Cryptosporidium* oocysts from the surface

pH	Sample Replicates	No. of oocysts/ spot		Release efficiency (%)	Average release efficiency (%)
		Capture	Release		
6.5	1	106	0	0.00	0.32
	2	103	1	0.97	
	3	108	0	0.00	
6.0	1	115	11	9.57	11.69
	2	107	12	11.21	
	3	105	15	14.29	
5.5	1	108	17	15.74	15.59
	2	109	14	12.84	
	3	110	20	18.18	
5.0	1	111	66	59.46	60.93
	2	102	64	62.75	
	3	104	63	60.58	
4.5	1	115	NCD	NCD	NCD*
	2	99	NCD	NCD	
	3	106	NCD	NCD	
4.0	1	113	NCD	NCD	NCD*
	2	105	NCD	NCD	
	3	99	NCD	NCD	
1.0	1	108	108	100.00	99.40
	2	110	110	100.00	
	3	111	109	98.20	

*NCD= Not countable due to damage

Table B.6: pH dependent release efficiency in terms of different time period

Release period (Min)	Sample Replicates	No. of oocysts/ spot		Release efficiency (%)	Average release efficiency (%)
		Capture	Release		
15	1	119	73	61.34	59.76
	2	105	61	58.10	
	3	117	70	59.83	
30	4	110	70	63.64	61.08
	5	112	68	60.71	
	6	107	63	58.88	
60	7	110	71	64.55	62.78
	8	116	74	63.79	
	9	115	69	60.00	

Table B.7: Changes in capture efficiency with the subsequent use of the same surface

Spots	1	2	3
Cell load (oocysts/spot)	120	120	120
1 st round of capture	117	105	108
Average Capture efficiency (1 st round)	91.7%		
Average Release efficiency (1 st round)	56.8%		
Cell load (2 nd round)	120	120	120
2 nd round of capture	90(+47) = 137	78(+50) = 128	94(+45) = 139
Cells left after 2 nd release	99	89	98
Average Capture efficiency (2 nd round)	72.8%		
Average Release efficiency (2 nd round)	29.2%		
Cell load (3 rd round)	120	120	120
3 rd capture	50 (+99) = 149	63 (+89) = 152	44(+98) = 142
Average Capture efficiency (3 rd round)	43.6%		
Average Release efficiency (3 rd round)	16.5%		
Cell load (4 th round)	120	120	120
4 th capture	37 (+120) = 157	38 (+131) = 169	27(+119) = 146
Average Capture efficiency (4 th round)	28.3%		

Table B.8: Analysis of the presence of CPD in DNA of UV irradiated (40mJ/cm²) oocysts

Microscopic fields	CPD positive area	DAPI positive area	Total area indicating DNA	% CPD indicating areas	Average % CPD indicating areas
1	2	4	4	50	63.5
2	0	2	2	0	
3	1	2	2	50	
4	3	2	3	100	
5	2	2	3	67	
6	1	2	2	50	
7	4	6	7	57	
8	16	17	17	94	
9	4	2	4	100	
10	2	3	3	67	

Appendix C: Statistical analyses outputs

Table C.1: One-way ANOVA for *C. parvum* vs. IgG3

ANOVA (efficiency)

	Sum of Squares	df	Mean Square	F	Sig.
Between Groups	.002	2	.001	1.225	.358
Within Groups	.004	6	.001		
Total	.006	8			

Table C.2: One-way ANOVA for *C. parvum* vs. IgG1

ANOVA (efficiency)

	Sum of Squares	df	Mean Square	F	Sig.
Between Groups	.002	2	.001	.749	.512
Within Groups	.008	6	.001		
Total	.009	8			

Table C.3: One-way ANOVA for *C. muris* vs. IgG3

ANOVA (efficiency)

	Sum of Squares	df	Mean Square	F	Sig.
Between Groups	.002	2	.001	5.337	.047
Within Groups	.001	6	.000		
Total	.003	8			

Post Hoc Tests (Homogeneous Subsets)

Student-Newman-Keuls (efficiency)

Slide	N	Subset for alpha = 0.05	
		1	2
6	3	.9149	
4	3	.9422	.9422
5	3		.9505
Sig.		.054	.493

Means for groups in homogeneous subsets are displayed.

a. Uses Harmonic Mean Sample Size = 3.000.

Table C.4: One-way ANOVA for *C. muris* vs. IgG1

ANOVA (efficiency)

	Sum of Squares	df	Mean Square	F	Sig.
Between Groups	.004	2	.002	2.464	.166
Within Groups	.005	6	.001		
Total	.009	8			

Table C.5: One-way ANOVA for *C. hominis* vs. IgG3

ANOVA (efficiency)

	Sum of Squares	df	Mean Square	F	Sig.
Between Groups	.005	2	.003	5.759	.040
Within Groups	.003	6	.000		
Total	.008	8			

Post Hoc Tests (Homogeneous Subsets)
Student-Newman-Keuls (efficiency)

Slide	N	Subset for alpha = 0.05	
		1	2
8	3	.8078	
9	3		.8542
7	3		.8618
Sig.		1.000	.673

Means for groups in homogeneous subsets are displayed.

a. Uses Harmonic Mean Sample Size = 3.000.

Table C.6: One-way ANOVA for *C. hominis* vs. IgG1

ANOVA (efficiency)

	Sum of Squares	df	Mean Square	F	Sig.
Between Groups	.001	2	.001	.373	.704
Within Groups	.010	6	.002		
Total	.011	8			

Table C.7: One-way ANOVA for IgG3 vs. all 3 *Cryptosporidium* species

ANOVA (efficiency)

	Sum of Squares	df	Mean Square	F	Sig.
Between Groups	.049	2	.024	33.850	.000
Within Groups	.017	24	.001		
Total	.066	26			

Post Hoc Tests (Homogeneous Subsets)
Student-Newman-Keuls (efficiency)

recode_org	N	Subset for alpha = 0.05	
		1	2
3	9	.8413	
1	9		.9260
2	9		.9359
Sig.		1.000	.443

Means for groups in homogeneous subsets are displayed.

a. Uses Harmonic Mean Sample Size = 9.000.

Table C.8: One-way ANOVA for IgG1 vs. all 3 *Cryptosporidium* species

ANOVA (efficiency)

	Sum of Squares	df	Mean Square	F	Sig.
Between Groups	.185	2	.093	75.969	.000
Within Groups	.029	24	.001		
Total	.214	26			

Post Hoc Tests (Homogeneous Subsets)
Student-Newman-Keuls (efficiency)

recode_org	N	Subset for alpha = 0.05		
		1	2	3
3	9	.5413		
2	9		.6584	
1	9			.7432
Sig.		1.000	1.000	1.000

Means for groups in homogeneous subsets are displayed.

Uses Harmonic Mean Sample Size = 9.000.

Table C.9: t-test IgG3 vs. IgG1 for *C. parvum*

Ab_recode		N	Mean	Standard Deviation	Standard Error Mean
Efficiency	IgG3	9	.9260	.02794	.00931
	IgG1	9	.7432	.03423	.01141

		Levene's Test for Equality of Variances		t-test for Equality of Means				
		F	Sig.	t	df	Sig. (2-tailed)	Mean Difference	Std. Error Difference
Efficiency	Equal variances assumed	.095	.762	12.412	16	.000	.18281	.01473
	Equal variances not assumed			12.412	15.382	.000	.18281	.01473

Table C.10: t-test IgG3 vs. IgG1 for *C. muris*

Ab_recode		N	Mean	Standard Deviation	Standard Error Mean
efficiency	IgG3	9	.9359	.02015	.00672
	IgG1	9	.6584	.03348	.01116

		Levene's Test for Equality of Variances		t-test for Equality of Means				
		F	Sig.	t	df	Sig. (2-tailed)	Mean Difference	Std. Error Difference
Efficiency	Equal variances assumed	2.352	.145	21.305	16	.000	.27751	.01303
	Equal variances not assumed			21.305	13.126	.000	.27751	.01303

Table C.11: t-test IgG3 vs. IgG1 for *C. hominis*

Ab_recode		N	Mean	Std. Deviation	Std. Error Mean
Efficiency	IgG3	9	.9359	.02015	.00672
	IgG1	9	.6584	.03348	.01116

		Levene's Test for Equality of Variances		t-test for Equality of Means				
		F	Sig.	t	df	Sig. (2-tailed)	Mean Difference	Std. Error Difference
Efficiency	Equal variances assumed	2.352	.145	21.305	16	.000	.27751	.01303
	Equal variances not assumed			21.305	13.126	.000	.27751	.01303

Table C.12: Statistical analysis of antibody concentration

ANOVA (efficiency)

	Sum of Squares	df	Mean Square	F	Sig.
Between Groups	1.369	4	.342	549.579	.000
Within Groups	.006	10	.001		
Total	1.375	14			

Post Hoc Tests (Homogeneous Subsets)

Student-Newman-Keuls (Efficiency)

ab_conc	N	Subset for alpha = 0.05			
		1	2	3	4
.00	3	.00321			
12.50	3		.41026		
25.00	3		.44551		
50.00	3			.58974	
100.00	3				.93910
Sig.		1.000	.114	1.000	1.000

Means for groups in homogeneous subsets are displayed.

a. Uses Harmonic Mean Sample Size = 3.000.